Open Source GIS in India: Present Scenario

Conveners

T V Ramachandra	*T G Sitharam*	*M S Mohan Kumar*	*S Narendra Prasad*
Chairman, OSGeo India Software Development Committee	Chairman C*i*STUP, IISc	Secretary KSCST	Chairman, OSGEO India, Education and Training Committee

Centre for *Infrastructure*, Sustainable Transportation and Urban Planning [C*i*STUP]

Indian Institute of Science

Bangalore 560 012, India

http://cistup.iisc.ernet.in

http://wgbis.ces.iisc.ernet.in/foss

Open Source GIS in India: Present Scenario

Centre for *Infrastructure*, Sustainable Transport and Urban Planning (CiSTUP)
Indian Institute of Science
Bangalore 560 012, Tel 08022932521

CiSTUP jointly with OSGEO (India Chapter) and KSCST announces

Discussion meeting

Open Source GIS in India: Present Scenario

Date: 16th November 2009 (Monday), Time: 9 to 3 30 pm, Registration: 9 am
Venue: CiSTUP, Conference Hall (SID Building), IISc Campus

Inauguration: 9 30 am

CiSTUP and Geoinformatics Initiative - Overview: Prof. T G Sitharam, Chairman,
Inaugural talk: Geoinformatics in India 9 30 to 10 am

Tea (10-1030 am)

Presentations (10 30-1300 hours)
    Session: OS GIS in India: Present Scenario
    1. OS GIS Development : Progress in India
         Mr. Ravi, Member, OSGEO International Board of Directors
    2. A Web GIS Using FOSS tools- Select case studies
         Dr. S.N.Prasad,SACON and Chairman, OSGEO India, Education and
                          Training Committee
    3. Role of IIIT in OS GIS development: approaches
         Dr. Rajan, IIIT, Hyderabad & OSGeo, India, Treasurer
    4. GRDSS: Evolution and scope
         Dr. T V Ramachandra, CES, CST & CiSTUP,IISc
         Chairman, OSGeo India Software Development Committee
    5. GRDSS: Applications and case study
         Uttam Kumar, CST & MS, IISc, Member, OSGEO India chapter
    6. Application of OS GIS in Decentralised planning (panchayath and in an academic
       institution) -   Jaisen N D, CES, IISc: Case study
    7. Experiments with FOSS - Dr. Gururaja K V, CiSTUP
    8. Geoinformatics at NRDMS: DST- KSCST Initiative
                          Dr. Subhas Sondur, NRDMS, KSCST
Lunch (1300 -1400 hours)

1400-1530: Interactive session on OS GIS in India – Scope and Strategies

1530 Feedback and Concluding Session

1530 - Evening Tea

Back ground:

Discussion Meeting – Open Source GIS In India: Present Scenario

The growth of GIS is hindered by highly priced proprietary softwares and unavailability of public geodata. Many of such licensed softwares remain unutilized in various government offices because they require either extensive training or easy availability on multiple locations. All this can be changed by the use of Free/Opensource software tools. This is significant since all government data and most educational institutions work in local language media. FOSS GIS or Free/Opensource Geospatial softwares are more powerful and usable for developing systems where more and more public participation is sought. In this regard the proposed discussion meeting helps to understand the potential and limitations of OS GIS apart from exploring the possible developments.

Centre for infrastructure, Sustainable Transportation and Urban Planning (CiSTUP) was established at IISc (http://cistup.iisc.ernet.in) with the financial aid from the Government of Karnataka to develop a unique expertise having an interface in the areas of infrastructure, sustainable transportation and urban planning. CiSTUP is actively engaged in several activities such as basic and applied research and development, academic activities, training programmes, workshops and consultancy projects in the areas of infrastructure, sustainable transportation and urban planning. Geoinformatics lab has been set up at CiSTUP with the state of the art gadgets in spatial and temporal analysis.

The Karnataka State Council for Science and Technology (KSCST) is actively involved in Natural Resources Data Management System (NRDMS) program (http://kscst.org.in/nrdms.html) - a multi-disciplinary and multi-institutional program aimed at developing methodologies for building and promoting the use of spatial data management and analysis technologies in local area planning.

The Open Source Geospatial Foundation (http://osgeo.org) created to support and build the highest-quality open source geospatial software. The goal is to encourage the use and collaborative development of community-led projects. The OSGeo-India is actively involved in the capacity building in Open Source Geospatial software encouraging student and researchers by conducting lectures and workshops in collaboration with the academic institutions (http://wiki.osgeo.org/wiki/India_Chapter_Report_2007). The India OSGeo Chapter is aiding individuals and institutions interested in Open Source Geospatial Solutions and related issues, covering all activities associated with the application, development and promotion of Open Source Geospatial solutions in India.

FOSS for Geoinformatics (FOSS4G)

Ramachandra T V and Uttam Kumar

Geoinformatics Laboratory

Centre for *Infrastructure*, Sustainable Transport and Urban Planning

Indian Institute of Science, Bangalore 560 012

E Mail: cestvr@cistup.iisc.ernet.in

Geoinformatics constitute a vital component of information science for addressing the problems of geography, geosciences and related branches of engineering. This domain combines geospatial analysis and modeling, development of geospatial databases, information systems design, human-computer interaction and both wired and wireless networking technologies. Geoinformatics uses geocomputation for analysing geoinformation. One of the major applications of geoinformatics in recent times is the study of variation in landscapes over multiple spatial and temporal scales encompassing a variety of domains – land use and land cover change, climate change, water resources, urban development, natural disaster mitigation, etc. Geoinformatics include geographic information systems, spatial decision support systems, global positioning systems (GPS), and remote sensing.

Geographic Information Systems (GIS) are increasingly being used as the principal tool for digital exploration of variation in landscapes, as they provide the necessary functions for spatial data collection, management, analysis and representation (Turner et al., 2001; Longley et al., 2005; Steiniger and Weibel, 2009; Ramachandra et al., 2004). These tools

provide new and critical ways of understanding our earth and its biogeochemical cycle. GIS software used for this kind of studies fulfill several GIS functionality including:

i.) Ensure world wide development, advancement and application of solutions.
ii.) Allow studying of data, methods and algorithm implementation.
iii.) Furthermore, developed models and algorithms need not be reimplemented by others in order to continue research or validate previous results.

Apart from these, researchers should have access to libraries of the original models for analysis, validation, development and implementation (Steiniger and Hay, 2009; Jolma et al., 2008b) for further improvement and customisation depending on the local requirement.

Over the last years the paradigm of Free and Open Source Software (FOSS) development has taken root in the GIS community, resulting in the creation of several sophisticated GIS software projects whose aim is to develop free software for numerous purposes. GIS software fulfilling the specific requirements have been distributed with licenses that grant more freedoms of use and that support openness, such as licenses used by FOSS GIS projects (for example: http://grass.itc.it/; http://wgbis.ces.iisc.ernet.in/grass).

FOSS have proved to be promising tools that allow us to see and change the *software codes* written in any programming language. FOSS is generally synonymous with *free software* and *open source software*, and describes similar development models, but with differing cultures and philosophies. Because of the way it is licensed, it has the potential to be legally given away for free or for very little cost and copied and shared with others.

FOSS, F/OSS or FLOSS (for *Free/Libre/Open Source Software*) is liberally licensed to grant the right of users to study, change, and improve its design through the availability of its source code. It has more scope for being available in multiple languages and for being adapted or tweaked to particular needs. This can be very useful for students, researchers, teachers, scientists wanting to use legal software that is appropriate to their needs and fits within their modest budgets. This approach has gained both momentum and acceptance as the potential benefits have been increasingly recognised by many (Steiniger and Hay, 2009). This is proving to be the boon to researchers from economically disadvantaged countries.

The open source definition is used by the Open Source Initiative to determine whether or not a software license can be considered open source. Under the open source definition, licenses must meet the following ten conditions in order to be considered open source licenses:

- Free redistribution: the software can be freely given away or sold. (This was intended to expand sharing and use of the software on a legal basis.)
- Source code: the source code must either be included or freely obtainable. (Without source code, making changes or modifications can be impossible.)

- Derived works: redistribution of modifications must be allowed. (To allow legal sharing and to permit new features or repairs.)
- Integrity of the author's source code: licenses may require that modifications are redistributed only as patches.
- No discrimination against persons or groups: no one can be locked out.
- No discrimination against fields of endeavor: commercial users cannot be excluded.
- Distribution of license: the rights attached to the program must apply to all to whom the program is redistributed without the need for execution of an additional license by those parties.
- License must not be specific to a product: the program cannot be licensed only as part of a larger distribution.
- License must not restrict other software: the license cannot insist that any other software it is distributed with must also be open source.
- License must be technology neutral: no click-wrap licenses or other medium-specific ways of accepting the license must be required.

There is a distinction between open source software and free software. Open source software are those, for which the human-readable source code is made available under a copyright license (or arrangement such as the public domain) that meets the Open Source Definition. This permits users to use, change and improve the software, and to redistribute it in modified or unmodified form. It is often developed in a collaborative manner in a public domain. Public domain comprises the body of knowledge and innovation (especially creative works such as writing and inventions) in relation to which no person or other legal entity can establish or maintain proprietary interests within a particular legal jurisdiction. This body of information and creativity is considered to be part of a common cultural and intellectual heritage, which, in general, anyone may use or exploit, whether for commercial or non-commercial purposes. Public domain software is not protected by copyright and may be copied and used without payment (http://www.fsf.org/; wikipedia).

On the other hand, free software is software that can be used, studied, and modified without restriction, and which can be copied and redistributed in modified or unmodified form either without restriction, or with restrictions only to ensure that further recipients can also do these things. To make these acts possible, the human readable form of the program (called the source code) must be made available. The source code can be placed in the public domain, accompanied by a software license saying that the copyright holder permits these acts (a free software licence), etc. (http://www.fsf.org/).

The first formal definition of free software states that software is free software if people who receive a copy of the software have the following four freedoms:

1.) Freedom 0: The freedom to run the program for any purpose.
2.) Freedom 1: The freedom to study and modify the program.
3.) Freedom 2: The freedom to copy the program so you can help your neighbor.

4.) Freedom 3: The freedom to improve the program, and release your improvements to the public, so that the whole community benefits.

Freedoms 1 and 3 require source code to be available because studying and modifying software without its source code is highly impractical (http://www.fsf.org/).

Proprietary software has restrictions on copying and modifying as enforced by the proprietor. Restrictions on modification and copying are sought by either legal or technical means or sometimes both. Technical means include releasing machine-readable binaries to users and withholding the human-readable source code. Legal means can involve software licensing, copyright, and patent law.

Copyleft is a form of licensing and may be used to modify copyrights for works such as computer software, documents, etc. In general, copyright law allows an author to prohibit others from reproducing, adapting, or distributing copies of the author's work. In contrast, an author may, through a copyleft licensing scheme, give every person who receives a copy of a work permission to reproduce, adapt or distribute the work as long as any resulting copies or adaptations are also bound by the same copyleft licensing scheme. A widely used and originating copyleft license is the GNU General Public License.

The GNU General Public License (GNU GPL or simply GPL) is a widely used free software license, originally written by Richard Stallman for the GNU project. It is the license used by the Linux kernel. The GPL is the most popular and well-known example of the type of strong copyleft license that requires derived works to be available under the same copyleft. Under this philosophy, the GPL is said to grant the recipients of a computer program the rights of the free software definition and uses copyleft to ensure the freedoms are preserved, even when the work is changed or added to. This is in distinction to permissive free software licences, of which the BSD (Berkeley Software Distribution) licenses are the standard examples. The GNU Lesser General Public License (LGPL) is a modified, more permissive, version of the GPL, intended for some software libraries.

FOSS has become an essential component in geoinformatics research. Many free and open source software are available that facilitate customisation, provide good support via forums and email lists and have up-to-date documentation. Among the many GIS tools that are frequently used are Desktop GIS, Mobile GIS, Remote Sensing and Image Processing software, GIS extensions and libraries, Spatial Database Management Systems, Map Server and Geostatistical tools (Steiniger and Hay, 2009).

Next, we present a non-comprehensive list of the FOSS commonly used in GIS applications along with their web address for further references.

	Application	Software	References
1	GIS	Sav GIS	http://www.savgis.org
2		Forestry GIS	http://www.forestpal.com/fgis.html
3		GRASS	http://wgbis.ces..isc.ernet.in/grass
4		QGIS	http://qgis.org
5	Image	ILWIS	http://ilwis.org
6	Processing /	uDIG	http://udig.refractions.net
7	Raster, Vector	SAGA	http://saga-gis.org
8	Analysis	OpenJUMP	http://openjump.org
9		MapWindow	http://mapwindow.org
10		gvGIS	http://gvsig.gva.es
11		InterImage	http://www.lvc.ele.puc-rio.br/projects/
12		Landserf	http://www.landserf.org
13		OSSIM	http://www.ossim.org
14	Landscape Analysis	r.li (GRASS)	http://grass.itc.it/grass70/manuals/html70_user/r.li.html
15		Fragstats	http://www.umass.edu/landeco/research/fragstats/fragstats.html
16	Spatial DBMS	MySQL	http://www.mysql.org
17		PostGIS for Postgre SQL	http://postgis.refractions.net
18	Web	GeoServer	http:// www.geoserver.org
19	MapServer	MapServer	http:// www.mapserver.org
20	Statistical	R	http://www.r-project.org/
21	software	Gstat	http://www.gstat.org
22		Past	http://folk.uio.no/ohammer/past/
23	Exploratory	GeoDa	http://geodacenter.asu.edu/software
24	Data Analysis	GeoVista	http://www.geovistastudio.psu.edu
25		STARS	http://regionalanalysislab.org/index.php/Main/STARS
26		GDAL/OGR	http://gdal.osgeo.org
27		Generic Mapping Tool	http://gmt.soest.hawaii.edu/
28		JAMA/GNU	http://math.nist.gov/javanumerics/jama/
29	Libraries	JTS Topology Suite	http://tsusiatsoftware.net/jts/main.html
30		LUPOLib	http://www.ufz.de/index.php?en=4302
31		OpenBugs	http://mathstat.helsinki.fi/openbugs/
32		Sextane	http://forge.osor.eu/projects/sextante/
33		TerraLib	http://www.terralib.org/
34		MASON	http://cs.gmu.edu/~eclab/projects/mason/
35	Multi Agent	Rapast Simphony	http://repast.sourceforge.net/
36		SWARM	http:// www.swarm.org
37		Netlogo	http://ccl.northwestern.edu/netlogo/

38		(Open-)Start Logo	http://education.mit.edu/openstarlogo/
39		OBEUS	http://www.tau.ac.il/~bennya/research1.html
40	CMS	Drupal	http://drupal.org/
41		Joomla	http://www.joomla.org/
42		Atutor	http://www.atutor.ca/
43	Modelling	Open Modeller	http://openmodeller.sourceforge.net/
44		Desktop GARP	http://www.nhm.ku.edu/desktopgarp/index.html
45		Maxent	http://www.cs.princeton.edu/~schapire/maxent/
46		Landisview	http://sourceforge.net/projects/landisview
47	Miscellaneous	PCRaster	http://pcraster.geo.uu.nl
48		SANET	http://ua.t.u-tokyo.ac.jp/okabelab/atsu/ sanet/
49		S-Distance	http://www.prd.uth.gr/res_labs/spatial_analysis/software/SdHome_en.asp
50		TAS	http://www.uoguelph.ca/~hydrogeo/TAS/
51		Harvest	http://www.nrs.fs.fed.us/tools/harvest/
52		Qrule	http://www.al.umces.edu/Qrule.htm

Proprietary software licenses impose several restrictions on the use of software such as not allowing users to distribute the software or to install it on a second computer or to give it to others. The licenses also prohibit a reverse engineering of the software and modifying the software. If the source code is not available, then it is not possible to study how algorithms are implemented and it is not possible to improve the software. FOSS licenses, such as the GPL and the LGPL, explicitly allow users to study, modify and re-distribute software. Consequently the following three benefits of FOSS have been identified (Steiniger and Bocher, in press):

(i) FOSS avoids 'reinventing the wheel',
(ii) in terms of the source code, FOSS provides the best 'documentation' available, and
(iii) users can adapt the software to their own needs without restrictions.

All three points are essential for research, when considering that

- research should not be limited by the functionality that is provided by the software,
- research experiments need to be repeatable and reproducible, and
- research can progress faster when models can be analysed, validated, and improved directly, i.e. based on source code, without the problem of misinterpretation, as may be the case when knowledge is obtained/interpreted from articles (Steiniger and Hay, 2009).

In addition to these general research advantages, the use of FOSS licenses have enhanced education and knowledge transfer, particularly in developing countries that don't have the (financial) resources. Students and researchers can freely and legally download the software and study the algorithms. Finally it benefits society in general, as the use of free

software licenses can facilitate the application of new technologies and knowledge that enables a sustainable use of resources (Jolma et al., 2008b). If such unified software development and research efforts could be initiated then we see great potential to accelerate geoinformatics research world wide.

References:
- Jolma, A., Ames, D.P., Horning, N., et, al., 2008a. Free and open source geospatial tools for environmental modelling and management. In: Jakeman, A.J., Voinov, A.A., Rizzoli, A.E., Serena, H.C. (Eds.), Environmental Modelling, Software and Decision Support. Elsevier, Amsterdam, pp. 163–180.
- Jolma, A., Ames, D.P., Horning, N., et, al., 2008b. Environmental modeling using open source tools. In: Shekhar, S., Xiong, H. (Eds.), Encyclopedia of GIS. Springer, New York, pp. 275–279.
- Longley, P.A., Goodchild, M.F., Maguire, D.J., and Rhind, D.W., 2005. Geographic information systems and science, 2nd ed. Wiley, Chichester.
- Steiniger, S., and Bocher, E., in press. An overview on current free and open source desktop GIS developments. International Journal of Geographical Information Science. doi:10.1080/13658810802634956.
- Steiniger, S., and Hay, G. J., 2009. Free and open source geographic information tools for landscape ecology. Ecological Informatics, 4, 183-195.
- Steiniger, S., and Weibel, R., 2009. GIS software — a description in 1000 words. Available from:
  http://www.geo.unizh.ch/publications/sstein/gissoftware_steiniger2008.pdf.
- Turner, M.G., Gardner, R.H., and O'Neill, R.V., 2001. Landscape ecology in theory and practice pattern and processes. Springer, New-York.

Useful links:

- http://wgbis.ces.iisc.ernet.in/foss
- http://www.opensourcegis.org
- http://www.spatialserver.net/osgis
- http://www.spatialanalysisonline.com
- http://www.ai-geostats.org
- http://ces.iisc.ernet.in/grass Mirror site for GRASS in India
- http://ces.iisc.ernet.in/biodiversity Geoinformatics Applications
- http://ces.iisc.ernet.in/energy

Geographic Resources Decision Support System – an Open Source GIS

T. V. Ramachandra (*,+), Uttam Kumar (*), S.N. Prasad (#) & Vaishnav B(*)
* Centre for Ecological Sciences, Indian Institute of Science
+ Centre for Sustainable Technologies, Indian Institute of Science
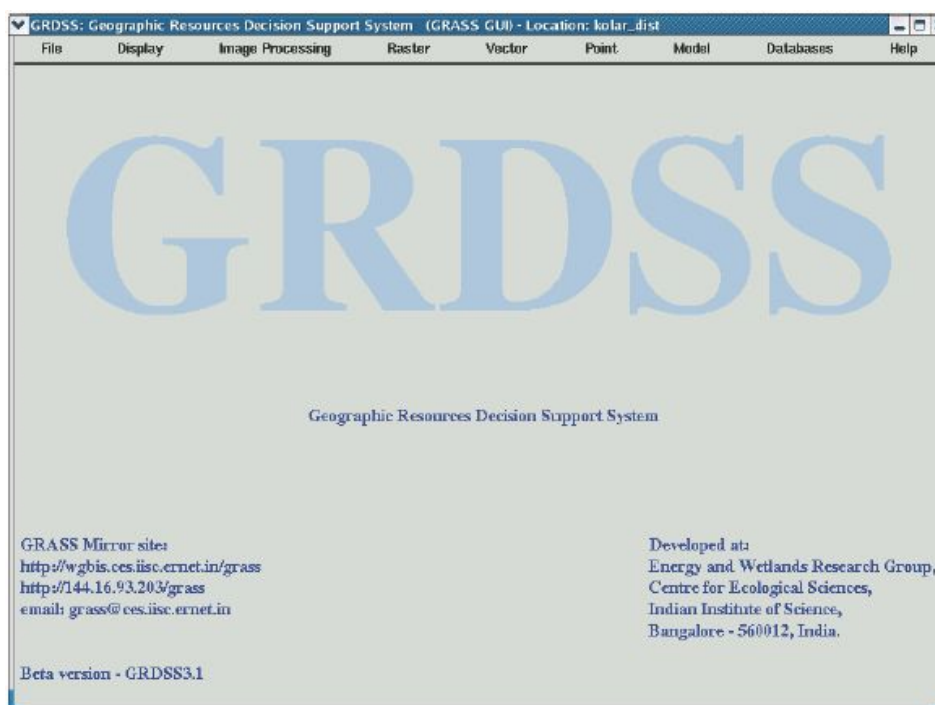# Salim Ali Centre for Ornithology and Natural History, Dehradun

Figure 1: GRDSS

The process of developing the GUI also involved undertaking the task of identifying the commands and implementation of the interfacing code. The layout of the interface had to be altered to suit the end user's perspective. Figure 2 shows the structural diagram of the GRDSS graphical user interface.

Address for Correspondence :
Dr. T.V. Ramachandra
Energy & Wetlands Research Group
Centre for Ecological Sciences
Indian Institute of Science,
Bangalore – 560 012, INDIA

Tel :
91-80-23600985/22932506/22933099

Fax :
91-80-23601428/23600085/23600683[CES-TVR]

E-mail :
cestvr@ces.iisc.ernet.in
cestvr@hamsadhvani.sers.iisc.ernet.in
energy@ces.iisc.ernet.in

URL :
http://ces.iisc.ernet.in/energy/index.htm

Abstract

Fully structured and matured open source spatial and temporal analysis technology seems to be the official carrier of the future for planning of the natural resources especially in the developing nations. This technology has gained enormous momentum because of technical superiority, affordability and ability to join expertise from all sections of the society. Sustainable development of a region depends on the integrated planning approaches adopted in decision making which requires timely and accurate spatial data. With the increased developmental programmes, the need for appropriate decision support system has increased in order to analyse and visualise the decisions associated with spatial and temporal aspects of natural resources. In this regard Geographic Information System (GIS) along with remote sensing data support the applications that involve spatial and temporal analysis on digital thematic maps and the remotely sensed images. Open source GIS would help in wide scale applications involving decisions at various hierarchical levels (for example from village panchayat to planning commission) on economic viability, social acceptance apart from technical feasibility. GRASS (Geographic Resources Analysis Support System, http://wgbis.ces.iisc.ernet.in/grass) is an open source GIS that works on Linux platform (freeware), but most of the applications are in command line argument, necessitating a user friendly and cost effective graphical user interface (GUI). Keeping these aspects in mind, Geographic Resources Decision Support System (GRDSS) has been developed with functionality such as raster, topological vector, image processing, statistical analysis, geographical analysis, graphics production, etc. This operates through a GUI developed in Tcltk (Tool command language / Tool kit) under Linux as well as with a shell in X-Windows. GRDSS include options such as Import /Export of different data formats, Display, Digital Image processing, Map editing, Raster Analysis, Vector Analysis, Point Analysis, Spatial Query, which are required for regional planning such as watershed Analysis, Landscape Analysis etc. This is customised to Indian context with an option to extract individual band from the IRS (Indian Remote Sensing Satellites) data, which is in BIL (Band Interleaved by Lines) format. The integration of PostgreSQL (a freeware) in GRDSS aids as an efficient

database management system.   11

Introduction

GIS (Geographic Information System) is a system of hardware, software and procedures to facilitate the management, manipulation and analyses of spatial-temporal data. Its application is wide ranging from micro level to macro level planning. However this boundless capabilities are limited by ones ability to visualise its implications. It has become an important component in regional planning with a pivotal role in major decisions related to earth resources. This includes urban sprawl analysis involving growth and migration of population, location of industries, employment activities, basic infrastructure (water, electricity, etc.), transportation (railway and road networks), drainage system (river basin quality, etc.), town planning, etc.

With the growing incidence of ecological and environmental impacts, GIS has been used to analyse the impact of human activities on the ecosystems. This is possible due to the options to display and analyse changes in the geo-referenced temporal and spatial data. This helps to solve complex problems regarding planning and management of resources and also biophysical modeling. The data input includes spatial, statistical and thematic data derived from a combination of existing maps, aerial photographs, interpretation of remotely sensed images and secondary data from the government agencies (census data, land use data, etc.). Digital image processing technique aids in restoration and rectification of data, segmentation of data and also in visualisation. The integration of spatial and temporal technology help in addressing challenges faced by the environment. The integration of GIS with remote sensing data offers enhanced capability for inventorying, mapping, monitoring and modeling to understand many environmental processes. This integration also helps in using remotely sensed image to update the GIS and also maps. The GIS thematic data and attributes are used to guide image classification. GRASS, a GIS based open source software distributed under the GNU GPL (General Public License) integrates these two technologies resulting in numerous advantages.

GRASS was originally developed by the U.S. Army Construction Engineering Research Laboratories, a branch of the US Army Corp of Engineers, as a tool for land management and environmental planning by the military. GRASS is a raster/vector GIS, image processing system, and graphics production system (http://wgbis.ces.iisc.ernet.in/grass). GRASS contains over 350 programs and tools to render maps and images on monitor and paper; manipulate raster, vector, and sites data; process multi spectral image data; and create, manage, and store spatial data. GRASS has the options to interface with printers, plotters, digitizers, and databases to develop new data as well as manage existing data. GRASS uses both intuitive windows interface as well as command line syntax for ease of operations and is supported by developers and users worldwide. Numerous sub modules existed in GRASS but most of them are in command line arguments. The command line syntax for GRASS was cumbersome and time consuming for individuals, who were not exposed to computer programming and did not possess any programming skills. In order to overcome this difficulty, it was the necessity for an economically viable, technically superior and a more flexible spatial and temporal analyses tools that led to the development of a user friendly graphical user interface (GRDSS) for GRASS GIS along with the database component as depicted in figure 1.
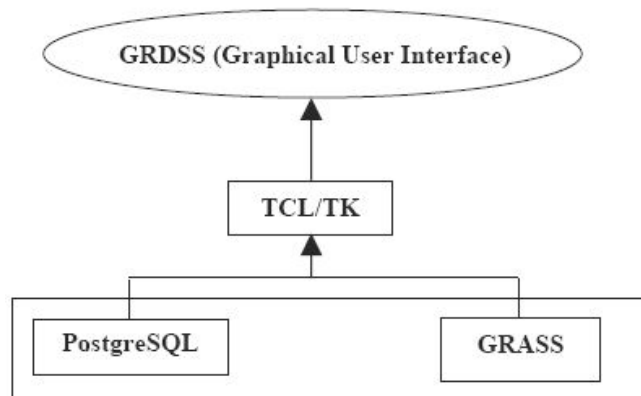

Figure 2: GRDSS - GUI structural diagram

Methodology   T

The current development in GRDSS in the allied technologies of remote sensing and GIS is to build an integrated spatial decision support system (SDSS). Recent advances in the development of graphical user interface based programming have enabled rapid prototyping, testing, and application development. Various GIS packages such as MapInfo (http://mapinfo.com), Idrisi (http://www.idrisi.clarku.edu), Geomedia (http:// w ww.intergraph.com) etc were comparatively studied as per the set criteria listed in table 1.

Sl. No.	Characteristics	MAPINFO	IDRISI	GEOMEDIA	GRDSS
1.	Menus and user interface	Y	Y	Y	Y
2.	Command line syntax	N	N	N	Y
3.	Data Import/Export	Y	Y	Y	Y
4.	IRS LISS–MSS Data extraction (Data in BIL and BSQ format to individual spectral bands)	N	Y	N	Y
5.	Map Registration & projection	Y	Y	Y	Y
6.	Digitization (vector data)	Y	Y	Y	Y
7.	Coordinate transformation	N	Y	Y	Y
8.	Buffer generation	Y	Y	Y	Y
9.	Digital Image analysis	N	Y	Y	Y
10.	Map Algebra	N	Y	Y	Y
11.	Terrain Modelling (DTM)	Y	Y	Y	Y
12.	Distance calculation	Y	Y	Y	Y
13.	Database support	Y	Y	Y	Y
14.	Error Explanation	Y	Y	Y	Y
15.	Help	Y	Y	Y	Y
16.	Online manuals and tutorials	Y	Y	Y	Y
17.	Proprietary software	Y	Y	Y	N
18.	Open source	N	N	N	Y
19.	Free software	N	N	N	Y
20.	Mailing List	N	N	Y	Y
21.	Digital Elevation Model (DEM)	Y	Y	Y	Y
22.	Fly through and animation	N	Y	Y	Y
23.	Fusion	N	N	N	Y

Y = features present
N = features not present

Table 1: **Comparative analyses of GIS softwares**

The limitations of the commercial GIS softwares were also considered while implementing the GRDSS to offer optimal performance. The following feature characterises GRDSS development.

i. System requirements - The GRDSS GUI sources can be compiled on all PC's running LINUX. It is a full system with X Window graphical user interface. Minimum PC can be 486 (or better), with "LINUX". The Linux- system with a three-button mouse, 32 MB RAM (64 MB recommended) and a hard disk space of 250MB (beside DOS/Windows partition). GRDSS binaries require only 45-50 MB and to compile additional 150 MB disk space is required (to store the sources). The GRDSS source code can be compiled using a GNU "C" compiler.

ii. User friendly interface and menu organisation - The user interface is designed to suit to the users in India and those who are not much exposed to programming. The interface is customized and simplified comparable to proprietary softwares in the market. The menu is organised sequentially in a user-friendly environment that satisfies both specific and common users.

iii. Functional capabilities - GRDSS is equipped with the functional capabilities such as data import/export in different formats (including the IRS data format), map analysis, data modeling, buffer generation, spatial and non spatial statistical calculation, digital image processing (spatial, spectral and temporal data analysis), raster, vector and point analysis and query, map calculator, terrain modeling, erosion modeling, report generation and can also handle spatial and non-spatial database (both spatial data and attribute information), etc.

iv. Help facilities – GRDSS extends all the help facilities present in GRASS. All the commands with their functions and options are present in help to get started with the GRDSS. There is a mailing list and mailing list archive where users can post their doubts and can discuss through e-mails worldwide. The help facilities andthe documents available on the GRASS official website provide enough information to start with the software.

v. Error explanation and manual support - GRDSS is equipped with error explanation, which automatically renders error messages through the mail facility in Linux. Beside many sample data sets are available on the GRASS official website, including online tutorials and manuals.
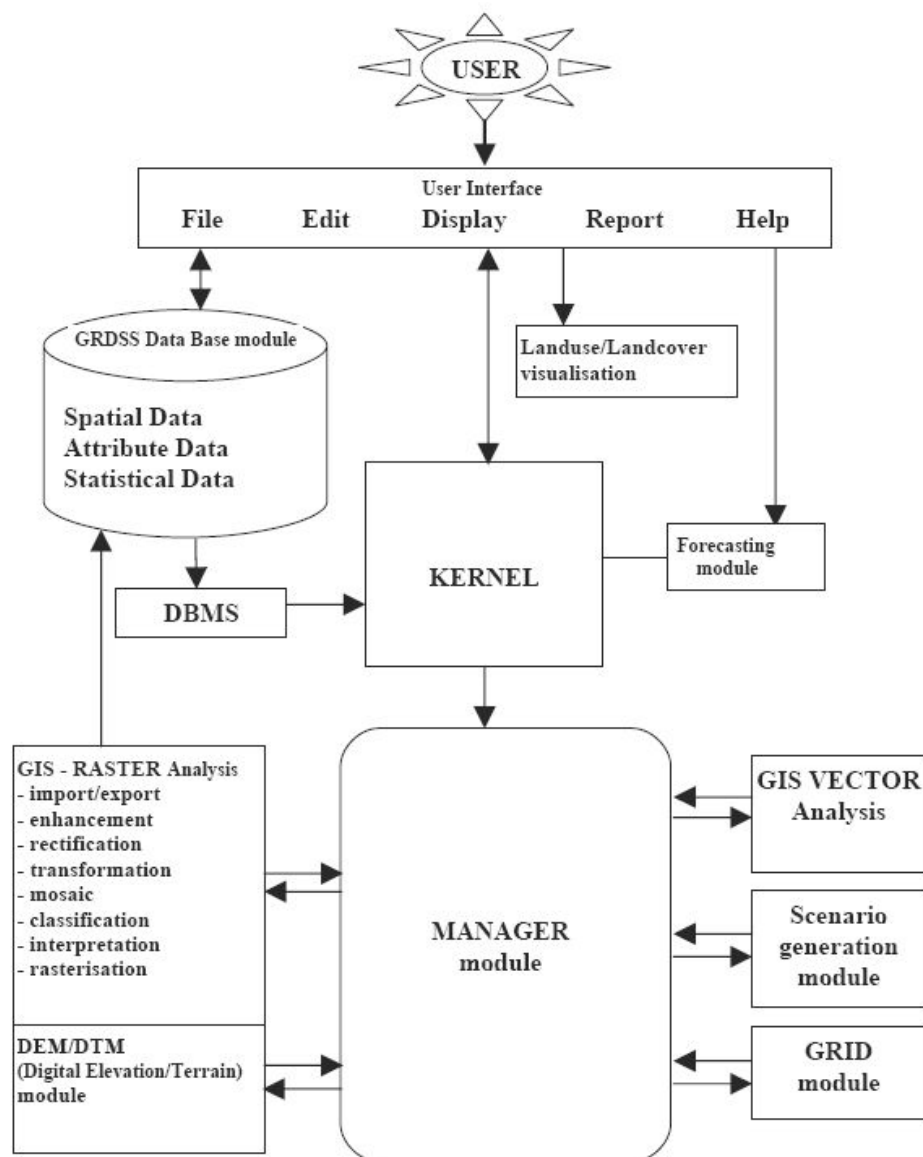
13

Figure 3: The GRDSS design and conceptual diagram.

Overview and description of GRDSS

T

GRDSS supports all basic features required by any GIS package.

  i. It supports a wide range of data Import/Export that are also supported by other standard GIS including IRS (LISS3 and PAN) data extraction and DTEM/DTED (Digital Terrain Elevation Model / Digital Terrain Elevation Data) extraction.
 ii. It has capabilities for displaying the raster/vector images. GRDSS can further interact with commercial plotters and printers and is capable of color management.
iii. GRDSS has the image processing capabilities (rectification, enhancement, transformation, classification, data analysis, etc.).
 iv. GRDSS has the capability of manipulating raster, vector and point data. This includes digitization, topology creation, map overlay, arithmetic operations, DEM generation, decision support, distance, area and statistical report, etc.
  v. It can perform wetland analysis, terrain modeling with slope, aspect, relief, profile, cost between two locations to analyze terrain data, runoff-modeling, etc.
 vi. Thematic data preparation, histogram generation, and charts of different formats.
vii. Database (PostgreSQL) management system.
viii. Online tutorials with help manuals and sample datasets. Figure 4 depicts the GRDSS hierarchical menu arrangement.
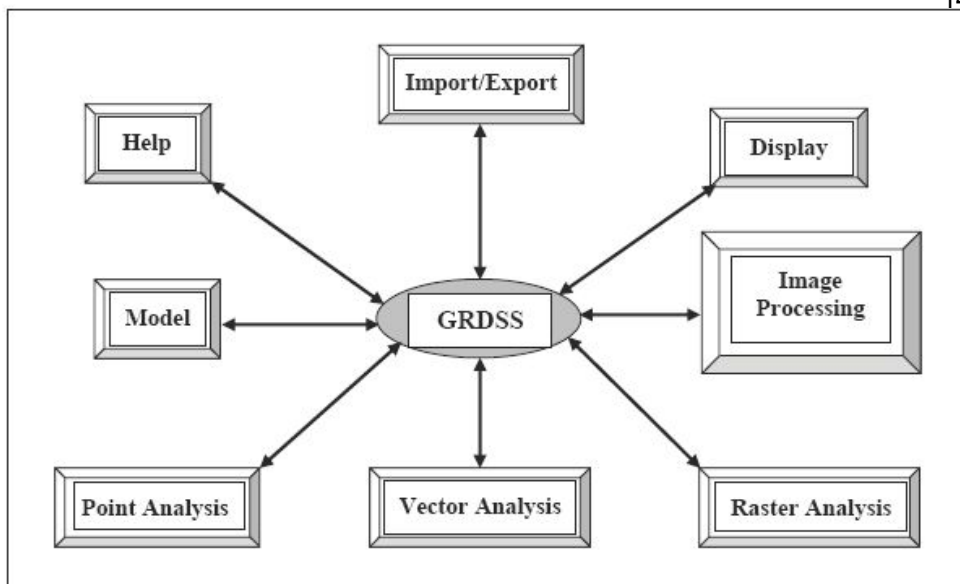
14

Figure 4: GRDSS hierarchical menu arrangement.Table 2: Functions of GRDSS modules

Import/Export (supported data formats)	Point (site) data formats
• **Raster formats –** IRS Data format (.bil – band interleaved by lines), Binary, Bsq (band sequential format), tiff (Tagged Image File Format), geotiff, img (image file), jpeg (joint photographic expert group), ppm (Portable Pixel Map), png (Portable Network Graphics), pbm (Portable Bit Map), pgm (Portable Gray Map), utm (Universal Transverse Mercator) sunraster, arcinfo, Esri, Erdas, ascii, tang, gridatb, Landsat tape formats, Idrisi etc. **Vector formats –** Autocad (dxf-Drawing eXchange Format), Atlas, shp (shape file), ascii, Esri, Arcinfo (dlg-Digital Line Graphs), Mapinfo (mif-MapInfo Interchange File), Sdts (Spatia Data Transfer Standard), Moss, xyz etc. • **Site formats –** Ascii, Shp (shape file), Dbf (data base file), Esri, etc. • **DEM/DTED extraction module.**	• Basic information attributes. • Quadrat counts, univariate statistics. • Buffer generation • Reprojection • Triangulation • Interpolation • Rainfall data preparation • Conversion tools – point to raster, vector, grid 3d etc. **Image Processing** • Segmentation • Rectification and restoration • Georegistration (geocorrection) • Transformation • Image enhancement • False color composite • Signature development • Clustering • Classification (land use analysis) • Vegetation indices (land cover analysis) **Models** • Wetland • Watershed • Landscape • Wildfire • Erosion tools

15

Vector format	Database (PostgreSQL)
- Digitize - Basic information about layers attributes, statistical calculation. - Report - Distance operators - Length, Perimeter, areas etc. - Reprojection - Grid generation - Conversion tool – vector to raster, vector to point, areas to line etc.	- Import /Export attribute data from different formats. - Select database/select table - Display table - Modify (add/delete) values - Query table - List table, list columns - Query raster, vector, sites data - Display raster, vector, sites data
Raster Analysis	Display
- Image information, report, area, category range, and statistical calculations. - Map algebra, regression analyses. - Distance operators, buffer creation. - Coordinate conversion tools - Topographic variables - Digital elevation model - Decision support - Grid generation, reclass, rescale, recode, color management. - Subimage extraction - Change resolution - Digitise - Conversion tools raster to vector lines, vector areas, point etc. - Cropping - Mosaic	- Display raster, vector, sites, 3d map. - Color management. - Display HIS, RGB, north arrow, frame, legend, map title. - Generate 3d view. - Animation. - Fly through. - Draping multiple raster, vector, site data. - Zoom, pan. - Generate histogram, pie chart, bar chart. - Select font size, symbols, appearance, style, width, and orientation. - Colors, line and polygon fill. - Placing text strings, map title, labels on raster, vector and point data.

Table 2: Functions of GRDSS modules

16
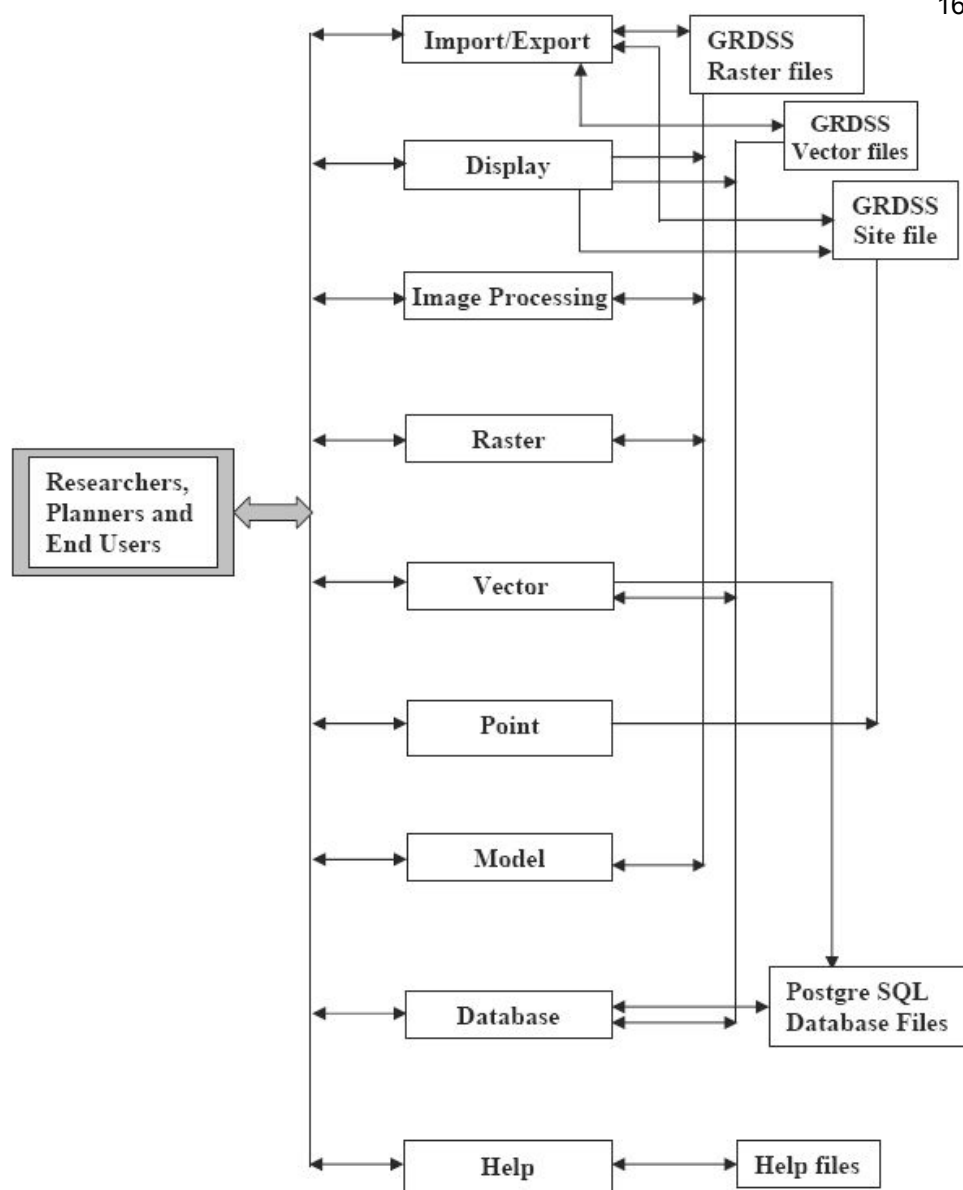
Figure 5: **GRDSS data flow diagram.**

Database connectivity   T

GRDSS uses PostgreSQL (a freeware) as a database for data storage, data retrieval, query and manipulation of both spatial and attribute information. It is the most advanced open source database server used primarily for data storage and retrieval, and complex data analysis. PostgreSQL is a sophisticated object-relational database management system (ORDBMS). An ORDBMS is an extension of the more traditional relational database management systems (RDBMS). For the advanced developer, PostgreSQL even supports extensibility of its data types and procedural languages. PostgreSQL has comprehensive SQL support, referential integrity, MVCC or Multi- Version Concurrency Control to avoid unnecessary locking that increases the reliability of the database by logging changes before they are written to the database.

Applications

GRDSS provide a support for spatial data as well as attribute data by integrating GIS, image processing, GPS (global positioning system) and other techniques.

Land cover analysis: This has been done by computing both slope based and distance based vegetation indices as the district had varying extent of vegetation covers. The result of land cover analysis is listed in table 3.

Kolar	Cutoff point	Area in hectares		Area in percentage 17	
		Non-vegetation	Vegetation	Non-vegetation	Vegetation
RATIO	1	444659	379184	53.98	46.03
NDVI	0	418783	401654	51.05	48.96
RVI	1	82824.8	68955.7	54.56	45.43
NRVI	0.99	401647	369692	52.08	47.93
TVI	0.71	444099	379183.2	53.94	46.06
CTVI	0.707	418203	379183.2	52.46	47.55
TTVI	0.73	364415.1	305628	54.39	45.61
PVI	26.00	446960	376808	54.26	45.74
PVI1	7.00	453558	369512	55.10	44.89
PVI2	104	435853	387416	52.95	47.05
PVI3	3850	448812	375025	54.47	45.53
DVI	45	452326	371438	54.91	45.09
AVI	1	468967	354879	56.92	43.08
SAVI	0.02	72405.7	55919.4	56.42	43.58
TSAVI1	0.0199	409483	390422	51.19	48.81
TSAVI2	0.024	453360	370482	55.03	44.97
MSAVI1	0.17	451548	372294	54.81	45.19
MSAVI2	0	444626	355103	55.60	44.41
WDVI	42.01	450160	373627	54.65	45.35

Table 3: Vegetation Indices

Land use analysis: GRDSS through its capability of analyzing the statistical, raster and vector data with options for map overly, map algebra and other operators aid in analyzing the landuse pattern. Both supervised and unsupervised classification approaches were tried to identify landuse categories in the district using Gaussian maximum likelihood classifier (GMLC). The level of accuracy in GMLC was 94.67% compared to unsupervised classifier (78.07%). The composition of land use categories (agriculture, forest, plantation, built-up and wasteland) are listed in the table 4.

Categories	Supervised		Unsupervised	
	Area (in ha)	Area (%)	Area (in ha)	Area (%)
Agriculture	233519	28.34	222416	27.00
Builtup	131468	15.96	70970	8.62
Forest	68300	8.29	85295	10.35
Plantation	70276	8.53	84716	10.28
Waste land	320284	38.88	360450	43.75

Table 4: Land use details of Kolar district

Accuracy Estimation   **T**

Accuracy estimation in terms of producer's accuracy, user's accuracy, overall accuracy and Kappa $\hat{k}$ coefficient were calculated after generating confusion matrix for supervised classification (table 5) and unsupervised classification (table 6).

Classification data	Agriculture	Builtup	Forest	Plantation	Waste land	Row Total
Agriculture	42	1	0	0	0	43
Built up	0	16	0	0	0	16
Forest	0	0	20	3	0	23
Plantation	0	0	2	34	0	36
Waste land	2	0	0	0	30	32
Column Total	44	17	22	37	30	150

Table 5: Error Matrix Resulting from Classifying Training Set Pixels.

Classification data	Agriculture	Builtup	Forest	Plantation	Waste land	Row Total
Agriculture	33	0	0	0	1	34
Built up	0	17	0	0	4	21
Forest	0	0	38	13	0	51
Plantation	0	0	0	28	0	28
Waste land	8	8	5	2	30	53
Column Total	41	25	43	43	35	187

Table 6: Error Matrix for Unsupervised Classification.

The producer's accuracy, user's accuracy corresponding to the various categories and overall accuracy results obtained are summarized in table 7.

Category	Supervised Classification			Unsupervised Classification		
	Producer's Accuracy	User's accuracy (%)	Overall accuracy (%)	Producer's accuracy (%)	User's accuracy (%)	Overall accuracy (%)
Agriculture	95.45	97.67		80.49	97.06	
Builtup	94.11	100.00		68.00	80.95	
Forest	90.90	86.96	94.67	88.37	74.51	78.07
Plantation	91.89	94.44		65.16	100.00	
Waste land	100.00	93.75		85.71	56.60	

Table 7: Producer's accuracy, user's accuracy and overall accuracy.

A $\hat{k}$ value was computed (0.931577) which is as an indication that an observed classification is 93 percent better than one resulting from a chance.

GRDSS was also used to study the watershed status in Kolar district along with land use and land cover analyses. The digital elevation model generated for the district is depicted in figure 6. Draping a land use data on the DEM enabled to assess the status of the catchment of major water bodies. The temporal analysis of Kolar district provided a picture of land use changes. The analysis indicates the unplanned developmental activities without proper planning have lead to the conversion of large scale productive land to waste land (43.75%).

Watershed mismanagement and conversion of waterbodies for various anthropogenic activities (agriculture, buildings, etc.) were the prime reasons for the depletion of the water table along with increasing ecological problems such as salinization, runoff, etc.
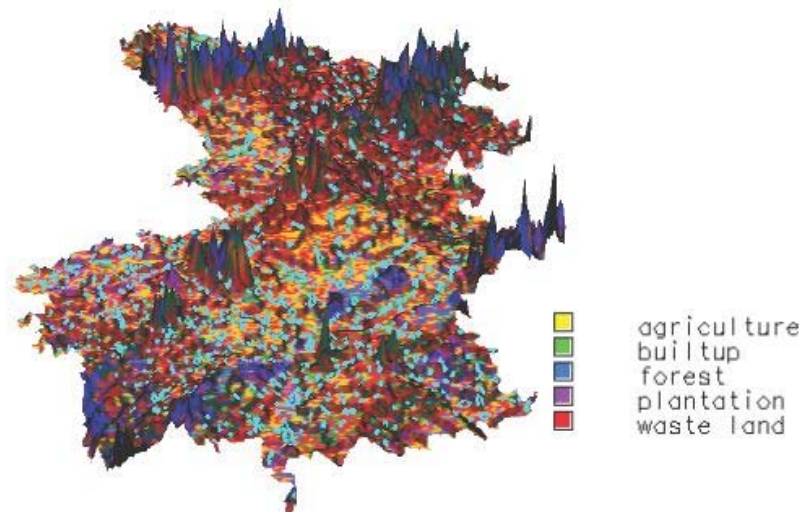
Figure 6: 3d-view of the Kolar district with landuse map draped on the image.

The land cover and land use analyses showed NRVI, CTVI, PVI1 results are comparable to GMLC in terms of percentage area. The assessment of the watershed and holistic approaches in landuse planning considering the actual ground condition could help in ensuring the sustainable development.

Summary

GRDSS a open source GIS with capabilities such as raster analysis, vector analysis, image processing, map algebra and other functionalities is comparable to any commercial software available in the market for various applications including natural resource management. An economical (free ware) with user friendly GUI's, GRDSS is hoped to penetrate in all sections of decision making and contribute to the sustainable development of India.

19   T

References :

1. GRASS official website : http://grass.itc.it
2. GRASS mirror site in India : http://wgbis.ces.iisc.ernet.in/grass/welcome.html
3. GRASS mailing list and mailing list archive : http://wgbis.ces.iisc.ernet.in/grass/support.html
4. GRASS software download page : http://wgbis.ces.iisc.ernet.in/grass/download.html
5. Requirements to compile GRASS GIS :http://wgbis.ces.iisc.ernet.in/grass/grass5/source /REQUIREMENTS.html
6. Mapinfo : http://www.mapinfo.com/location/integration
7. Idrisi : http://www.idrisi.clarku.edu
8. Geomedia : http://www.intergraph.com/dynamicdefault.asp

E-mail | Sahyadri | ENVIS | Energy | GRASS | CES | IISc | E-mail

Home | About Us | Site Map   Subscribe Newsletter | Search Site

Directory

Applications
AudioCast
Careers
Companies
Downloads
Education
Events
GIS Development
Glossary
Guest Book
History
Interviews
News
Policy
Proceedings
Professionals
Publications
Technology
Thesis
Tutorials

Announcement

Page 1 of 1

Engaging Web for better administration

Dr S Narendra Prasad
Senior Principal Scientist, Salim Ali
Centre for Ornithology and Natural
History, Deccan Regional Station,
Hyderabad and Secretary,
OSGeo
snarendra.prasad@gmail.com

Santosh Gaikwad
IT Officer , Salim Ali Centre for
Ornithology and Natural
History
Deccan Regional Station ,
Hyderabad
santosh@osgeo.in

Dr KS Rajan
Associate Professor,
International
Institute of Information
Technology
Hyderabad and Treasurer,
OSGeo
rajan@iiit.ac.in

India has been witnessing tremendous growth, the like of which has not been observed since Independence. The rapid pace of development has impacted practically every aspect of environment and the common man.

It has, therefore, become imperative to put in place effective governance systems with major emphasis on efficiency, accessibility and transparency and at the same time being able to understand the problems and issues faced by the society. Whether it is delivery of proper health care to the citizens, access to safe drinking water, social infrastructure like schools and other quality of life (QoL) concerns of the residents, the knowledge and understanding of geography or 'location' plays an important role in making the right decisions by the respective agencies or departments of the government machinery.

The governance systems, therefore, would require accurate and timely information and data, which is location specific in nature.

A WEB GIS FOR RAJAHMUNDRY

GIS is an indispensable tool to provide a spatial data infrastructure (SDI) for implementing e-governance. A GIS has been developed for the Rajahmundry Parliamentary Constituency, East Godavari district, Andhra Pradesh, which focuses on both the urban and rural regions, integrates data from multiple sources - remote sensing imagery, GPS surveys and field studies - and brings everything together on to an Open Source GIS platform for the development of a Spatial Decision Support System for civil and public administration from a desktop to Web enabled GIS. A Web GIS has been created both in English as well as in the local language, Telugu.

The work is unique in that multiple stakeholders were involved at various stages of development of the GIS. First, Member of Parliament V Aruna Kumar readily saw the possibilities and potential of developing such a system for the benefit of common man and funded the project through the MPLADS scheme.

The collector of East Godavari district, in turn, appreciated the merits of implementing such a project and facilitated its administration and implementation. The OSGeo India chapter endorsed the project and the Salim Ali Centre for Ornithology and Natural History executed the project. M.Sc students of Adi Kavi Nannaya University, Rajahmundry,

Data flow using Google Maps API
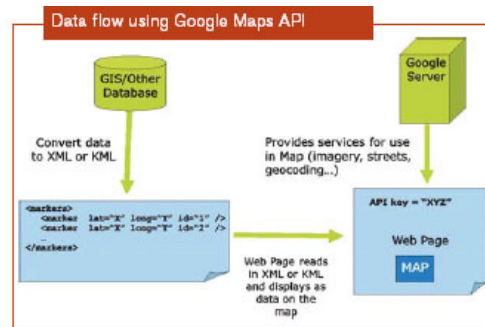
were trained to carry out the project work in part fulfillment of their course requirements.

A PIGGYBACK RIDE ON GOOGLE MAPS APIS

Google Maps provides a highly responsive, intuitive mapping interface with embedded, detailed street and aerial imagery data. Google Maps provides not only the map, satellite image or a hybrid of both but also a range of operations on the map including zooming, panning, information pop-ups and overlays. Google Maps API provides an interface into these operations through JavaScript objects. The GIS application for Rajahmundry parliamentary constituency has been developed using Google Maps API.

A spatial database was developed for it in PostgreSQL/ PostGIS database. The advan- GIS DEVELOPMENT 50 Open Source Engaging Web for better administration DECEMB E R 200 8 Data flow using Google Maps API tage of creating spatial database for Rajahmundry was having all the data in a central database including well defined privileges which makes it possible to extend the more standard SQL queries with spatial queries.

Search

Google [ ] Go

DATASETS USED FOR RAJAHMUNDRY PARLIAMENTARY CONSTITUENCY

21

The following shape files were used while developing the spatial database for Rajahmundry Parliamentary Constituency.

Point data

Bank and ATM centres, cemeteries, bus stations, police stations, places of worship, cinema halls, clubs, commercial complexes, community centres, customer care centres, e-Seva centres, educational centres , electric sub-stations.

Polygon data

Rajahmundry parliamentary constituency

Figure 1
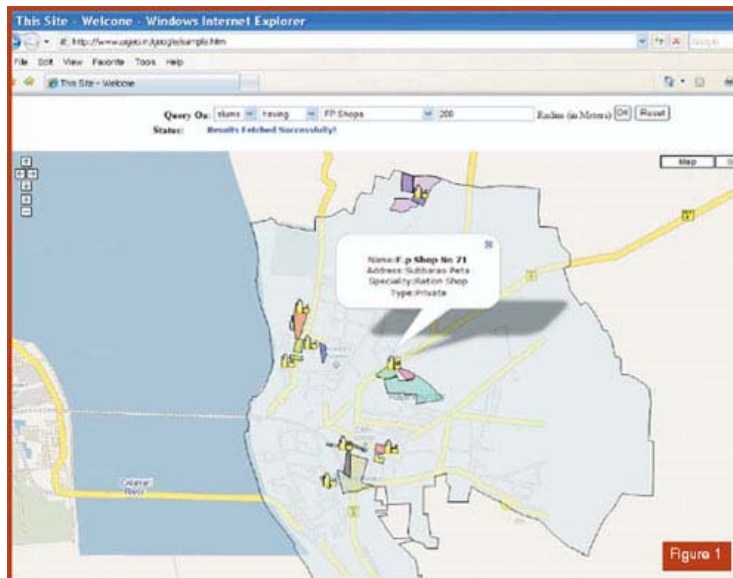
boundary, slums in Rajahmundry parliamentary constituency.

Steps involved in developing the Web-GIS application

The following are prerequisites that ensured the development of Web-GIS application for Rajahmundry parliamentary constituency.

• An Apache Web server running PHP and PostgreSQL/PostGIS
• Spatial data in PostGIS database for Rajahmundry.
• Populating the spatial data into Post- GIS database
• Outputting XML with PHP
• Generating HTML page for map visualisation

The URL for Rajahmundry parliamentary constituency Web-GIS application is http://www.osgeo.in/google /sample. htm. The interface which was developed for Rajahmundry Parliamentary Constituency Web-GIS application allows users to query against spatial data available in the PostgreSQL/Post- GIS database.

FEATURES

• Intuitive user interface for querying the spatial data

General public is familiar with Google Maps interface and its basic navigation. In this, we added a simple query tool. In Figure 1, the results have been showed by the query slums having fair price (FP) shops within the radius of 100 meters. A user can click on the FP shops marker icons which will pop up an info window to show the information about the particular FP shop. User can even

Advantages

• Free (except for developer time)
• Quick development time - depending on complexity of application
• End product is light weight application, client side scripting
• Intuitive user interface - general public already familiar with Google Maps interface and basic navigation
• Fast, good response time
• Google provides solid background services (satellite data, roads, traffic data, street view, geocoding)
• Effective for displaying selected GIS data - not every mapping application requires multiple, complex map layers
• Great on-line resources for learning, multitude of samples and tutorials
• Best for focussed applications
• Best for small municipalities, companies (not huge datasets)

Limitations

• Limited functionality compared to some commercial products
• Difficult to overlay more complex GIS data
• Difficult to overlay multiple GIS layers

• Cannot read directly from GIS database, must convert to other formats (XML, KML) (but parts of process can be automated with scripting)

22

Figure 2
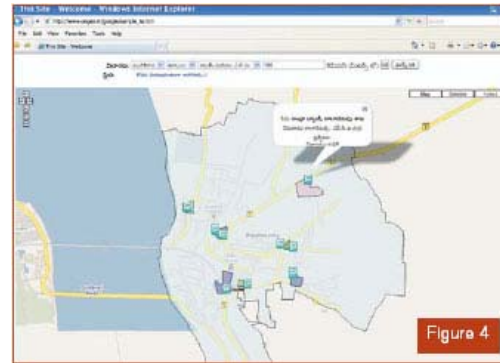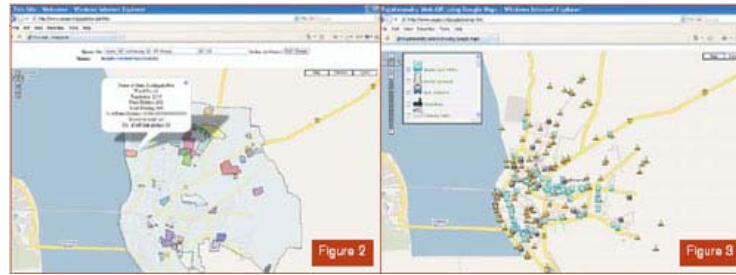
Figure 3

Figure 4

get the information about slums by clicking on slums polygon. The interface allows the user to query slums not having FP shops within the radius of 100 meters to know which slums don't have the FP shops nearby. Figure 2 shows the result for the query slums not having FP shops within the radius of 100 meters.

• Light weight Web-GIS application
This application gets loaded faster on the browser and even the querying time is less. Results too get displayed faster.

• Google provides background data such as satellite data, roads etc.

• This application is useful for common public, policy makers, decision makers, government officials etc.

A simple Web- GIS application showing point of interests in the Rajahmundry parliamentary constituency was developed to get the information about point of interests such as parks and gardens, Banks and ATM centres, Police stations etc (Figure 3). Following the URL for it http:// www.osgeo.in/google. overlay. htm. In this application, point of interests can be overlaid by checking the respective point of interest check boxes.

The Rajahmundry parliamentary constituency Web-GIS is also available in the regional language Telugu (Figure 4). Following the URL for Telugu version of Rajahmundry parliamentary constituency Web-GIS application http:// www.osgeo.in/google/sample_ te.htm http://www.osgeo.in/ google /overlay_te.htm.

The Indic IME for Telugu software from www.bhashaindia. com was used to type the data in Telugu. The PostgreSQL database was encoded to UTF-8 and then the data was loaded into PostgreSQL database.

THE WAY FORWARD

We increasingly see the use of Open Source tools by a large number of stakeholders in virtually all thematic areas of concern. Combined with the power of the use of Indic languages as a preferred medium, the Web GIS will emerge as one of the most potent tools for societal benefit.

ACKNOWLEDGEMENTS

Page 1 of 1

Land Surface Temperature with Land Cover Dynamics: Multi-Resolution, Spatio-Temporal Data Analysis of Greater Bangalore

Ramachandra, T. V.,[1] and Uttam, K.,[2]
[1]Energy and Wetlands Research Group, Centre for Ecological Sciences & Centre for Infrastructure, Sustainable Transportation and Urban Planning [CiSTUP], Indian Institute of Science, Bangalore – 560 012 India, E-mail: cestvr@ces.iisc.ernet.in, energy@ces.iisc.ernet.in
[2]Centre for Sustainable Technologies, Department of Management Studies, Indian Institute of Science

Abstract

Bangalore is experiencing unprecedented urbanisation in recent times due to concentrated developmental activities with impetus on IT (Information Technology) and BT (Biotechnology) sectors. The concentrated developmental activities has resulted in the increase in population and consequent pressure on infrastructure, natural resources, ultimately giving rise to a plethora of serious challenges such as urban flooding, climate change, etc. One of the perceived impact at local levels is the increase in sensible heat flux from the land surface to the atmosphere, which is also referred as heat island effect. In this communication, we report the changes in land surface temperature (LST) with respect to land cover changes during 1973 to 2007. A novel technique combining the information from sub-pixel class proportions with information from classified image (using signatures of the respective classes collected from the ground) has been used to achieve more reliable classification. The analysis showed positive correlation with the increase in paved surfaces and LST. 466% increase in paved surfaces (buildings, roads, etc.) has lead to the increase in LST by about 2 ℃ during the last 2 decades, confirming urban heat island phenomenon. LSTs' were relatively lower (~ 4 to 7 ℃) at land uses such as vegetation (parks/forests) and water bodies which act as heat sinks.

1. Introduction

Many cities in developing countries are now undergoing rapid urbanisation evident from the increase in urban population from 13% (220 million) in 1900, to 29% (732 million) in 1950, to 49% (3.2 billion) in 2005 and is projected to rise to 60% (4.9 billion) by 2030 (WUP, 2005). Accurate and timely information in land use (LU) and LU changes is crucial for long-term economic development planning and also for short-term land management. Increase in paved land covers (LC) consequent to the concentrated human activities often leads to increased land surface temperatures (LST). Enhanced LST in certain urban pockets compared to its immediate surroundings consequent to the increase in paved surfaces is known as urban heat island (UHI) phenomenon (Landsbeg, 1981). Specifically, surface and atmospheric temperatures are increased by anthropogenic heat discharge due to energy consumption, increased land surface coverage by artificial materials having high heat capacities and conductivities, and the associated decreases in vegetation and water impervious surfaces, which reduce surface temperature through evapotranspiration (Kato and Yamaguchi, 2005). Temperatures have been monitored through space borne remote sensing (RS) sensors, which measure top of the atmosphere (TOA) radiances in the Thermal Infrared (TIR) region. TOA radiance is the net result of emitted radiance from the Earth's surface, upwelling radiance from the atmosphere, and downwelling radiance from the sky. Brightness temperatures (also known as blackbody temperatures) can be derived from the TOA radiance (Dash et al., 2002). These brightness temperatures are further corrected with spectral emissivity values prior to the computation of LST to account for the roughness properties of the land surface, the amount and nature of vegetation cover, and the thermal properties and moisture content of the soil (Friedl, 2002). However, lack of knowledge of emissivity can introduce an error ranging from 0.2 to 1.2 K for mid-latitude summers and from 0.8 to 1.4 K for the winter conditions for an emissivity of 0.98 and at the ground height of 0 km (Dash et al., 2002). Two approaches have been developed to recover LST from multispectral TIR imagery (Schmugge et al., 1998). The first approach utilises a radiative transfer equation to correct the at-sensor radiance to surface radiance, followed by an emissivity model to separate the surface radiance

into temperature and emissivity (Friedl, 2002). The second approach applies the split-window technique for sea surfaces to land surfaces, assuming that the emissivity in the channels used for the split window is similar (Dash et al., 2002). TIR region corresponding to 8 -14 μm in the electromagnetic spectrum is being used in quantifying the thermal urban environment (as per Wien's displacement law) as well as mapping heat islands in the urban areas. Currently available RS data pertaining to visible, near infrared (NIR) and thermal range in different spatial resolution and temporal coverage are used for LU/LC classification and LST estimations. Spatial resolution of the data plays an important role in classification scheme and studies have been carried out to understand the role of various resolutions for LU classification. Multi-sensor RS data were analysed for terrain cover classification over the Greater Sydney region by Forghani et al., (2007). National terrain surface roughness was generated, using MODIS (Level 1-areas with no major towns), Landsat/ASTER/SPOT 2/4 (Level 2-areas with major towns), SPOT-5 (Level 3-areas with capital/major cities), and IKONOS/QuickBird (Level 4-areas containing significant critical infrastructure). The study highlights that Landsat TM/ETM+ imagery is suited for derivation of 30 m and 100 m resolution terrain maps. UHI was investigated earlier through LST measurements using NOAA AVHRR data (Li et al., 2004, Balling and Brazell, 1988, Gallo et al., 1993, Gallo and Owen, 1998 and Kidder and Wu, 1987), TM TIR data (Carnahan and Larson, 1990), Landsat TM data (Tanaka et al., 2005), ASTER and ETM+ data (Kato and Yamaguchi, 2005), Landsat-5 TM and Landsat-7 ETM+ data (Nikolakopoulos et al., 2003, Stathopoulou and Cartalis, 2007 and Weng et al., 2004), Corine LC with Landsat ETM+ data (Stathopoulou and Cartalis, 2007). However, there are no studies to understand the LST with LU dynamics in a rapidly urbanising region such as Greater Bangalore. Hence, the objective of this study is to investigate the LST with LU dynamics to understand the urban heat island phenomenon in Greater Bangalore considering multi - senor, multi - resolution and temporal RS data acquired through space borne sensors. This involved:

i) Temporal LU change analysis (during 1973 to 2007);
ii) Computation of LST and NDVI (Normalized Difference Vegetation Index) from Landsat TM (1992) and MODIS data (2000 and 2007) of summer month;
iii) Investigation of the role of NDVI in LST;
iv) Deriving sub-pixel proportion of LU using linear mixture model (LMM) on bands of ETM+

(excluding thermal and panchromatic) and investigate its relationship with LST;
v) Deriving improved supervised classified LC map through Bayesian classifier using abundance values obtained from LMM as a prior probability along with information from classified map obtained using spectral signatures (training polygons).

2. Data and Methods
2.1Data
Data used in the study are Landsat MSS (1973), TM (1992), IRS LISS-III MSS (1999), Landsat ETM+ (2000), IRS LISS-III (2006), MODIS 7 bands reflectance product (2002, 2007), MODIS Land Surface Temperature/Emissivity (V004 and V005): 8-Day, L3 Global 1km products (2000, 2007) and Google Earth (http://earth.google.com).

2.2 Study Area
Greater Bangalore is the principal administrative, cultural, commercial, industrial, and knowledge capital of the state of Karnataka with an area of 741 km^2 and lies between the latitudes 12°39′00″ to 13°3′00″ N and longitude 77°22′00″ to 77°52′00″ E. Bangalore city administrative jurisdiction was widened in 2006 by merging the existing area of Bangalore city spatial limits with 8 neighboring Urban Local Bodies (ULBs) and 111 Villages of Bangalore Urban District. Thus, Bangalore has grown spatially more than ten times since 1949 (69 km^2). Now, Bangalore (Figure 1) is the fifth largest metropolis in India currently with a population of about 7 million (Ramachandra and Kumar, 2008).

Figure 1: Study area – Greater Bangalore, India

2.3 Methods
2.3.1 Land use analysis
This was done with Landsat data of 1973 (79 m spatial resolution), 1992 and 2000 (30 m), IRS

LISS-III data of 1999 and 2006 (23.5 m) and MODIS data of 2002 and 2007 (250 m to 500 m spatial resolution) using supervised pattern classifiers based on Gaussian maximum likelihood (GML) estimation followed by a Bayesian statistical approach. This technique quantifies the tradeoffs between various classification decisions using probability and costs that accompany such decisions (Duda et al., 2000). It makes assumptions that the decision problem is posed in probabilistic terms, and that all of the relevant probability values are known with a number of design samples or training data collected from field that are particular representatives of the patterns to be classified. The mean and covariance are computed using maximum likelihood estimation with the best estimates that maximises the probability of the pixels falling into one of the classes. LU analysis considering temporal data (1973, 1992, 1999, 2000, 2002, 2006 and 2007) was done using the open source programs (i.gensig, i.class and i.maxlik) of Geographic Resources Analysis Support System (http://wgbis.ces.iisc.ernet.in/grass).

2.3.2 Change detection
LU change detection is performed by change/no-change recognition followed by boundary delineation on images of two different time periods. Pixels which show significant changes are checked and validated on the ground and the boundaries of the changed patches are category wise delineated. This is supplemented with visual interpretation and online digitisation. Many LU change detection techniques have been developed, but no single algorithm is suitable for all cases (Lu et al., 2004), as the implementation of change detection analysis is dependent on the data itself (Zhang and Zhang, 2007). Bi-temporal multispectral images have been analysed to understand LU dynamics through:

- **Principal Component Analysis** (PCA) – PCA has been an effective tool for change detection (Fung and LeDrew, 1987 and Michener and Houhoulis, 1997). Major components of the time two (t_2) data are subtracted from the corresponding components of the time one (t_1) data to obtain differences related to changes in LU. This method provides a better result than simple image differencing when the radiometric differences between the two images are too large due to different imaging circumstances and cannot be effectively dealt with by the radiometric normalisation process (Zhang and Zhang, 2007). Landsat MSS (1973) and IRS LISS-III (2006) scenes having different radiometry were used with PCA to understand the overall changes across a period of 33 years.

- **Tasseled Cap** (TC) or Kauth-Thomas (KT) transformation – Here, multi-temporal TM and ETM+ data are transformed into the brightness-greenness-wetness space, then changed areas are generated by differencing the brightness (ΔB) and greenness (ΔG) values (Kauth and Thomas, 1976). Changes in brightness (ΔB) are associated with most LU changes, especially constructed related changes. TC results can be physically interpreted as its coefficients are predetermined and independent of each image scene, while PCA coefficients are not. However, for the purpose of simply detecting change/no-change areas, PCA is better than TC in many cases, although the physical interpretation is difficult. TC transformations were performed on Landsat TM (1992) and ETM+ (2000) data.

- **Image Differencing** (ID) – ID is effective for identifying LU changes from visible and NIR band pairs acquired in similar circumstances (imaging conditions) using same sensor over two different time periods (Macleod and Congalton, 1998). IRS LISS-III (1999 and 2006) data used to visualise the LU changes through ID.

2.3.3 Derivation of LST from Landsat TM and Landsat ETM+
LST were computed (Weng et al., 2004) from TIR bands (Landsat TM and ETM+). Emissivity correction for the specified LC is carried out using surface emissivities as per Synder et al., (1998); Stathopoplou et al., (2007) and Landsat 7 science data user's handbook (2008). The emmissivity corrected land surface temperature (Ts) are computed as per Artis and Carnahan (1982)

$$T_s = \frac{T_B}{1 + (\lambda \times T_B / \rho) \ln \varepsilon}$$

Equation 1

Where, λ is the wavelength of emitted radiance for which the peak response and the average of the limiting wavelengths (λ = 11.5 μm) (Markham and Barker, 1985) were used, ρ = h x c/σ (1.438 x 10^{-2} mK), σ = Stefan Bolzmann's constant (5.67 x 10^{-8} Wm^{-2}K^{-4} = 1.38 x 10^{-23} J/K), h = Planck's constant (6.626 x 10^{-34} Jsec), c = velocity of light (2.998 x 10^8 m/sec), and ε is spectral emissivity.

2.3.4 LST from MODIS
MODIS LST/Emissivity 16-bit unsigned integer data with 1 km spatial resolution are multiplied by a scale factor of 0.02 (http://lpdaac.usgs.gov/modis-/dataproducts.asp#mod11) and are converted to degree Celsius.

International Journal of Geoinformatics, Vol 5, No. 3, September, 2009

45

Land Surface Temperature with Land Cover Dynamics: Multi-Resolution, Spatio-Temporal Data Analysis of Greater Bangalore 43-53

2.3.5 NDVI from Landsat TM, ETM+ and MODIS

NDVI was computed using visible Red (0.63 – 0.69 μm) and NIR (0.76 – 0.90 μm) bands of Landsat TM (1992)/ETM+ (2000) and Red (0.62 – 0.68 microns) and NIR (0.77 – 0.86 microns) bands of LISS-III data of 2006.

2.3.6 Estimation of abundance maps

Linear unmixing method was adopted for solving the mixed pixel problem as the spectral radiance measured by a sensor consists of the mixture of radiances reflected in proportion to the sub-pixel area covered (Kumar et al., 2008). Endmembers corresponding to pure pixels are given by the reference spectra of each of the individual pure materials. Spectra corresponding to sub-pixel areas in a pixel are assumed to be linearly independent, and the target pixel spectra are a combination of these spectra (which is proportional to respective LC in a pixel). The spectrum measured by a sensor is a linear combination of the spectra, therefore,

$$y_i = \sum_{j=1}^{n} (a_{ij} x_j) + e_i$$

Equation 2

where n = the number of distinct LU classes; y_i = Spectral reflectance of respective pixels in a band; a_{ij} = Spectral reflectance of the jth component in the pixel for i^{th} spectral band; x_j = Proportion value of the jth component in the pixel; j = 1, 2, 3 ... n (number of land classes assumed); i = 1, 2, 3 ... m (number of multispectral bands) and e_i = error term for the ith spectral band. The error term (e_i) is due to the assumption made that the response of each pixel in any spectral wavelength is a linear combination of the proportional responses of each component. Assuming that the error term is 0, equation 2 can be written as:

$$AX=Y$$

Equation 3

where A is a m x n matrix (a_{11}, a_{12}, …, a_{mn}), X is a n x 1 vector (x_1, x_2, …, x_n) and Y is a n x 1 vector (y_1, y_2, …, y_n) written as:

$$\begin{bmatrix} a_{11} & a_{12} & ... & a_{1n} \\ a_{21} & a_{22} & ... & a_{2n} \\ \vdots & \vdots & \vdots & \vdots \\ a_{m1} & a_{m2} & ... & a_{mn} \end{bmatrix} \begin{bmatrix} x_1 \\ x_2 \\ \vdots \\ x_n \end{bmatrix} = \begin{bmatrix} y_1 \\ y_2 \\ \vdots \\ y_n \end{bmatrix}$$

Equation 4

$$X_{constrained} = (A^T A)^{-1} A^T Y + \frac{(1 - 1^T ((A^T A)^{-1} A^T Y))}{1^T (A^T A)^{-1}} (A^T A)^{-1} 1$$

Equation 5

Equation 5 gives the Constrained Least Squares (CLS) estimate of the abundance expressed in terms of matrix A, X and Y. The reflected spectrum of a pure feature is called a reference or endmember spectrum. Endmembers are extracted using scatter plot or through automatic endmember extraction techniques (Kumar et al., 2008).

2.3.7 LC derivation from abundance values along with training polygons using Bayesian classification

Abundances of each category (pixel wise) are used as a prior probability of the class. In the Baye's classifier for the multispectral data, the posterior probability of the class given the observation is computed by multiplying the prior probability of the class with the conditional probability P(x|k), where x denotes the multispectral observation vector and k any class. The class label assigned to the pixel is:

$$l = \arg \min_k \frac{P(k \,|\, i, j) P(x \,|\, k)}{P(x)}$$

Equation 6

3. Results

Temporal LU details are displayed in figure 2 and class statistics are listed in table 1. The classified images of 1973, 1992, 1999, 2000, 2002, 2006 and 2007 showed an overall accuracy of 72%, 75%, 71%, 77%, 60%, 73% and 55%. Accuracy assessment was performed which showed higher accuracy for high resolution data (~ 70-75% for Landsat and IRS LISS-III) and decreasing accuracy with coarse spatial resolution (~ 55-60% for MODIS). Figure 3 (a) – (f) depicts the LU change based on differencing techniques of PCA and TC. The disappearance of water bodies from 1973 to 2006 is given in Figure 4. 55% decline (from 207 to 93) in the number of water bodies and 61% decline in the spatial extent (of water bodies) is noticed from the temporal analysis. Validation was done considering training data and Google Earth image, covering approximately 15% of the study area. Then, pixels corresponding to urban category were extracted for further analysis. Figure 5 shows the LST and NDVI of Greater Bangalore in 1992, 2000 and 2007. The minimum (min) and maximum (max) temperature was 12 °C and 21 °C with a mean of 16.5±2.5 from Landsat TM (1992, winter). Similarly MODIS data of 2000 (summer) show the min, max and mean temperature of 20.23, 28.29 and 23.71±1.26 °C respectively. Corresponding values for 2007 (summer) are 23.79, 34.29 with a mean of 28.86±1.60 °C. LC wise NDVI and LST are listed in table 2.
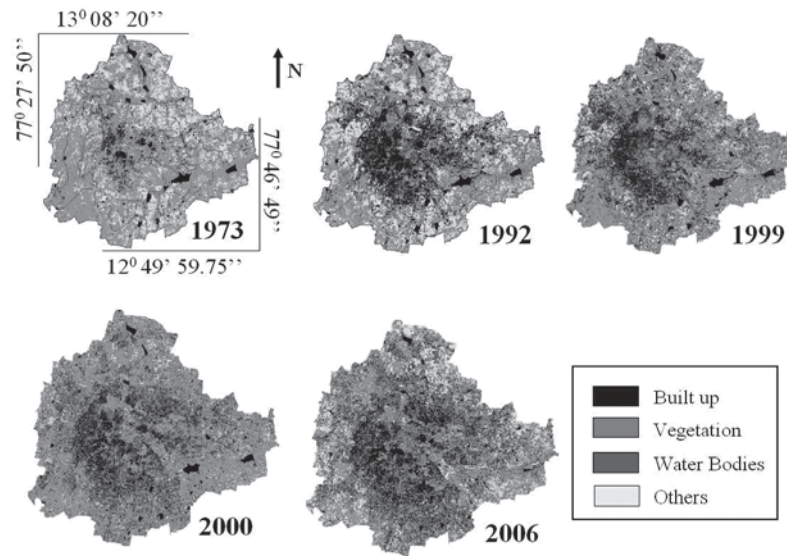
Figure 2: Greater Bangalore in 1973, 1992, 1999, 2000 and 2006
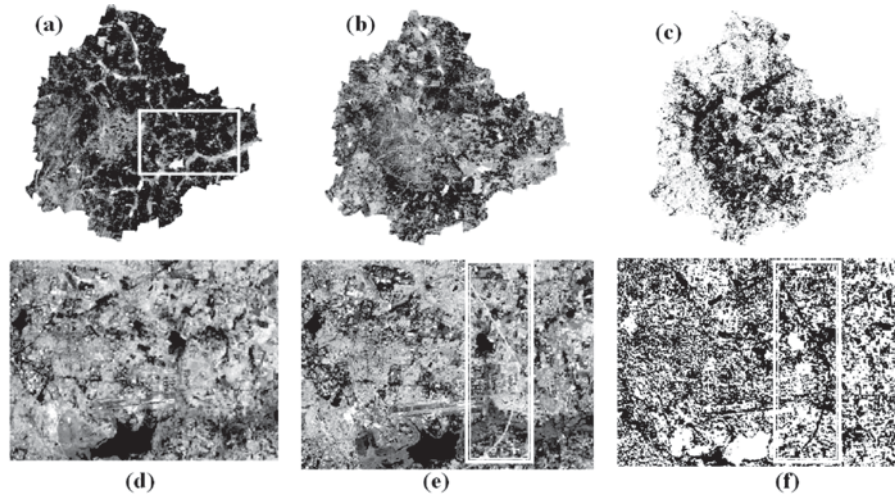
Figure 3: PC1 of Landsat MSS-1973 (a), PC1 of IRS LISS-III-2006 (b) and the change in LU is highlighted in (c) using PCA differencing methods. The highlighted box in (a) and (b) are further enlarged in (d) to (f). Brightness values from TC transformation on Landsat TM-1992 (d) and ETM+2000 (e). The changes are highlighted in (f) by differencing the brightness values emphasizing new built up

Table 1: Greater Bangalore land cover statistics

Class → Year ↓		Built up	Vegetation	Water Bodies	Others
1973	Ha	5448	46639	2324	13903
	%	7.97	68.27	3.40	20.35
1992	Ha	18650	31579	1790	16303
	%	27.30	46.22	2.60	23.86
1999	Ha	23532	31421	1574	11794
	%	34.44	45.99	2.30	17.26
2000	Ha	24163	31272	1542	11346
	%	35.37	45.77	2.26	16.61
2002	Ha	26992	28959	1218	11153
	%	39.51	42.39	1.80	16.32
2006	Ha	29535	19696	1073	18017
	%	43.23	28.83	1.57	26.37
2007	Ha	30876	17298	1005	19143
	%	45.19	25.32	1.47	28.01
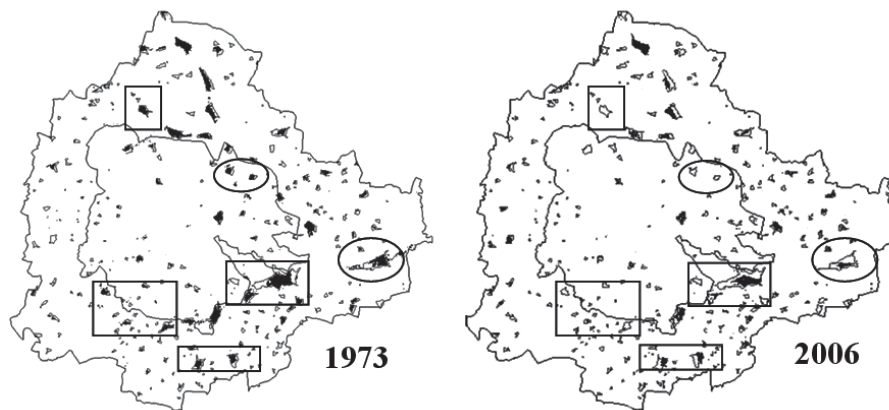
Figure 4: Temporal changes in water bodies from 1973 (using Landsat MSS) to 2006 (using IRS LISS-III) highlighted in rectangular boxes and circles.
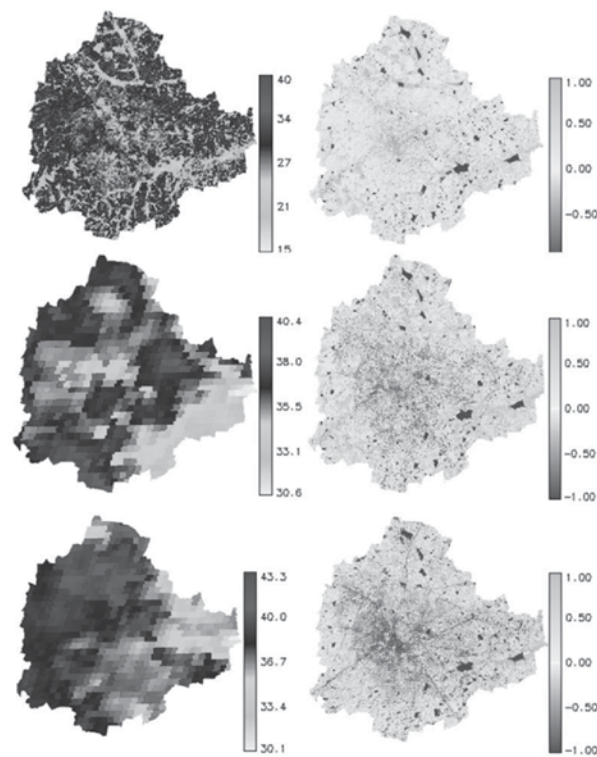
Figure 5: LST from Landsat TM (1992), MODIS (2000 and 2007), NDVI from Landsat TM (1992), Landsat ETM+ (2000) and IRS LISS-III (2006)

Table 2: NDVI and LST (°C) for respective land uses

Land cover	1992 (TM)		2000 (MODIS)		2007 (MODIS)	
	Mean LST (SD)	Mean NDVI (SD)	Mean LST (SD)	Mean NDVI (SD)	Mean LST (SD)	Mean NDVI (SD)
Builtup	19.03 (1.47)	-0.162 (0.096)	26.57 (1.25)	-0.614 (0.359)	31.24 (2.21)	-0.607 (0.261)
Vegetation	15.51 (1.05)	0.467 (0.201)	22.21 (1.49)	0.626 (0.27)	25.29 (0.44)	0.348 (0.42)
Water bodies	12.82 (0.62)	-0.954 (0.055)	21.27 (1.03)	-0.881 (0.045)	24.00 (0.27)	-0. 81 (0.27)
Open ground	17.66 (2.46)	-0.106 (0.281)	24.73 (1.56)	-0.016 (0.283)	28.85 (1.54)	-0.097 (0.18)

The relationship between LST and NDVI were investigated for each LC type through the Pearson's correlation coefficient (CC) at a pixel level, which are listed in table 3. It is apparent that values tend to negatively correlate with NDVI for all LC types. NDVI values ranges from -0.05 to -0.6 (built up) and 0.15 to 0.6 (vegetation). Temporal increase in temperature with the increase in the number of urban pixels is noticed during 1992 to 2007 (63%) and 'r' confirms this relationship for the respective years. The decrease in vegetation is reflected by the respective increase in temperature. Further analysis is done by considering vegetation abundance. Landsat ETM+ (band 1, 2, 3, 4, 5 and 7) were unmixed to get the abundance maps of 5 classes (1) dense urban (commercial/industrial/residential), (2) mixed urban (urban with vegetation and open ground), (3) vegetation, (4) open ground and (5) water bodies. We considered only dense urban, mixed urban and vegetation abundance for further

analysis as shown in figure 6. The min and max temperature from ETM+ data was 13.49 and 26.32 °C with a mean of 21.75±2.3. These abundance images were further analysed to see their contribution to the UHI by separating the pixels that contains 0-20%, 20-40%, 40-60%, 60-80% and 80-100% of the commercial/industrial/residential (dense urban), mixed urban and vegetation. Table 4 gives the mean and standard deviation (SD) of the LST for various LU. Application of decision based unmixing approach, systematically exploited the information from both the sources (sub-pixel class proportions and classified image based on training data collected from the ground) for achieving more reliable classification, shown in figure 7. Table 5 lists LC wise LST, NDVI and correlation coefficient. Relationship of population density with LST (Landsat ETM+) is evident in figure 8, which corroborate that the increase in LST is due to urbanisation and consequent increase in population.
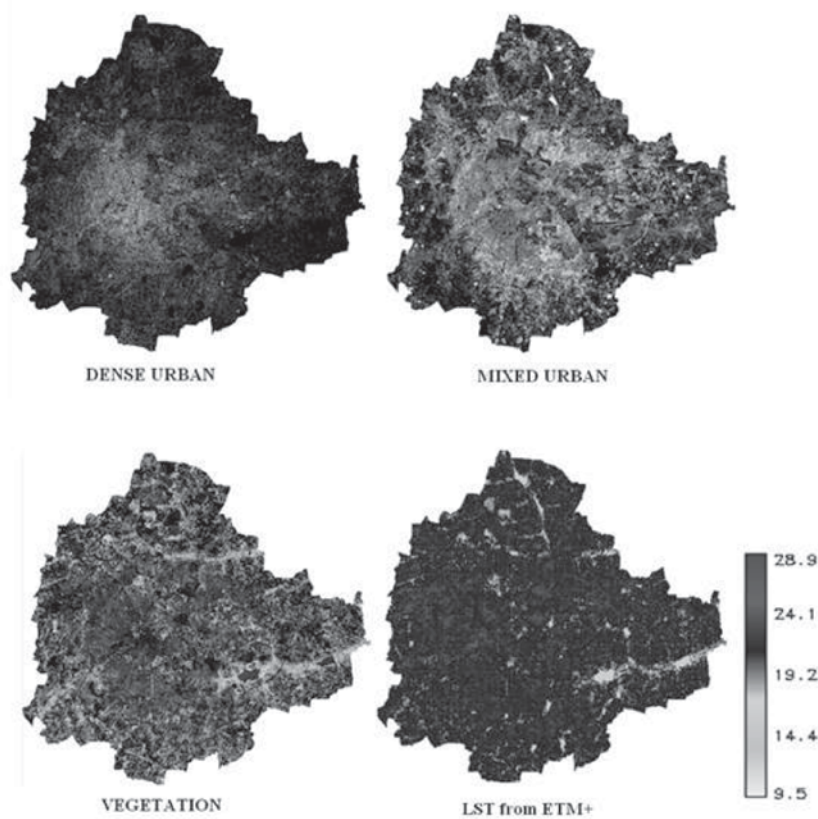
Figure 6: Abundance maps and LST obtained from Landsat ETM+ data (2000)

Table 3: Correlation coefficients between LST and NDVI by LC type (significant at 0.05 level)

LU	1992	2000	2007
Builtup	-0.7188	-0.7745	-0.7900
Vegetation	-0.8720	-0.6211	-0.6071
Open ground	-0.6817	-0.5837	-0.6004
Water bodies	-0.4152	-0.4182	-0.4999

Table 4: Mean LST for different LC classes for various abundances

Class → Abundance ↓	Mean Temperature ± SD of dense urban	Mean Temperature± SD of mixed urban	Mean Temperature± SD of vegetation
0-20%	21.99±2.37	21.57±2.36	17.91±2.19
20-40%	22.06±2.15	21.58±2.36	17.39±1.37
40-60%	22.27±2.00	21.67±2.41	17.22±0.89
60-80%	22.33±2.22	22.28±2.02	17.13±0.85
80-100%	22.47±1.96	22.37±2.17	17.12±0.91
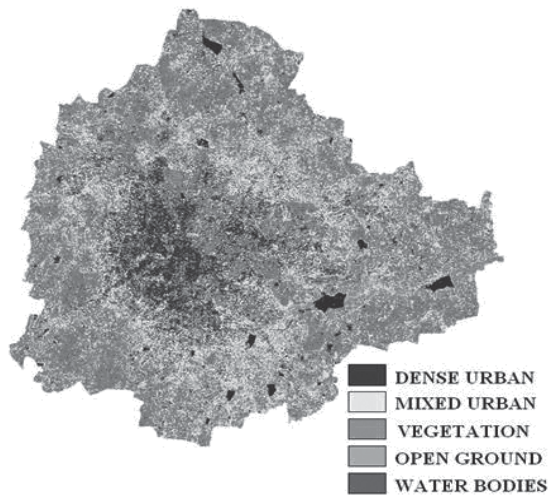
Figure 7: Classified image obtained from combining unmixed images and classified image using spectral signatures from ground as input to Baye's classifier from 6 MSS bands of Landsat ETM+
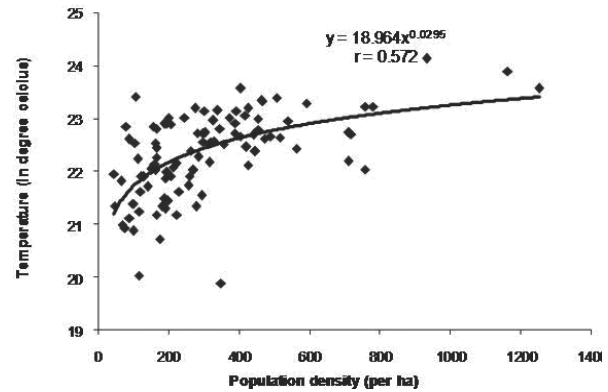
Figure 8: LST with ward wise population density

Table 5: LST, NDVI and correlation coefficient for different LC classes

Landuse	LST Mean ± SD	NDVI Mean ±SD	Correlation coefficient between LST and NDVI
Dense builtup	23.09± 1.16	-0.2904± 0.395	-0.7771
Mixed builtup	22.14± 1.06	-0.138± 0.539	-0.6834
Vegetation	19.27± 1.59	0.3969± 0.404	-0.8500
Open Ground	22.40± 1.97	-0.0193± 0.164	-0.6319
Water Bodies	19.57± 1.72	-0.301± 0.47	0.2319

Table 6: MMU sizes for different RS data sources used

Data source	MODIS	Landsat MSS	Landsat TM/ETM+	IRS LISS-III
MMU (ha)	6.25	0.62	0.09	0.055

4. Discussion

The analysis showed that there has been a 466% increase in built up area from 1973 to 2007 as evident from temporal analysis leading to a sharp decline of 61% area in water bodies. LU changes were more prominent in the city during the last 2 decades consequent to rapid urbanisation accompanied with urban sprawl with IT (Information Technology) and BT (Biotechnology) boom and consequent migration of people from different regions. Identification of the changed patches or specific region that underwent changes (from one LU to other) is not easily achievable in a highly dynamic and large urbanising environment considering the varying range of spatial resolutions (23.5 to 250 m) across time (1973 to 2007). This requires the development and maintenance of database for each LU across a large time-scale (Zhang and Zhang, 2007).

A newly constructed flyover or road (for example see a new road in Figure 3 (e) running from south to north highlighted in a rectangular box in the second half of the image), was detected as a broken line in figure 3 (f) due to shadow or getting merged with other classes (mixed pixels), etc. This was obtained by differencing TC transformed 92 and 2000 brightness values and the changed patches were identified using Region Growing Method (RGM) along with thresholding. The exact delineation of the boundary for every recognised change patch also depends on the minimum mapping unit (MMU) and its proper selection (Zhang and Zhang, 2007). Large MMU changes result in significant differences in the accuracy estimates of LC classification. They make change detection more accurate but often miss real and small LU changes. A small MMU present detailed LU changes but also increase the uncertainty of the RS derived change product. MMU for various pixel sizes are listed in table 6. The minimum built up size in residential areas is ~ 0.011 ha to 0.037 ha and often extend up to 1 ha (in case of multi-storied buildings) while industrial buildings can spread from 50 to 150 ha approximately. One way to delineate such features is to perform interactive on-screen editing along with visual interpretation in a synergistic way. MODIS and Landsat MSS present significant challenge due to mixed pixel problems. Landsat TM/ETM+ and IRS LISS-III are adequate for detecting pixel patch changes, yet most of the objects fall on boundaries of two adjacent pixels and they are smaller than the MMU size (form mixed pixels). Hence, these data tend to overestimate the LU classes. The area derived from RS data is closer to the area on the ground when patch size increases. However, area measurements from high spatial resolution were more accurate. The correlation (r) between NDVI and temperature of 1992 (based on TM data) was 0.88. Similarly for 2000, r was 0.72 (MODIS 2000) and 0.65 (MODIS 2007) respectively. Analysis of LST with NDVI suggests that the extent of LC with vegetation plays a significant role in the regional LST. Although many factors can contribute to the variations of LST, the spatial arrangement and aerial extent of various LU types is a fundamental one. Within the city, if we consider the LU nature, then we see that temperature falls from densely builtup area to medium builtup area and again from medium builtup to vegetative land. The temperature close to vegetation and wetlands were lower by 4 and 5-7 ºC respectively (see table 2). This highlights that LU characteristics play a significant role in maintaining the ambient temperature and also in the regional heat island phenomenon. Vegetation and water

bodies are negatively correlated with temperature suggesting that these LU aid as heat sinks and hence maintains salubrious regional climate. Accuracy of the unmixing decision based approach considering information from sub-pixel class proportions and classified map obtained using training data was 85.46%. This approach is apt for fusing the information obtained from multi-sensors (such as MODIS and IRS). MODIS based sub-pixel information obtained from one of the unmixing techniques can be fused with IRS LISS-III MSS classified information. The endmembers for MODIS data unmixing can be extracted from the image itself (Kumar et al., 2008), while IRS LISS-III MSS classification is done with the training data. This technique would be helpful in optimising the benefits of higher spectral and spatial resolutions of multi-sensors. Certain areas in the city with sparsely located building having parks and lakes in the surroundings have lower air temperature compared to completely urbanised regions. UHI is evident with the enhanced surface temperatures in urbanised landscapes compared to their surroundings (non-urbanised). Temperature profile with respect to human population density is depicted in figure 8, suggesting that dense urban areas have higher temperatures. When the population of a region exceeds its carrying capacity, it exerts pressure on the local natural resources (land, water, etc.). Correlations among LST and NDVI are the result of unique signatures of the biophysical parameters due to interactions between thermal and vegetation dynamics in each LU.

5. Conclusion
This study analysed the role of increased urbanisation through spatial change analysis on LST, which is positively correlated with urbanising landscapes and negatively correlated with vegetation and water bodies. Abundance maps with pixels having 80-100% dense builtup and mixed builtup class proportions show increase in urban temperature by an average of 2 °C. LST were comparatively lower in areas having parks, healthy vegetation and lakes that aid as heat sinks. Although the algorithms adopted here seems to work satisfactorily, the classification and change detection methods in use were not very suitable for handling multi-sensor, multi-resolution condition as the classification accuracies obtained from MODIS data were low. These require advanced image fusion and LU classification algorithms or machine learning techniques to be adopted to achieve higher classification accuracies. The unmixing decision based approach adopted in this paper is an attempt to achieve classification results with higher

accuracies per class. This could be automated to obtain LU classes and bring out changes across multi-temporal data routinely. Methods of change detection from multi-resolution images integrating spectral, structural and textural features to generate changed patches and change attribute is also desirable and a challenging area of research.

References

Artis, D. A., and Carnahan, W. H., 1982, Survey of Emissivity Variability in Thermography of Urban Areas. *Remote Sensing of Environment*, 12, 13-329.

Balling, R. C., and Brazell, S. W., 1988, High Resolution Surface Temperature Patterns in a Complex Urban Terrain. *Photogrammetric Engineering and Remote Sensing*, 54, 289-1293.

Carnahan, W. H., and Larson, R. C., 1990, An analysis of an urban heat sink. *Remote Sensing of Environment*, 33, 65-71.

Dash, P., Gottsche, F. M., Olesen, F. S., and Fischer, H., 2002, Land Surface Temperature and Emissivity Estimation from Passive Sensor Data: Theory and Practice-Current Trends. *International Journal of Remote Sensing*, 23(13), 2563–2594.

Duda, R. O., Hart, P. E., and Stork, D. G., 2000, *Pattern Classification*, A Wiley-Interscience Publication, Second Edition, ISBN 9814-12-602-0.

Forghani, A., Cechet, B., and Nadimpalli, K., 2005, Object-Based Classification of Multi-Sensor Optical Imagery to Generate Terrain Surface Roughness Information for Input to wind Risk Simulation. *Proceedings of the Geosciences and Remote Sensing Symposium,* 2007, IGARSS '07, 23-27 July, 2007, Barcelona, Spain, IEEE International Publication, 3090-3095.

Friedl, M. A., 2002, Forward and Inverse Modeling of Land Surface Energy Balance using Surface Temperature Measurements. *Remote Sensing of Environment*, 79, 344-354.

Fung, T., and LeDrew, E., 1987, Application of Principal Component Analysis for Change Detection. *Photogrammetric Engineering and Remote Sensing*, 53(12), 1649-1658.

Gallo, K. P., and Owen, T. W., 1998, Assessment of Urban Heat Island: A Multi-Sensor Perspective for the Dallas-Ft. Worth, USA Region. *Geocarto International*, 13, 35– 41.

Gallo, K. P., McNab, A. L., Karl, T. R., Brown, J. F., Hood, J. J., and Tarpley, J. D., 1993, The use of NOAA AVHRR Data for Assessment of the Urban Heat Island Effect. *Journal of Applied Meteorology*, 32, 899– 908.

Kato, S., and Yamaguchi, Y., 2005, Analysis of Urban Heat-Island Effect using ASTER and ETM+ Data: Separation of Anthropogenic Heat Discharge and Natural Heat Radiation from Sensible Heat Flux. *Remote Sensing of Environment*, 99, 44–54.

Kauth, R. J., and Thomas, G. S., 1976, The Tasseled Cap-A Graphic Description of The Spectral-Temporal Development of Agricultural Crops as seen by LANDSAT. *Proceedings of the Symposium on Machine Processing of Remotely Sensed Data*, Purdue University of West Lafayette, Indiana, 4B-41-4B – 51.

Kidder, S. Q., and Wu, H. T., 1987, A Multispectral Study of the St. Louis Area Under Snow-Covered Conditions using NOAA-7 AVHRR Data. *Remote Sensing of Environment*, 22, 159– 172.

Kumar, U., Kerle, N., and Ramachandra T. V., 2008, Contrained Linear Spectral Unmixing Technique for Regional Land Cover Mapping using MODIS Data. *In: Innovations and Advanced Techniques in Systems, Computing Sciences and Software Engineering,* Edited by Khaled Elleithy. Berlin: Springer, ISBN: 978-1-4020-8734-9, 87 - 95.

Landsat 7 Science Data User's Handbook, Landsat Project Science Office, Goddard Space Flight Center, 2002, URL: http://ltwww.gsfc.nasa.gov-/IAS/handbook/handbook_toc.html (last accessed: 25 March, 2008).

Landsbeg, H. E., 1981, *The Urban Climate*, (New York: Academic Press).

Li, F., Jackson, T. J., Kustas, W., Schmugge, T. J., French, A. N., Cosh, M. L., and Bindlish, R., 2004, Deriving land surface temperature from Landsat 5 and 7 during SMEX02/SMACEX. *Remote Sensing of Environment*, 92, 521 – 534.

Lu, D., Mausel, P., Brondizio, E., and Moran, E., 2004, Change Detection Techniques. *International Journal of Remote Sensing*, 25(12), 2365-2407.

Macleod, R. D., and Congalton, R. G., 1998, A Quantitative Comparison of Change-Detection Algorithms for Monitoring Eelgrass from Remotely Sensed Data. *Photogrammetric Engineering and Remote Sensing*, 64(3), 207-216.

Markham, B. L., and Barker, J. K., 1985, Spectral Characteristics of the LANDSAT Thematic Mapper Sensors. *International Journal of Remote Sensing*, 6, 697-716.

Michener, W. K., and Houhoulis, P. F., 1997, Detection of Vegetation Associated with Extensive Flooding in a Forest Ecosystem.

Photogrammetric Engineering and Remote Sensing, 63(12), 1363-1374.

Nikolakopoulos, K. G., Vaiopoulos, D. A., and Skianis, G. A., 2003, Use of Multitemporal Remote Sensing Thermal Data for the Creation of Temperature Profile of Alfios River Basin, *Proceedings of the Geoscience and Remote Sensing Symposium, 2003, IGARSS '03*, 21-25 July 2003. IEEE International Publication, 4:2389-2391, ISBN: 0-7803-7929-2.

Ramachandra, T. V., and Kumar, U., 2008, Wetlands of Greater Bangalore, India: Automatic Delineation through Pattern Classifiers. *Electronic Green Journal*, 26, WebURL: http://egj.lib.uidaho.edu/index.php/egj/article/view/3171

Schmugge, T., Hook, S. J., and Coll, C., 1998, Recovering Surface Temperature and Emissivity from Thermal Infrared Multispectral Data. *Remote Sensing of Environment*, 65, 121– 131.

Snyder, W. C., Wan, Z., Zhang, Y., and Feng, Y. Z., 1998, Classification Based Emissivity for Land Surface Temperature Measurement from Space. *International Journal of Remote Sensing*, 19, 2753– 2774.

Stathopoplou, M., Cartalis, C., and Petrakis, M., 2007, Integrating CORINE Land Cover Data and landsat TM for Surface Emissivity Definitions: An Application for the Urban Areas of Athens, Greece. *International Journal of Remote Sensing,* 28, 3291-3304.

Stathopoulou, M., and Cartalis, C., 2007, Daytime Urban Heat Island from Landsat ETM+ and Corine land Cover Data: An application to Major Cities in Greece. *Solar Energy*, 81, 358-368.

Tanaka, Y., Shibata, S., and Gotoh, K., 2005, Appearance Characteristic Analysis of Heat Island Phenomenon by Using Satellite Remote Sensing and GIS. *Proceedings of the Geosciences and Remote Sensing Symposium, 2005, IGARSS '05*, 25-29 July 2005, IEEE International Publication, 3:1855-1858, ISBN: 0-7803-9050-4.

Weng, Q., Lu, D., and Schubring, J., 2004, Estimation of Land Surface Temperature – Vegetation Abundances Relationship for Urban Heat Island Studies. *Remote Sensing of Environment*, 89, 467-483.

WUP (World Urbanization Prospects): The 2005 Revision, Population Division, Department of Economic and Social Affairs, UN.

Zhang, J., and Zhang, Y., 2007, Remote Sensing Research Issues of the National Land Use Change Program of China. *Photogrammetry & Remote Sensing*, 62(6), 461-472.

Land Surface Temperature with Land Cover Dynamics: Multi-Resolution, Spatio-Temporal Data Analysis of Greater Bangalore   43-53

International Journal of Geoinformatics, Vol 5, No. 3, September, 2009

53

Fusion of Multisensor Data: Review and Comparative Analysis

Uttam Kumar
Department of Management
Studies & Centre for Sustainable
Technologies, Indian Institute of
Science, Bangalore, India.
e-mail: uttam@ces.iisc.ernet.in

Chiranjit Mukhopadhyay
Department of Management
Studies, Indian Institute of Science,
Bangalore, India.
e-mail: cm@mgmt.iisc.ernet.in

T. V. Ramachandra, *SM, IEEE*
Centre for Ecological Sciences &
Centre for Sustainable
Technologies, Indian Institute of
Science, Bangalore, India.
e-mail: cestvr@ces.iisc.ernet.in

Abstract— **Image fusion is a formal framework which is expressed as means and tools for the alliance of multisensor, multitemporal, and multiresolution data. Multisource data vary in spectral, spatial and temporal resolutions necessitating advanced analytical or numerical techniques for enhanced interpretation capabilities. This paper reviews seven pixel based image fusion techniques – intensity-hue-saturation, brovey, high pass filter (HPF), high pass modulation (HPM), principal component analysis, fourier transform and correspondence analysis. Validation of these techniques on IKONOS data (Panchromatic band at 1 m spatial resolution and Multispectral 4 bands at 4 m spatial resolution) reveal that HPF and HPM methods synthesises the images closest to those the corresponding multisensors would observe at the high resolution level.**

Keywords-multiresolution, multisensor, image fusion

I. INTRODUCTION

Earth observation satellites provide data covering different portions of the electromagnetic spectrum at different spatial, spectral and temporal resolutions. Satellites, such as QuickBird, IKONOS, IRS, bundle a 1:4 ratio of a high resolution (HR) panchromatic (PAN) band and low resolution (LR) Multispectral (MS) bands in order to support both spectral and best spatial resolutions while minimising on-board data handling needs [1]. Fusion of data from multiple sensors aids in delineating objects with comprehensive information due to the integration of spatial information present in the PAN image and spectral information present in the LR MS images. For example, fusion of 1 m IKONOS PAN image with 4 m MS images, permits identification of objects approximately one meter in length on the Earth's surface, especially useful in urban areas because the characteristic of urban objects are determined not only by their spectra but also by their structure. Remote sensing (RS) data fusion techniques integrate both PAN and MS data and can be performed at pixel [2], feature [3] and decision [4] levels. This paper reviews the outcome of seven pixel based image fusion techniques.

II. IMAGE FUSION TECHNIQUES

RS data are radiometrically and geometrically corrected (at pixel level) and georegistered considering the topographic undulations. For all methods discussed here, it is assumed that LR MS images are upsampled to the size of HR PAN image.

A. Intensity-Hue-Saturation (IHS)

In RGB – IHS algorithm, the LR MS data (DN^l_{MS1}, DN^l_{MS2}, DN^l_{MS3}) are transformed to the IHS (Intensity, Hue, Saturation) color space (equation 1) which separates the colour aspects in its average brightness (intensity). This corresponds to the surface roughness, its dominant wavelength contribution (hue) and its purity (saturation) [5]. V_1 and V_2 are the intermediate variables. I is replaced with HR image – $DN^{h'}_{PAN}$ and is contrast stretched to match the original PAN image. The fused images of HR are obtained by performing an inverse transformation (equation 2).

$$\begin{pmatrix} DN^l_{PAN} \\ V_1 \\ V_2 \end{pmatrix} = \begin{pmatrix} \frac{1}{3} & \frac{1}{3} & \frac{1}{3} \\ \frac{-1}{\sqrt{6}} & \frac{-1}{\sqrt{6}} & \frac{2}{\sqrt{6}} \\ \frac{1}{\sqrt{6}} & \frac{-1}{\sqrt{6}} & 0 \end{pmatrix} \begin{pmatrix} DN^l_{MS1} \\ DN^l_{MS2} \\ DN^l_{MS3} \end{pmatrix} \quad (1)$$

$$I = DN^l_{PAN} \quad H = \tan^{-1}\left(\frac{V_2}{V_1}\right) \quad S = \sqrt{V_1^2 + V_2^2}$$

Since the forward and backward transformations are linear, replacing V_1 and V_2 in equation (2) by V_1 and V_2 from (1) yields the mathematical model (equation 3) where DN^l_{PAN} = (1/3) (DN^l_{MS1} + DN^l_{MS2} + DN^l_{MS3}) and $DN^{h'}_{PAN}$ is DN^h_{PAN}, stretched to have same mean variance as DN^l_{PAN}.

$$\begin{pmatrix} DN^h_{MS1} \\ DN^h_{MS2} \\ DN^h_{MS3} \end{pmatrix} = \begin{pmatrix} 1 & \frac{-1}{\sqrt{6}} & \frac{3}{\sqrt{6}} \\ 1 & \frac{-1}{\sqrt{6}} & \frac{-3}{\sqrt{6}} \\ 1 & \frac{2}{\sqrt{6}} & 0 \end{pmatrix} \begin{pmatrix} DN^{h'}_{PAN} \\ V_1 \\ V_2 \end{pmatrix} \quad (2)$$

$$\begin{pmatrix} DN^h_{MS1} \\ DN^h_{MS2} \\ DN^h_{MS3} \end{pmatrix} = \begin{pmatrix} DN^l_{MS1} \\ DN^l_{MS2} \\ DN^l_{MS3} \end{pmatrix} + \left(DN^{h'}_{PAN} - DN^l_{PAN} \right) \begin{bmatrix} 1 \\ 1 \\ 1 \end{bmatrix} \quad (3)$$

IEEE
computer
society

B. Brovey Transform (BT)

BT is based on the chromaticity transform with a limitation that only three bands are involved [6]. It normalises the three MS bands used for RGB display and to multiply the result by any other desired data to add the intensity or brightness component to the image (equation 4) where $DN^l_{PAN} = (1/3) (DN^l_{MS1} + DN^l_{MS2} + DN^l_{MS3})$.

$$\begin{pmatrix} DN^h_{MS1} \\ DN^h_{MS2} \\ DN^h_{MS3} \end{pmatrix} = \begin{pmatrix} DN^l_{MS1} \\ DN^l_{MS2} \\ DN^l_{MS3} \end{pmatrix} + \left(DN^h_{PAN} - DN^l_{PAN} \right) \begin{bmatrix} \dfrac{DN^l_{MS1}}{DN^l_{PAN}} \\ \dfrac{DN^l_{MS2}}{DN^l_{PAN}} \\ \dfrac{DN^l_{MS3}}{DN^l_{PAN}} \end{bmatrix} \qquad (4)$$

C. High pass filtering (HPF)

The high spatial resolution image is filtered with a small high-pass (HP) filter or taking the original HR PAN image and subtracting the LR PAN image, which is the low-pass (LP) filtered HR PAN image resulting in the high frequency part of the data which is related to the spatial information. This is pixel wise added to the LR bands. It preserves a high percentage of the spectral characteristics, since the spatial information is associated with the high-frequency information of the HR MS images, which is from the HR PAN image, and the spectral information is associated with the low-frequency information of the HR MS images, which is from the LR MS images (equation 5) [6].

$$DN^h_{MSS} = DN^l_{MS} + (DN^h_{PAN} - DN^l_{PAN}) \qquad (5)$$

where $DN^l_{PAN} = DN^h_{PAN} * h_0$ and h_0 is a LP filter (average or smoothing filter).

D. High pass modulation (HPM)

This transfers the high frequency information of PAN to LR MS data, with modulation coefficients, which equal the ratio between the LR MS images and the LR PAN image [6] where $DN^l_{PAN} = DN^h_{PAN} * h_0$ and h_0 is the same LP filter as used in the HPF method.

$$DN^h_{MS} = DN^l_{MS} + (DN^h_{PAN} - DN^l_{PAN}) \frac{DN^l_{MS}}{DN^l_{PAN}} \qquad (6)$$

E. Principal Component Analysis (PCA)

This transforms multivariate data into a data set of new un-correlated linear combinations of the original variables. It follows the idea similar to the IHS, of increasing the spatial resolution of MS images by introducing a HR PAN image, with the main advantage that an arbitrary number of bands can be used. The channel which will replace PC1 is stretched to the variance and average of PC1. The HR image

replaces PC1 since it contains the information which is common to all bands while the spectral information is unique for each band. PC1 accounts for maximum variance which can maximise the effect of the HR data in the fused image. Finally, HR MS images are determined by performing the inverse PCA transform. The transformation matrix v contains the eigenvectors, ordered with respect to their eigenvalues. It is orthogonal and determined either from the covariance or correlation matrix of the input LR MS images [6].

$$\begin{bmatrix} PC1 \\ PC2 \\ ... \\ PCn \end{bmatrix} = \begin{bmatrix} v11 & v21 & ... & vn1 \\ v12 & v22 & ... & vn2 \\ ... & ... & ... & ... \\ v1n & v2n & ... & vnn \end{bmatrix} \begin{bmatrix} DN^l_{MS1} \\ DN^l_{MS2} \\ ... \\ DN^l_{MSn} \end{bmatrix} \qquad (7)$$

where the transformation matrix

$$v = \begin{bmatrix} v11 & v12 & ... & v1n \\ v21 & v22 & ... & v2n \\ ... & ... & ... & ... \\ vn1 & vn2 & ... & vnn \end{bmatrix}$$

$$\begin{bmatrix} DN^h_{MS1} \\ DN^h_{MS2} \\ ... \\ DN^h_{MSn} \end{bmatrix} = \begin{bmatrix} v11 & v12 & ... & v1n \\ v21 & v22 & ... & v2n \\ ... & ... & ... & ... \\ vn1 & vn2 & ... & vnn \end{bmatrix} \begin{bmatrix} DN^{h'}_{PAN} \\ PC2 \\ ... \\ PCn \end{bmatrix} \qquad (8)$$

Similar to IHS method, equation 7 and 8 can be merged as follows:

$$\begin{bmatrix} DN^h_{MS1} \\ DN^h_{MS2} \\ ... \\ DN^h_{MSn} \end{bmatrix} = \begin{bmatrix} DN^l_{MS1} \\ DN^l_{MS2} \\ ... \\ DN^l_{MSn} \end{bmatrix} + (DN^{h'}_{PAN} - DN^l_{PAN}) \begin{bmatrix} v11 \\ v21 \\ ... \\ vn1 \end{bmatrix} \qquad (9)$$

where $DN^l_{PAN} = PC1$ and $DN^{h'}_{PAN}$ is DN^l_{PAN}, stretched to have same mean and variance as PC1.

F. Fourier transformation (FT)

FT or filter fusion transfers the high spatial frequency content of the HR image to the MS imagery by combining the LP filter version of the duplicated LR MS image and a HP filter version of the more highly resolved PAN [7]. This preserves a high percentage of the spectral characteristic, since the spectral information is associated with the low spatial frequencies of the MS imagery. The spatial resolution data is extracted by HP filtering the more highly resolved PAN band. The cut-off frequencies of the filters have to be chosen in such a way that the included data does not influence the spectra of the opposite data. A sensible value is the Nyquist frequency of the MS imagery. The fusion process is shown in equation (10) where FT denotes the Fourier transformation.

$$MS^H_i = FT^{-1}\{LPF\{FT(MS^L_i)\} + HPF\{FT(PAN)\}\}$$
$$(10)$$

The usage of the spatial frequency domain is convenient

for the filter design and allows a faster computation for large imagery. After fusing both filtered spectra, the inverse Fourier transform (FT^{-1}) leads back into the image domain. The limitation of the approach is the introduction of false edges if the LR MS bands and the HR PAN exhibit a weak correlation.

G.   Correspondence Analysis (CA)

Here, the data table (X) is transformed into a table of contributions of the Pearson chi-square statistic [1]. First, pixel (Xij) values are converted to proportions (Pij) by dividing each pixel (Xij) value by the sum (x++) of all pixels in data set. The result is a new data set of proportions (table Q), and the size is r x c. Row weight pi+ is equal to xi+/x++, where xi+ is the sum of values in row i. Vector [p+j] is of size c. The Pearson chi-square statistic, χ2p, is a sum of squared χij values computed for every cell 'ij' of the contingency table:

$$X_{ij} = \frac{O_{ij} - E_{ij}}{\sqrt{E_{ij}}} = \sqrt{x_{++}} \left[\frac{p_{ij} - p_{i+}p_{+j}}{\sqrt{p_{i+}p_{+j}}} \right] \quad (11)$$

If we use q_{ij} values instead of X_{ij} values, so that $q_{ij} = \chi_{ij} / \sqrt{\chi_{++}}$, eigenvalues will be smaller than or equal to 1 which is more convenient. We used the q_{ij} values to form matrix $\overline{Q}_{r \times c}$ which is

$$\overline{Q}_{r \times c} = \left[q_{ij} \right] = \left[\frac{p_{ij} - p_{i+}p_{+j}}{\sqrt{p_{i+}p_{+j}}} \right]. \quad (12)$$

After this point, the calculation of eigenvalues and the eigenvectors is similar to the PCA methods. Matrix U produced by $U_{c \times c} = \overline{Q}_{c \times r}^T \overline{Q}_{r \times c}$ (13) is similar to the covariance matrix of PCA. MS data are then transformed into the component space using the matrix of eigenvectors. A difference between CA and PCA fusion is the substitution of the last component with the high spatial resolution imagery as opposed to the substitution of the first component in the PCA. Two methods can be used in this part of the CA fusion process. The first is the substitution of the last component with PAN, which is stretched to have same range and variance with the last CA component. Second is the inclusion of details from the PAN band into the last component. Spatial details can be represented as the ratios of pixel values at the lower resolutions of the same imagery and can be included into the last component by

$$CA_{SimComp} = \frac{Pan_{High}}{Pan_{mean}} * CA_{LastComp} \quad (14)$$

where CA$_{SimpComp}$ is the new simulated last component image with the spatial resolution of Pan$_{High}$ which is the high spatial resolution PAN image. Pan$_{Mean}$ is the image with local mean values of Pan$_{High}$ over neighbourhoods equivalent to footprints of CA$_{LastComp}$ image pixels. Noting that Pan$_{Mean}$ can be calculated either by block averaging pixels within the footprints of the low spatial resolution image pixels, or using smoothing convolution filters [8] such as a LP filter so that values are calculated once for each LR pixel block as an average of the high spatial resolution pixels within the block. Finally, the components image is transformed back to the original image space using the inverse matrix of eigenvectors.

III.   DATA ANALYSIS AND RESULTS

Validation of the techniques discussed above was done using IKONOS PAN (525.8 – 928.5 μm, 1 m, acquired on February 23, 2004) and 4 m resolution MS bands (Blue, Green, Red and NIR, acquired: November 24, 2004). The size of PAN and MS images, covering a portion of Bangalore city, India, is 1200 x 1600 and 300 x 400 respectively. The pairs of the images were geometrically registered and the LR images were upsampled to 1200 x 1600 by nearest neighbour algorithm. IKONOS data were collected at 11-bits per pixel (2048 gray tones). The processing and evaluation were based on the original 11-bit and the data were converted to 8-bit for display purpose only. Fig. 1 (1 and 2) shows the PAN image and the natural colour composite of the R-G-B combination resampled at 1 m pixel size. The study area is composed of various features such as buildings, race course, buses, parks, etc. ranging in size from 1 m to 100 m. The correlation coefficients (CCs) between PAN (downsampled to 4 m pixel size) and the original Blue band was 0.41, PAN and Green was 0.44, PAN and Red was 0.47 and PAN and NIR was 0.59. CC of the NIR band is higher than CCs of other bands, indicating that IKONOS NIR band is very important to the IKONOS PAN band. IHS and BT methods can handle only three bands so G-R-NIR combination was chosen for false colour composite (FCC). The resolution ratio between the IKONOS MS and PAN is 1:4, therefore, in the HPF and HPM methods, a 5 x 5 filter was used. The FCC of the G-R-NIR bands (at 1 m) and the fused result of the IHS, BT, HPF, HPM, PCA, FT and CA methods are displayed in Fig. 1 (3-10) respectively.

FT based fusion was performed in spectral domain as shown in Fig. 2. The aim of fusion here is to simulate MS data acquired at LR (4 m) to HR level (1 m), which is identical to MS images originally acquired at HR (1 m) had there been an ideal sensor that would acquire MS bands at 1 m. The performance of the techniques is evaluated in terms of the quality of synthesis of both spatial and spectral information. Visual inspection indicated that the spatial resolutions of the resultant images are higher than that of the original image as features (such as buses, trees, buildings, roads) which were not interpretable in the original image

420
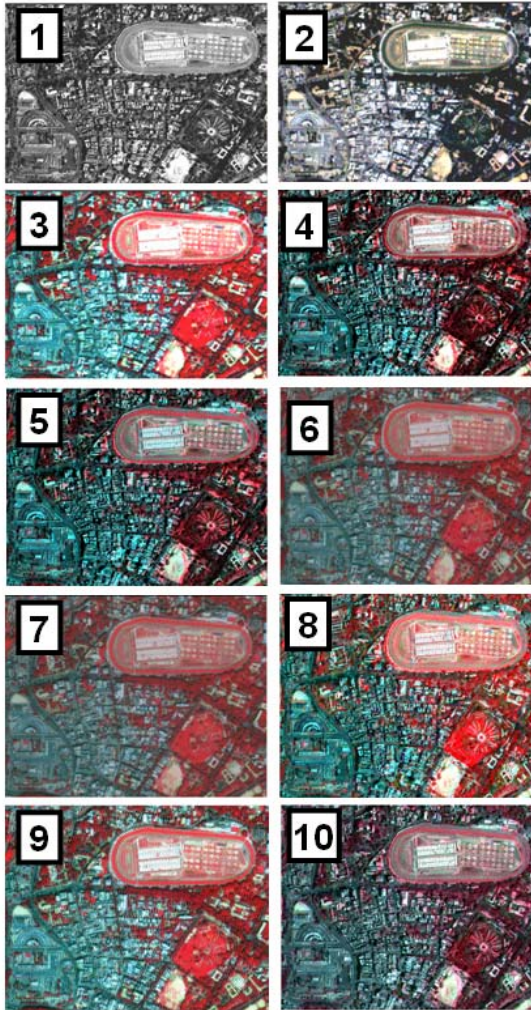
Figure 1. Original PAN image (1), original LR MS image (B-G-R) resampled at 1 m pixel size (2), original LR MS image (G-R-NIR) resampled at 1 m pixel size (3), Fusion through IHS (4), BT (5), HPF (6), HPM (7), PCA (8), FT (9) and CA (10).
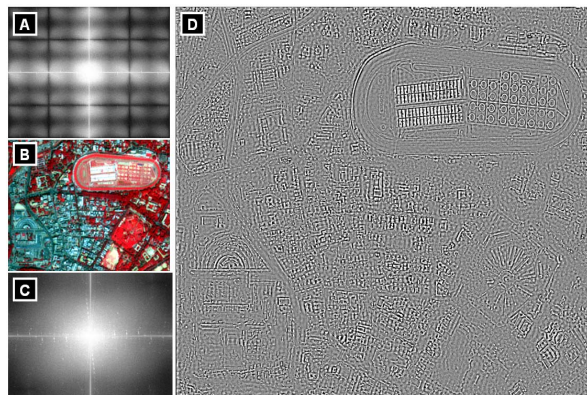
Figure 2. (A) FT on MS (B) Inverse FT on MS, (C) FT on PAN, (D) Inverse FT on PAN.

[Fig. 1 (3)] are identifiable in the resultant images [Fig. 1 (4-10)]. IHS, BT, and CA [Fig. 1 (4, 5 and 10)] produce significant color distortion, while HPF, HPM, PCA and FT methods [Fig. 1 (6, 7, 8 and 9)] produce slight colour distortion in buildings/builtup area. HPF, HPM and FT exhibit more sharpness. This is probably due to over-enhancement along the edge area because these additive methods have considered the differences in high-frequency information between the PAN and the MS bands. Overall, by visual inspection HPF, HPM, PCA and FT methods gives the synthesised result closest to what is expected with least colour distortion. The performance of these techniques were also analysed quantitatively by checking the CC that is often used as a similarity metric in image fusion. However, CC is insensitive to a constant gain and bias between two images and does not allow subtle discrimination of possible fusion artifacts. In addition, a universal image quality index (UIQI) [6] is used to measure the similarity between two images. UIQI is designed by modeling any image distortion as a combination of three factors: loss of correlation, radiometric distortion, and contrast distortion and is given by:

$$Q = \frac{\sigma_{AB}}{\sigma_A \sigma_B} \cdot \frac{2\mu_A \mu_B}{\mu_A^2 + \mu_B^2} \cdot \frac{2\sigma_A \sigma_B}{\sigma_A^2 + \sigma_B^2} \qquad (15)$$

The first component is the CC for A (original MS band) and B (fused MS band). The second component measures how close the mean gray levels of A and B is, while the third measures the similarity between the contrasts of A and B. The dynamic range is [-1, 1]. If two images are identical, the similarity is maximal and equals 1. The synthesised HR MS images (1 m) are spatially degraded to the resolution level of the original LR MS images (4 m). UIQI are computed between the degraded HR MS images and the original LR MS images at the 4 m resolution level. Table 1 shows that the UIQI values of HPF and HPM are higher than the UIQI values of other methods. These two methods also showed higher scores in the NIR band. Since, PAN band includes the most important information from the NIR band (PAN and NIR exhibited highest correlation), therefore from the UIQI method, it is apparent that HPF is superior to all other methods but only slightly better than HPM, which is also reported in [6].

TABLE 1. UIQI OF FUSED AND ORIGINAL IMAGE

	Blue	Green	Red	NIR
HIS	-	0.17	0.27	0.12
BT	-	0.89	0.97	0.54
HPF	**0.85**	**0.94**	**0.96**	**0.98**
HPM	**0.83**	**0.94**	**0.97**	**0.95**
PCA	0.68	0.63	0.63	0.46
FT	0.43	0.22	0.73	0.81
CA	0.27	-0.01	0.06	-0.00

TABLE 2. CORRELATION BETWEEN IKONOS HR PAN AND
CORRESPONDING LR PAN IMAGES FROM DIFFERENT METHODS

IHS	BT	HPF	HPM	PCA	FT	CA
0.32	0.32	**0.95**	**0.95**	0.32	-	0.27
p value for all CC = 2.2e-16						
Both IHS and BT are limited to 3 bands (G, R and NIR). IHS and BT use the same low resolution PAN image. HPF and HPM use the same low resolution PAN image. There is no generation of low resolution PAN in FT.						

The closeness between two images was also quantified in terms of correlation function where each original IKONOS MS band was correlated with respect to each fused band obtained from the 7 techniques (except in IHS and BT where only three bands – G, R, and NIR were considered). Table 2 shows the correlation between the IKONOS HR PAN image and the corresponding LR PAN images by different methods (computed at 1 m pixel size). It can be seen from Table 1 and 2 that the degree of similarity between the HR PAN image and the LR PAN image correspond to the degree of spectral distortion of each band. The lower the similarity between the HR PAN image and the LR PAN image, the higher the spectral distortion and vice versa. HPF and HPM produce very high correlation of more than 0.9 with band 2, 3 and 4. BT has a high correlation in band 2 and 3. IHS and CA produce least correlation, while PCA and FT has medium correlation contrary to the earlier report in [1]. Statistical parameters – minimum, maximum and standard deviation were also used as a measure to examine the spectral information preservation for all the bands. HPM, HPF and PCA were closest to the minimum values of the original bands. For the maximum values, all bands from the HPF and HPM methods were very close to the maximum of original bands. All other methods induced changes in the maximum values in all the fused bands. The standard deviation values for the HPF, HPM, BT and PCA were similar to the original bands of the IKONOS. All other methods showed deviations. These parameters indicated that HPF and HPM are better compared to other methods, however, it could not clearly indicate which method among HPF and HPM is better since some values were closer to original bands in HPF while some were closer to original band values in HPM. By combining the visual inspection and the quantitative results, it was observed that the IHS, BT, and CA methods produce considerable spectral distortion, the FT and PCA methods produce slight spectral distortion and the HPF and HPM method produces the images closest to those the corresponding multisensors would observe at the HR level. However, if the contribution of the NIR band is considered in image fusion then HPF is slightly better than HPM.

IV. CONCLUSION

This paper reviews and analyses seven fusion techniques: IHS, BT, HPF, HPM, PCA, FT and CA. The performance of each method is determined by two factors: how the low resolution PAN image is computed and how the modulation coefficients are defined. If the low resolution PAN image is approximated from the low resolution MS image, it usually has a weak correlation with the high resolution PAN image, leading to color distortion in the fused image. If the low resolution PAN is a low-pass filtered high resolution PAN image, it usually shows less spectral distortion. If the modulation coefficient is set as a constant value, the reflectance differences between the PAN and the MS bands are unaccounted, and the fused images bias the color of the pixel toward the gray. By combination of the visual inspection results and the quantitative results, it is possible to see that the experimental results are in conformity with the theoretical analysis. HPF method followed by HPM produces the synthesised images closest to those the corresponding multi-sensors would observe at the high-resolution level.

REFERENCES

[1] H. I. Cakir, and S. Khorram, "Pixel Level Fusion of Panchromatic and Multispectral Images Based on Correspondence Analysis," Photogrammetric Engineering & Remote Sensing, vol. 74(2), 2008, pp. 183-192.

[2] P. Cheng, T. Toutin, and C. Pohl, "A comparison of geometric models for multisource data fusion," Proceedings of International Symposiumon Remote Sensing, GIS and GPS in Sustainable Development and Environmental Monitoring, GeoInformatics '95 - Hong Kong, 26-28 May 1995.

[3] M. Mangolini, "Apport de la fusion d'images satellitaires multicapteurs au niveau pixel en teÂ leÂ deÂ tection et photo-interpreÂtation," Dissertation published at the University ofNice, Sophia Antipolis, France, 15 November 1994.

[4] S. S. Shen, "Summary of types of data fusion methods utilized in workshop papers," Multisource Data Integration in Remote Sensing, Proceedings of Workshop, Maryland, U.S.A., 14-15 June 1990, NASA Conference Publication 3099 (Greenbelt, MD: NASA), pp. 145-149.

[5] W. J. Carper, T. M. Lillesand, and R. W. Kieffer, "The use of Intensity-Hue-Saturation transformations for merging SPOT Panchromatic and multispectral image Data," Photogrammetric Engineering and Remote Sensing, 56, 1990, pp. 459-467.

[6] Z. Wang, D. Ziou, C. Armenakis, D. Li, and Q. Li, "A Comparative Analysis of Image Fusion Methods," IEEE Transactions of Geoscience and Remote Sensing, vol. 43 (6), 2005, pp. 1391-1402.

[7] R. A. Schowengerdt, Remote sensing models and methods for image processing. Academic Press, San Diego, CA, USA, 1997.

[8] J. G. Liu, "Smoothing filter-based intensity modulation: A spectral preserve image fusion technique for improving spatial details," International Journal of Remote Sensing, 21(18), 2000, pp. 3461-3472.

Fusion of multi resolution remote sensing data for urban sprawl analysis

Bharath H. Aithal[1], Uttam Kumar[2] and Ramachandra T.V.[3,*]

Abstract

Urban population is growing at around 2.3 percent per annum in India. This is leading to urbanisation and often fuelling the dispersed development in the outskirts of urban and village centres with impacts such as loss of agricultural land, open space, and ecologically sensitive habitats. This type of upsurge is very much prevalent and persistent in most places, often inferred as sprawl. The direct implication of such urban sprawl is the change in land use and land cover of the region and lack of basic amenities, since planners are unable to visualise this type of growth patterns. This growth is normally left out in all government surveys (even in national population census), as this cannot be grouped under either urban or rural centre. The investigation of patterns of growth is very crucial from regional planning point of view to provide basic amenities in the region. The growth patterns of urban sprawl can be analysed and understood with the availability of temporal multi-sensor, multi-resolution spatial data. In order to optimise these spectral and spatial resolutions, image fusion techniques are required. This aids in integrating a lower spatial resolution multispectral (MSS) image (for example, IKONOS MSS bands of 4m spatial resolution) with a higher spatial resolution panchromatic (PAN) image (IKONOS PAN band of 1m spatial resolution) based on a simple spectral preservation fusion technique - the Smoothing Filter-based Intensity Modulation (SFIM). Spatial details are modulated to a co-registered lower resolution MSS image without altering its spectral properties and contrast by using a ratio between a higher resolution image and its low pass filtered (smoothing filter) image. The visual evaluation and statistical analysis confirms that SFIM is a superior fusion technique for improving spatial detail of MSS images with the preservation of spectral properties.

Keywords: urbanisation, sprawl, resolution, image fusion, SFIM

INTRODUCTION

Urbanisation is the growth in response to many factors - economic, social, political, physical geography of an area, etc. There are two forms of urbanisation i) in the form of townships and ii) unplanned or organic. Many organic towns in India are under the influence of development with new roads, infrastructure improvements, etc. The urban population in India is growing at around 2.3% per annum with the global proportion of urban population increasing from 13% (220 million in 1900) to 49% (3.2 billion, in 2005) and is projected to rise to 60% (4.9 billion) by 2030 (Ramachandra and Kumar, 2008; World Urbanization Prospects, 2005). An increased urban population in response to the growth in urban areas is mainly due to migration. There are 35 urban agglomerations/cities having a population of more than one million in India (in 2001). Urbanisation leads to the dispersed development in the outskirts, which is known as sprawl. The direct implication of such urban sprawl is the change in land use and land cover of the region. These regions are devoid of any infrastructure and normally left out

in all government surveys (even in national population census), as this cannot be grouped under either urban or rural centre. Understanding this kind of growth is very crucial for regional planning to provide basic amenities in those regions. This would help developers and town planners to project growth patterns and facilitate various infrastructure facilities. It is imperative for planning and governance to facilitate, augment and service the requisite infrastructure over time systematically, which requires an understanding of landscape characterisation. Mapping landscapes on temporal scale provide an opportunity to monitor the changes, which is important for natural resource management and sustainable planning activities. Integration of remote sensing data with ancillary information from various other data sources (population, natural resources, etc.) help to arrive at appropriate decision for good governance. Multi resolution, temporal remote sensing data aid in capturing this dynamics.

Fusion of data from multiple sensors aids in delineating objects with comprehensive information due to the integration of spatial information present in the high resolution (HR) panchromatic (PAN) image and spectral information present in the low resolution (LR) Multispectral (MS) images. Remote sensing satellites, such as QuickBird, IKONOS, IRS, bundle a 1:4 ratio of a HR PAN band and LR MS bands in order to support both spectral and best spatial resolutions while minimising on-board data handling needs. Image fusion techniques integrate both PAN and MSS and can be performed at pixel (Cheng et al., 1995), feature (Mangolini, 1994) and decision (Shen, 1990) levels.

The objective of this work is to optimise multi-resolution data analysis to understand landscape dynamics in Greater Bangalore by image fusion and classification. Fusion permits identification of objects on the Earth's surface, especially useful in urban areas because the characteristic of urban objects are determined not only by their spectra but also by their structure. Thus, remote sensing image fusion techniques are useful to integrate a lower spatial resolution MSS image with a higher spatial resolution PAN image.

STUDY AREA AND DATA

Greater Bangalore (figure 1) is the administrative cultural, commercial, industrial, and knowledge capital of the state of Karnataka with an area of 741 sq. km. and lies between the latitudes 12°39'00'' to 13°13'00'' N and longitude 77°22'00'' to 77°52'00'' E. Bangalore city administrative jurisdiction was widened in 2006 by merging the existing area of Bangalore city spatial limits with 8 neighbouring Urban Local Bodies (ULBs) and 111 Villages of Bangalore Urban District. Bangalore has grown spatially more than ten times since 1949 (69 square kilometers) and is the fifth largest metropolis in India currently with a population of about 7 million (Ramachandra and Kumar, 2008).

The data used were IKONOS PAN from 525.8 – 928.5 μm at 1 m spatial resolution acquired on February 23, 2004 and 4 m resolution MSS bands in Blue, Green, Red and NIR part of the electromagnetic spectrum, acquired on November 24, 2004. The size of high resolution (HR) PAN and low resolution (LR) MSS images, covering a portion of Bangalore city, India, is 1200 x 1600 and 300 x 400 respectively. The pairs of the images

Fusion of multi resolution remote sensing data for urban sprawl analysis

were geometrically registered and the LR PAN image was upsampled to 1200 x 1600 by nearest neighbour algorithm. The other data used in the study were Landsat MSS bands of 1973, IRS LISS-III of 2006, and Google Earth image (http://earth.google.com).
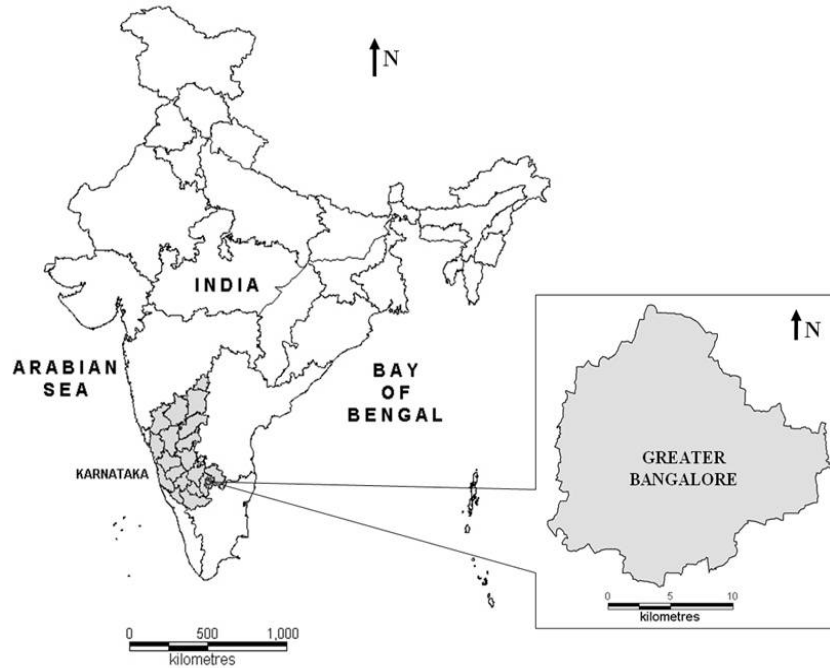
Figure 1: Study area – Greater Bangalore, India.

MODEL

Smoothing Filter-based Intensity Modulation (SFIM) is a general spectral preserve image fusion technique applicable to co-registered multi resolution images (Liu, 2000, Bharath, 2009). SFIM is based on a simplified solar radiation and land surface reflection model (equation 1). Spatial details can be modulated to a co-registered LR MSS band without altering its spectral properties and contrast by using a ratio between a HR image and its low pass (smoothing filter) filtered image.

Digital Number (DN) of an optical image in the reflective spectral band (λ) is dependent on irradiance $E(\lambda)$ and the spectral reflectance of the land surface $\rho(\lambda)$, is given by

$$DN(\lambda) = \rho(\lambda)\, E(\lambda). \tag{1}$$

Similarly DN value in a LR image of spectral band λ is represented by $DN(\lambda)_{low}$ and DN value of the corresponding pixel in a HR image of spectral band γ is given by $DN(\gamma)_{high}$. If the two images are taken in similar solar illumination conditions, then

$$DN(\lambda)_{low} = \rho(\lambda)_{low}\, E(\lambda)_{low} \tag{2}$$

$$DN(\gamma)_{high} = \rho(\gamma)_{high}\, E(\gamma)_{high}. \tag{3}$$

Fusion of multi resolution remote sensing data for urban sprawl analysis

SFIM is given by,

$$DN(\lambda)_{sim} = \frac{DN(\lambda)_{low}DN(\gamma)_{high}}{DN(\gamma)_{mean}} \tag{4}$$

$$= \frac{\rho(\lambda)_{low}E(\lambda)_{high}\rho(\gamma)_{high}E(\gamma)_{high}}{\rho(\gamma)_{low}E(\gamma)_{low}} \tag{5}$$

$$= \rho(\lambda)_{low}E(\lambda)_{high} \tag{6}$$

where $DN(\lambda)_{sim}$ is the simulated HR pixel corresponding to $DN(\lambda)_{low}$ and $DN(\gamma)_{mean}$ is the local mean of $DN(\gamma)_{high}$ over a neighbourhood equivalent to the resolution of $DN(\lambda)_{low}$. For a given solar radiation, irradiance upon a land surface is controlled by topography. If the two images are quantified to the same DN range, we can presume $E(\lambda) \approx E(\gamma)$ for any given resolution because both vary with topography in the same way (Liu et al., 1997). We can also presume $\rho(\lambda)_{low} \approx \rho(\gamma)_{high}$ if there is no significant spectral variation within the neighbourhood for calculating DN(γ)mean. Thus in

$$= \frac{\rho(\lambda)_{low}E(\lambda)_{high}\rho(\gamma)_{high}E(\gamma)_{high}}{\rho(\gamma)_{low}E(\gamma)_{low}} \tag{7}$$

$E(\lambda)_{low}$ and $E(\gamma)_{low}$ cancel each other; $\rho(\gamma)_{low}$ and $\rho(\gamma)_{high}$ also cancel each other; and $E(\gamma)_{high}$ can be replaced by $E(\lambda)_{high}$. We then have a final simple solution of (6). The local mean $DN(\gamma)_{mean}$ is calculated for every pixel of the HR image using a smoothing convolution filter. $DN(\gamma)_{mean}$ is considered as a simulated LR pixel derived from the HR image pixels by spatial smoothing. The image of $DN(\gamma)_{mean}$ is equivalent to the image of $DN(\lambda)_{low}$ in topography and texture because they both have a pixel size of the higher resolution image, and a spatial resolution of the lower resolution image. The final result, the image of $DN(\lambda)_{sim}$, is a product of the topography and texture of higher resolution, $E(\lambda)_{high}$, introduced from the higher resolution image, and the lower resolution spectral reflectance of the original lower image, $\rho(\gamma)_{low}$. It is therefore independent of the spectral property of the HR image used for intensity modulation. As the spectral difference between the lower and the higher resolution images is not fundamental to the operations, equation 6 can be rewritten as:

$$IMAGE_{SFIM} = \frac{IMAGE_{low}IMAGE_{high}}{IMAGE_{mean}} \tag{8}$$

where $IMAGE_{low}$ is a pixel of a LR image co-registered to a HR image of $IMAGE_{high}$, $IMAGE_{mean}$ is a smoothed pixel of $IMAGE_{high}$ using averaging filter over a neighbourhood equivalent to the actual resolution of $IMAGE_{low}$. The ratio between $IMAGE_{high}$ and $IMAGE_{mean}$ in equation (8) cancels the spectral and topographical contrast of the HR image and retains the higher resolution edges only. SFIM is therefore reliable to the spectral properties as well as contrast of the original lower resolution image.

Fusion of multi resolution remote sensing data for urban sprawl analysis

However, for SFIM operations, the lower resolution image must be interpolated to the same pixel size as the higher resolution image by the co-registration process. Also, $IMAGE_{low}$ must have the same pixel size as $IMAGE_{high}$ though with a lower resolution. Otherwise, the spatial information of HR image cannot be fully integrated into the LR image.

ANALYSIS AND RESULTS

The correlation coefficient (CCs) between PAN and the original Green band was 0.44, PAN and Red was 0.47 and PAN and NIR was 0.59. The SFIM result based on the fusion of IKONOS MSS and PAN data is given in Figure 2.

(a)   (b)
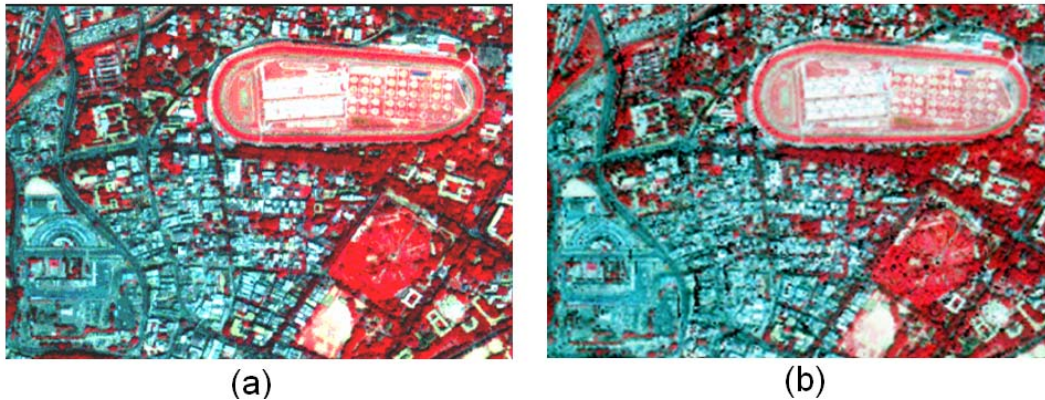
Figure 2: FCC of the IKONOS PAN and MSS (a) original bands at 4m, (b) fused bands at 1m.

The performance of the technique was analysed quantitatively by checking the CC that is often used as a similarity metric in image fusion as given in table 1. HIS (Hue-Intensity-Saturation) and BT (Brovey Transform) methods can handle only three bands so G (band 2) − R (band 3) − NIR (band 4) combination was chosen for false colour composite (FCC). CC between original band 2 and 3 and fused bands from Brovey and SFIM is almost equal. However, the CC of the original band 4 (NIR band) and SFIM fused band 4 is higher than Brovey and HIS. Since NIR band is very useful for vegetation and water discrimination and has the highest correlation (0.59) with PAN band, therefore, SFIM is better than the other two methods.

Table 1: CC between original bands and the fused bands from different techniques.

Fusion techniques	Band 2	Band 3	Band 4
HIS	0.22	0.32	0.17
Brovey	0.99	0.98	0.67
SFIM	0.96	0.98	**0.97**

In addition, a universal image quality index (UIQI) (Wang et al., 2005) was used to measure the similarity between two images. UIQI is designed by modeling any image

distortion as a combination of three factors: loss of correlation, radiometric distortion, and contrast distortion given by:

$$Q = \frac{\sigma_{AB}}{\sigma_A \sigma_B} \cdot \frac{2\mu_A \mu_B}{\mu_A^2 + \mu_B^2} \cdot \frac{2\sigma_A \sigma_B}{\sigma_A^2 + \sigma_B^2} \tag{9}$$

The first component is the CC for A (original MSS band) and B (fused MSS band). The second component measures how close the mean gray levels of A and B is, while the third measures the similarity between the contrasts of A and B. The dynamic range is [-1, 1]. If two images are identical, the similarity is maximal and equals 1. This index showed that the SFIM preserves spectral properties even better than Brovey and HIS techniques (Kumar et al., 2009) as given in table 2.

Table 2: UIQI values for the fused bands from different techniques.

Fusion techniques	Original		
	Band 2	**Band 3**	**Band 4**
HIS (Band 2)	0.17	0.27	0.11
Brovey (Band 3)	1.00	0.97	0.63
SFIM (Band 4)	0.97	0.97	0.97

SFIM is more sensitive to image co-registration accuracy. Inaccurate co-registration may result in blurring edges in the fused images. This problem can be resolved using a smoothing filter with a kernel, larger than the resolution ratio between the higher and lower resolution images. The HIS and Brovey transform fusion techniques are not sensitive to the co-registration accuracy as the topographic/textural features are totally replaced by the intensity replacement image. This may not necessarily be an advantage. The SFIM technique is not applicable for fusing images that are fundamentally different in physical properties, such as the fusion between optical images and radar images. SFIM fusion technique aided in integrating a lower spatial resolution MSS image with a higher spatial resolution PAN image. Spatial details were modulated to a co-registered LR MSS image without altering its spectral properties and contrast by using a ratio between a higher resolution image and its low pass filtered image. The visual evaluation and statistical analysis confirms that SFIM is a superior fusion technique for improving spatial detail of MSS images with the preservation of spectral properties.

Figure 3 shows the classified image of 1973 (79 m) and 2006 (23.5 m) obtained with four land use categories (built-up, vegetation, water and open land) for Greater Bangalore. The fused image has retained both the spectral and spatial properties and gives finer details not visible in the two LR classified images. Table 3 gives the details of the classified images.

Table 3: Landuse statistics of Greater Bangalore.

Year ↓ Class →		Built up	Vegetation	Water	Others
1973	**Ha**	5448	46639	2324	13903
	%	**7.97**	**68.27**	**3.40**	**20.35**
2006	**Ha**	29535	19696	1073	18017
	%	**43.23**	**28.83**	**1.57**	**26.37**

Temporal analysis of Greater Bangalore data showed that there has been a 466% increase in built up area from 1973 to 2006 leading to decline of 54% area in water bodies, attributing to intense urbanisation process. The rapid development of urban sprawl has many potentially detrimental effects including the loss of valuable agricultural and eco-sensitive (e.g. wetlands, forests) lands, enhanced energy consumption and greenhouse gas emissions from increasing private vehicle use (Ramachandra and Kumar, 2008).
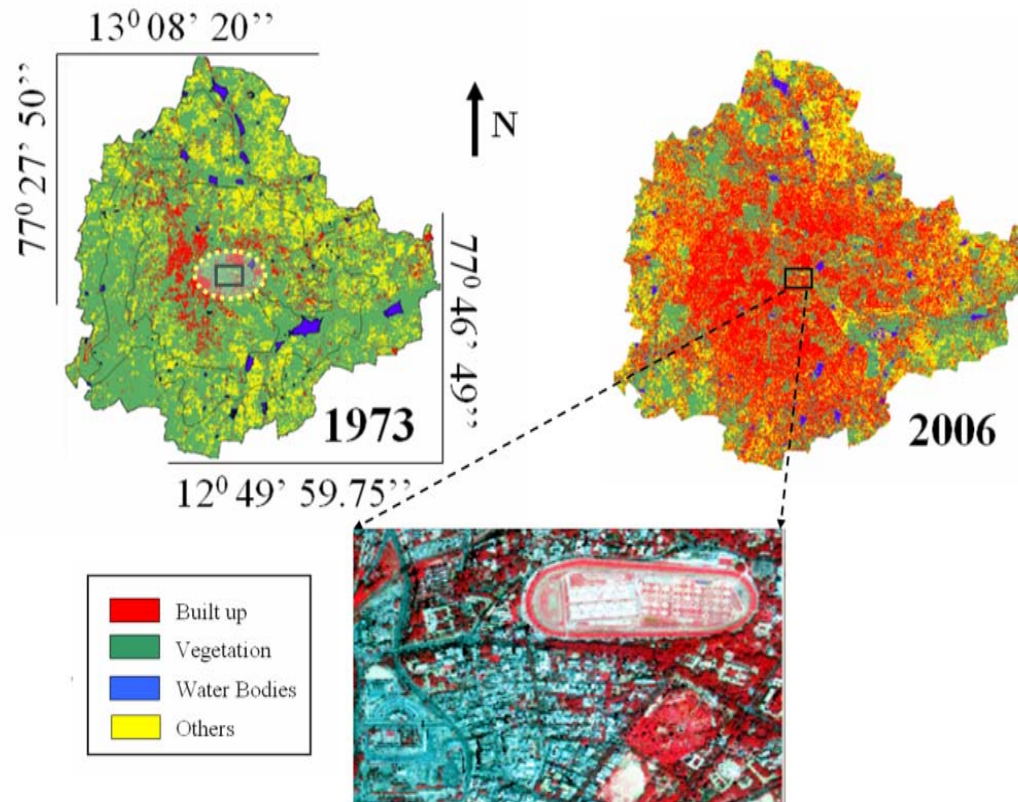
Figure 3: Classified images of 1973 and 2006. **Fused image of area highlighted in rectangular box in the two classified images.**

Vegetation has decreased by 58% from 1973 to 2006. Multi-storied buildings have come up on some lake beds that have totally intervene the natural catchment flow leading to artificial floods (Ramachandra and Kumar, 2008). Urbanisation has also enhanced land surface temperature in urban areas from the circumference ground creating heat island effects.

Fusion of multi resolution remote sensing data for urban sprawl analysis

CONCLUSIONS

The advantage of the SFIM over the HIS and Brovey fusion technique is that it improves spatial details with the fidelity to the image spectral properties and contrast. This technique can be used to perform high speed real-time image fusion process and visualisation. The SFIM technique is not applicable for fusing images that are fundamentally different in illumination conditions or physical properties such as the fusion between optical images and radar images. The case study unravels the pattern of growth in Greater Bangalore and its implication on local climate and also on the natural resources, necessitating appropriate strategies for the sustainable management. This would help developers and town planners to project growth patterns and facilitate various infrastructure facilities. The study reveals the type, extent and nature of sprawl taking place in a region. Methods of change detection from multi-resolution images integrating spectral, structural and textural features to generate change patches in a landscape are future scope of this work.

ACKNOWLEDGEMENTS

REFRENCES

1. Bharath H., (2009), Image fusion techniques in remote sensing, B.E. Dissertation, University Visvesvaraya College of Engineering, Bangalore
2. Cheng, P., Toutin, T., and Pohl, C., (1995), A comparison of geometric models for multisource data fusion. Proceedings of International Symposiumon Remote Sensing, GIS and GPS in Sustainable Development and Environmental Monitoring, GeoInformatics '95 - Hong Kong, 26-28 May 1995.
3. Kumar, U., Mukhopadhayay, C., and Ramachandra T. V., (2009), Fusion of Multisensor Data: Review and Comparative Analysis. In Proceedings of the 2009 WRI Global Congress on Intelligent Systems, 19-21 May 2009, Xiamen, China, pp. 418 – 422, DOI 10.1109/GCIS.2009.457, IEEE Computer Society, Conference Publishing Services, Los Alamitos, California.
4. Liu, J. U., (2000), Smoothing Filter-based Intensity Modulation: a spectral preserve image fusion technique for improving spatial details, International Journal of Remote Sensing, 21 (18):3461-3472
5. Mangolini, M., (1994), Apport de la fusion d'images satellitaires multicapteurs au niveau pixel en teÂ leÂ deÂ tection et photo-interpreÂtation. Dissertation published at the University ofNice, Sophia Antipolis, France, 15 November 1994.
6. Ramachandra T. V., and Kumar, U., (2008), Wetlands of Greater Bangalore, India: Automatic Delineation through Pattern Classifiers. Electronic Green Journal, Issue 26, Spring 2008 ISSN: 1076-7975.

7. Shen, S. S., (1990), Summary of types of data fusion methods utilized in workshop papers. Multisource Data Integration in Remote Sensing, Proceedings of Workshop, Maryland, U.S.A., 14-15 June 1990, NASA Conference Publication 3099 (Greenbelt, MD: NASA), pp. 145-149.

8. Wang, Z., Ziou, D., Armenakis, C., Li, D., and Li, Q., (2005), A Comparative Analysis of Image Fusion Methods. IEEE Transactions of Geoscience and Remote Sensing, vol. 43 (6), pp. 1391-1402.

9. World Urbanization Prospects, (2005), Revision, Population Division, Department of Economic and Social Affaris, UN.

AUTHOR REFERENCE

[1]Bharath H Aithal, Research scholar, Centre for Sustainable Technologies, Indian Institute of Science, Bangalore. E-mail: bharath@ces.iisc.ernet.in

[2]Uttam Kumar, Research scholar, Department of Management Studies, Indian Institute of Science, Bangalore. E-mail: uttam@ces.iisc.ernet.in

[3]Ramachandra T.V., Faculty, Centre for Ecological Sciences and Associate Faculty, Centre for Sustainable Technologies, and Centre for *Infrastructure*, Sustainable Transportation and Urban Planning (C*i*STUP), Indian Institute of Science, Bangalore. E-mail: cestvr@ces.iisc.ernet.in, energy@ces.iisc.ernet.in, Tel: 91-80-23600985/22932506/ 22933099, Fax: 91-80-23601428 [CES-TVR].
[*]Corresponding Author, cestvr@cistup.iisc.ernet.in

Spatial Data Mining
and
Modeling for Visualisation of Rapid Urbanisation

Uttam Kumar[1], **Mukhopadhyay C**[2]., & **Ramachandra T. V**[3]*

*[1] Department of Management Studies and Centre for Sustainable Technologies,
Indian Institute of Science, Bangalore.
[2] Department of Management Studies, Indian Institute of Science, Bangalore.
[3] Centre for Ecological Sciences, Centre for Sustainable Technologies,
Centre for Infrastructure, Sustainable Transportation and Urban Planning
Indian Institute of Science, Bangalore, India.*

*[1]uttam@ces.iisc.ernet.in, [2]cm@mgmt.iisc.ernet.in,
* Corresponding author: [3]cestvr@ces.iisc.ernet.in*

Abstract

Rapid urbanisation in India has posed serious challenges to the decision makers in regional planning involving plethora of issues including provision of basic amenities (like electricity, water, sanitation, transport, etc.). Urban planning entails an understanding of landscape and urban dynamics with causal factors. Identifying, delineating and mapping landscapes on temporal scale provide an opportunity to monitor the changes, which is important for natural resource management and sustainable planning activities. Multi-source, multi-sensor, multi-temporal, multi-frequency or multi-polarization remote sensing data with efficient classification algorithms and pattern recognition techniques aid in capturing these dynamics. This paper analyses the landscape dynamics of Greater Bangalore by: (i) characterisation of direct impervious surface, (ii) computation of forest fragmentation indices and (iii) modeling to quantify and categorise urban changes. Linear unmixing is used for solving the mixed pixel problem of coarse resolution super spectral MODIS data for impervious surface characterisation. Fragmentation indices were used to classify forests – interior, perforated, edge, transitional, patch and undetermined. Based on this, urban growth model was developed to determine the type of urban growth – Infill, Expansion and Outlying growth. This helped in visualising urban growth poles and consequence of earlier policy decisions that can help in evolving strategies for effective land use policies.

Keywords: *Landscape, orthogonal subspace projection, forest fragmentation, urban growth model*

1.   Introduction

Urbanisation is a form of metropolitan growth in response to incomprehensible combination of economic, social, and political forces and to the physical geography of an area. This could be planned (in the form of townships) or unplanned (organic). Many organic cities are now undergoing redevelopment for economic purposes with new roads, infrastructure improvements, etc. It results in the increase in population, in proportion to the region's rural population. This phenomenona is very rapid in India with urban population growing at around 2.3 percent per annum. The 21st century is witnessing "rapid urbanisation of the world's population", as the global proportion of urban population rose dramatically from 13% (220 million in 1900) to 29% (732 million, in 1950) to 49% (3.2 billion, in 2005) and is projected to rise to 60% (4.9 billion) by 2030 [1]. An increased urban population and growth in urban areas is inadvertent with dramatic increase in population mainly due to migration. There are 35 urban agglomerations/cities having a population of more than one million in India (in 2001). Of the 4000 plus urban agglomerations, about 38 percent reside in just 35 urban areas, thus indicating the magnitude of urbanisation. Overall rise in population of urban poor or increase in travel times owing to congestion in road networks are indicators of urban governance and planning. As Indian cities continue to urbanise, the land use (LU) plays a determining role in the quality of land, water and air environment. This pose serious challenges to the decision makers in the city planning and management process involving plethora of issues like infrastructure development, traffic congestion, and basic amenities (such as electricity, water, and sanitation), floods, heat island, loss of aquatic eco-system, carbon footprint, enhanced level of pollution, higher instances of diseases, etc. [2]. Thus, the administration at all levels: local bodies, federal and national governments are facing the brunt of rapid urban growth. It is imperative for planning and governance to facilitate, augment and service the requisite infrastructure over time systematically. This requires an understanding of landscape characterisation focusing on agents of urban dynamics.

Problem Statement – Identifying, delineating and mapping landscapes on temporal scale provide an opportunity to monitor the changes, which is important for natural resource management and sustainable planning activities. Multi-source, multi-sensor, multi-temporal, multi-frequency or multi-polarization remote sensing (RS) data [3] with pattern recognition techniques [4] aid in capturing the dynamics. Pattern classification and modeling are very useful in landscape characterisation for addressing the problems of sprawling cities and urban management. The objectives of this work are to understand the landscape dynamics in Greater Bangalore through visualization by i) modeling impervious surface, ii) computation of forest fragmentation indices, iii) quantification and categorisation of urban changes and (iv) modeling of urban dynamics.

Visuaisation - Current Trend and Techniques: Geovisualisation helps to explore real-world environments and model 'what if' scenarios based on spatio-temporal data. This aids as a tool for modeling the environmental interests in policy planning. Some of the well known applications are 3D photorealistic representations to simulate urban redevelopment and possible pollution diffusion over the next few years. Techniques used in geovisualisation are agent based cellular automata models, genetic algorithms, etc.

2.   Methods

2.1   Orthogonal Subspace Projection (OSP) – Pixel usually contain contributions from more than one class, when object size is smaller than the pixel resolution (mixed pixels) except in higher spatial resolution data. Standard classification techniques, which attribute a single class to the entire pixel, are therefore inappropriate to low spatial resolution satellite images from space-borne sensors. This motivates the development of algorithms which unmix the coarse spatial data or, in other words, perform classification at a sub-pixel level. The main objective is to find out the proportion of each category in a given pixel, or in other words, unmix the pixel to identify the categories present within the pixel. In order to address this problem, unmixing techniques have been developed to exploit sub-pixel level information for image analysis [5], where sub-pixel class composition is estimated through the use of techniques, such as linear mixture modeling [6], supervised fuzzy-c means classification and artificial neural networks, etc.

Linear unmixing is based on an assumption that the spectral radiance measured by the sensor consists of the radiances reflected collectively in proportion to the sub-pixel area covered by each material. Let K be the number of spectral bands in the multispectral / superspectral data set, and P, the number of distinct classes of objects in the physical scene. Associated with

each pixel is a K-dimensional vector $\mathbf{y}$ whose components are the gray values corresponding to the K bands. Let $\mathbf{E} = [e_1, e_2, ..., e_P]$, where $\{e_i\}$ is a column vector representing the spectral signature of the ith target material or category, and these values are the components of the P-dimensional abundance vector α. Assuming the linear mixture model, the observation vector $\mathbf{y}$ is related to $\mathbf{E}$ by

$$y = E\alpha + \bar{\eta} \qquad (1)$$

where $\bar{\eta}$ accounts for the measurement noise. We further assume that the components of the noise vector $\bar{\eta}$ are zero-mean random variables that are independent and identically distributed. Therefore, the covariance matrix of the noise vector is $\sigma^2\mathbf{I}$, where σ^2 is the variance, and $\mathbf{I}$ is K x K identity matrix. The conventional approach [7] to extract the abundance values is to minimise $\| y - E\alpha \|$, and the estimate for the abundance is

$$\alpha = (E^T E)^{-1} E^T \mathbf{y} \qquad (2)$$

which is termed as the Unconstrained Least Squares (ULS) estimate of the abundance. Imposing the sum-to-one constraint on the abundance values while minimising $\| y - E\alpha \|$, gives the Constrained Least Squares (CLS) estimate of the abundance as,

$$\alpha = (E^T E)^{-1}\left(E^T\mathbf{y} - \frac{\lambda}{2}1 \right) \qquad (3)$$

where,

$$\lambda = \frac{2(1^T(E^T E)^{-1}E^T\mathbf{y}-1)}{1^T(E^T E)^{-1}1} \qquad (4)$$

Chang (2005) [8] came up with a technique called Orthogonal Subspace Projection (OSP) in the signal processing domain, which is used here as a classification technique based on two aspects: 1) how to best utilise the target knowledge provided *a priori* and 2) how to effectively make use of numerous spectral bands. Briefly, the technique involves (i) finding an operator which eliminates undesired spectral signatures, and then (ii) choosing a vector operator which maximises the signal to noise ratio (SNR) of the residual spectral signature. In order to find the abundance of the pth target material (α_p), let the corresponding spectral signature of the desired target material be denoted as $\mathbf{d}$. The term $E\alpha$ in equation (1) can be rewritten to separate the desired spectral signature $\mathbf{d}$ from the rest as:

$$E\alpha = d\alpha_p + \mathbf{Rr} \qquad (5)$$

where $\mathbf{r}$ contains the abundance of the rest of the end-members, and $\mathbf{R}$ is a K x P - 1 matrix containing the columns of $\mathbf{E}$ except for the column vector $\mathbf{d}$. We rewrite (1) as

The column vectors of the K x P matrix $\mathbf{E}$ are called end-members. For a given pixel, the abundance fraction of the pth target material present in a pixel is denoted by α_p, and these values are the components of the P-

$$y = d\alpha_p + \mathbf{Rr} + \bar{\eta}. \qquad (6)$$

The interfering signatures present in $\mathbf{R}$ can be removed from (6) by the operator,

$$P = (\mathbf{I} - \mathbf{R}(\mathbf{R}^T\mathbf{R})^{-1}\mathbf{R}^T) \qquad (7)$$

which is used to project the vector $\mathbf{y}$ into a space orthogonal to the space spanned by the interfering spectral signatures. Therefore, operating on $\mathbf{y}$ with $\mathbf{P}$, and noting that $\mathbf{PR} = 0$, we get

$$Py = Pd\alpha_p + P\bar{\eta}. \qquad (8)$$

The next step is to find an operator w^T which maximizes the SNR given by

$$\text{SNR} = \frac{(w^T Pd\alpha_p)^2}{\varepsilon\{(w^T P\bar{\eta})^2\}} = \frac{w^T Pd\alpha_p^2 d^T P^T w)^2}{w^T P\varepsilon\{(\bar{\eta}\bar{\eta}^T)\}P^T w} \qquad (9)$$

$$= \left(\frac{\alpha_p^2}{\sigma}\right)^2 \frac{w^T Pdd^T P^T w}{w^T PP^T w}$$

Maximizing the SNR leads to the generalized eigenvalue problem: $Pdd^T P^T w = \lambda PP^T w$.

The eigenvector corresponding to the maximum eigenvalue is the vector '$\mathbf{w}$'. It can be shown that the $\mathbf{w}$ which maximises the SNR is given by

$$\mathbf{w = kd.} \qquad (10)$$

Therefore, an optimal estimate of α_p is given by

$$\alpha_p = \frac{y^T P^T Py}{d^T P^T Pd} \qquad (11)$$

In the absence of noise, the estimate matches with the exact value as in (6). The value of α is the abundance of the pth class (in an abundance map) ranging from 0 to 1 in any given pixel. 0 indicates absence of a particular class and 1 indicates full presence of that class in that particular pixel. There are as many abundance maps as the number of classes. Intermediate values between 0 and 1 may represent a fraction of that class. If the objective is to map the impervious surface, then OSP renders an impervious surface abundance map, where each abundance pixel shows the proportion of impervious material (buildings / houses / roads / paved surfaces, etc.) in that pixel.

2.2   Forest fragmentation – Forest fragmentation is the process whereby a large, continuous area of forest is both reduced in area and divided into two or more fragments. The decline in the size of the forest and the increasing isolation between the two remnant patches of the forest has been the major cause

of declining biodiversity [9]. The primary concern is direct loss of forest area, and all disturbed forests are subject to "edge effects" of one kind or another. Forest fragmentation is of additional concern, insofar as the edge effect is mitigated by the residual spatial pattern [10].

Land cover (LC) map indicate only the location and type of forest, and further analysis is needed to quantify the forest fragmentation. Total extent of forest and its occurrence as adjacent pixels, fixed-area windows surrounding each forest pixel is used for calculating type of fragmentation. The result is stored at the location of the centre pixel. Thus, a pixel value in the derived map refers to between-pixel fragmentation around the corresponding forest location. As an example [11] if Pf is the proportion of pixels in the window that are forested and Pff is the proportion of all adjacent (cardinal directions only) pixel pairs that include at least one forest pixel, for which both pixels are forested then, Pff estimates the conditional probability that, given a pixel of forest, its neighbour is also forest. The six fragmentation model that identifies six fragmentation categories are: (1) interior, for which $Pf = 1.0$; (2), patch, $Pf < 0.4$; (3) transtitional, $0.4 < Pf < 0.6$; (4) edge, $Pf > 0.6$ and $Pf-Pff > 0$; (5) perforated, $Pf > 0.6$ and $Pf-Pff < 0$, and (6) undetermined, $Pf > 0.6$ and $Pf = Pff$.

When Pff is larger than Pf, the implication is that forest is clumped; the probability that an immediate neighbour is also forest is greater than the average probability of forest within the window. Conversely, when Pff is smaller than Pf, the implication is that whatever is nonforest, is clumped. The difference ($Pf - Pff$) characterizes a gradient from forest clumping (edge) to nonforest clumping (perforated). When $Pff = Pf$, the model cannot distinguish forest or nonforest clumping. The case of $Pf = 1$ (interior) represents a completely forested window for which Pff must be 1.

Forest fragmentation indices [12] have two parts: (1) Total forest proportion (TFP) and Forest continuity (FC). TFP provides a basic assessment of forest cover in a region ranging from 0 to 1. FC value examines only the forested areas within the analysis region. Its measure specifically utilises the results from the forest fragmentation model.

$$TFP = \frac{total\ forest\ area}{total\ non-water\ area} \qquad (12)$$

$$FC = \frac{weighted\ forest\ area}{total\ forest\ area} * \frac{area\ of\ largest\ interior\ forest\ patch}{total\ forest\ area} \qquad (13)$$

Weighted values for the weighted forest area (WFA) are derived from the median Pf value for each fragmentation class (equation 14):

$$WFA = (1.0 * interior) + (0.8 * (perforated + edge + undertermined) + (0.5 + transitiojnal) + (0.2 * patch) \qquad (14)$$

The rationale is that, given two regions of equal forest cover, the one with more interior forest would have a higher weighted area, and thus be less fragmented. To separate further regions based on the level of fragmentation, the weight area ratio is multiplied by the ratio of the largest interior forest patch to total forest area for the region. FC ranges from 0 to 1.

2.3 Urban Dynamics Characterisation –

An urban dynamics model has spatially detailed data with fine spatial grain, examines the whole landscape and assesses urban growth in all areas, avoids spatial averaging, maintains spatial pattern and configuration, and is consistent over time. The urban growth model used here is based on the modified forest fragmentation model developed by Ritters *et al.*, (2000) [13]. The urban dynamics model uses urban and non-urban classes to create fragmentation image instead of forest and non-forest in forest fragmentation model. Input data consist of multi-dates LC with a minimum of three classes; urban (developed), non-urban (non-developed), and water. Instead of using a forest versus non-forest binary image to create a forest fragmentation map, the first step of the urban growth model uses a non-developed versus developed image to create a "non-developed" fragmentation image. The single date fragmentation map consist of three "fragmented" classes that are combination of the five classes previously described (interior, patch, transitional, edge and perforated). The first is interior, which occurs when all pixels in a *3 x 3* window are non-developed. The second class is perforated, which occurs when between 60 % and less than 100 % of pixels in a *3 x 3* window are non-developed. The final class is patch, which occurs when fewer than 60 % of pixels in a *3 x 3* window are non-developed. Two dates of fragmentation maps are used to create change map. There are three types of change classes – the first type consists of no change classes (including developed, water and interior), the second type includes improbable changes, likely due to classification error, and the third type consists of classes that represent urban growth. The classes that indicate urban growth are outlined in table 1 along with their corresponding urban growth classes. The change classes determine the type of urban growth. *Infill* is the development of a small area surrounded by existing developed land.

Expansion is the spreading out of urban LC from existing developed land. *Outlying growth* is an interior pixel that changes to developed, and is further classified as either *isolated*, *linear branching*, or *clustered branching* (see table 1).

Table 1: Change classes that represent urban growth and the corresponding growth types [13]

Significant Change Classes	Type of Growth
Patch to Developed	Infill Growth
Perforated to Developed	Expansion Growth
Interior to Developed	Outlying Growth: 1. *Isolated Growth,* 2. *Linear Branching Growth,* 3. *Clustered Branching Growth*

Their distinction is made using a set of rules. An isolated growth is defined as a new, small area of construction surrounded by non-urban land and some distance from other developed areas. A linear branching growth is a road, corridor, or linear development surrounded by non-urban land and some distance from other urban areas. A clustered branching growth is indicative of a new, large and dense development in a previously undeveloped area. The urban growth model produces an urban growth map, which consists of five types of growth as well as developed land, water, and non-developed land.

3.   Study area and Data

Greater Bangalore is the principal administrative, cultural, commercial, industrial, and knowledge capital of the state of Karnataka with an area of 741 square kilometers (sq. km) and lies between the latitudes 12°39'00'' to 131°3'00''N and longitude 77°22'00'' to 77°52'00''E (figure 1). Bangalore has grown spatially more than ten times (741 sq. km) since 1949 (69 sq. km.) and is the fifth largest metropolis in India currently with a population of about 7 million. The mean annual total rainfall is about 880 mm with about 60 rainy days a year over the last ten years. The summer temperature ranges from 18° C – 38° C, while the winter temperature ranges from 12° C – 25° C. Thus, Bangalore enjoys a salubrious climate all round the year.   Survey of India (SOI) toposheets of 1:50000 and 1:250000 scales were used to generate base layers of the city boundary and water bodies. Field data for ground control points (GCPs) and training sites for supervised classification of RS data were collected with a handheld GPS. RS data used are

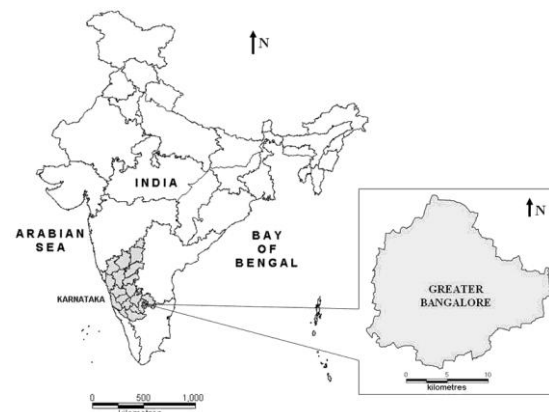- Landsat MSS of 1973, TM of 1992, ETM+ of 2000 [downloaded from http://glcf.umiacs.umd.edu/data/]

Figure 1: Study area – Greater Bangalore, India.
(Self Compiled)

- IRS (Indian Remote Sensing) LISS (Linear Imaging Self Scanner)-III of 1999 and 2006 [procured from NRSA, Hyderabad, India]
- MODIS of 2006, 2007 (Moderate Resolution Imaging Spectroradiometer) Surface Reflectance 7 bands product [downloaded from http://edcdaac.usgs.gov/main.asp]
- Google Earth data (http://earth.google.com) served in pre and post classification process and validation of the results.

4.   Results and discussions

4.1   Classification of IRS LISS-III (2006) data: IRS LISS-III data acquired on 28th March, 2006 having 3 spectral bands (Green, Red and NIR) with 23.5 m spatial resolution were georegistered with known GCPs and geometrically corrected and resampled to 25 m (1360 x 1400 pixels) which helped in pixel level comparison of abundance maps obtained by unmixing MODIS data (of 2006) with LISS-III classified map. The class spectral characteristics for four LC categories (buildings/urban, vegetation, water bodies and others) using LISS-III MSS bands 2, 3 and 4 were obtained from the training pixels spectra to assess their inter-class separability and the images were classified using Gaussian Maximum Likelihood classifier with training data uniformly distributed over the study area collected with pre calibrated GPS (figure 2). This was validated with the representative field data (training sets collected covering the entire city and validation covering ~ 10% of the study area) and also using Google Earth image (http://www.earth.google.com).   LC statistics, producer's accuracy, user's accuracy and overall accuracy computed are listed in table 2. The urban pixels were extracted from the
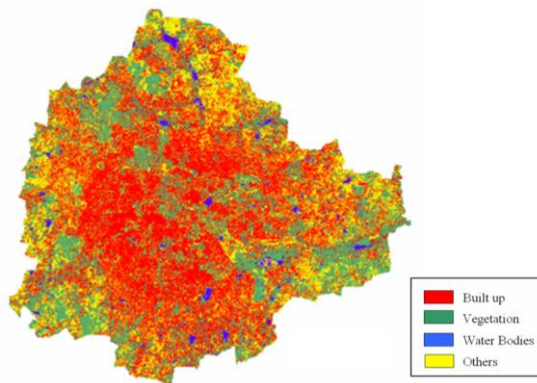
Figure 2: LC classification using LISS-III MSS (2006). (Self Compiled)

Table 2: LC details using LISS -III MSS (Self Compiled)

Class	Area (Ha)	Area (%)	P* (%)	U* (%)	O* (%)
Builtup	29535	43.2	85.2	84.5	
Vegetation	19696	28.8	83.5	88.1	84.6
Water bodies	1073	01.6	90.7	80.2	
Others	18017	26.4	78.3	77.7	

P* - Producer's Accuracy, U* - User's Accuracy, O* - Overall Accuracy

classified image and were used as a benchmark to validate the output obtained from OSP.

4.2 Unmixing of MODIS data using OSP: MODIS data (of 2006) having 7 bands with band 1 and 2 at 250 m and band 3 to 7 at 500 m spatial resolution were georegistered with GCPs, geometrically corrected and bands 3 to 7 were resampled to 250 m (136 x 140 pixels) so that all 7 bands are at same spatial resolution. Unmixing of MODIS data (250 m) were done to obtain abundance map of the impervious surface. Visual inspection as well as accuracy assessment of abundance image showed that OSP algorithm maps impervious surface spatially and proportionally similar to supervised classified image of LISS-III (of 2006). The proportions of urban pixels in the image (figure 3) range from 0 to 1, with 0 indicating absence and increasing value showing higher abundance.

Accuracy assessment at pixel level: A pixel of MODIS (250 m) corresponds to a kernel of 10 x 10 pixels of LISS-III spatially (resampled to 25 m). The builtup abundance map was validated pixel by pixel with the LISS-III builtup map. The proportion of builtup percentage obtained in these 136 x 140 cells were compared using three measures of performance – Root Mean Square (RMS) error (0.160), Bivariate Distribution Functions (BDFs) between LISS-III
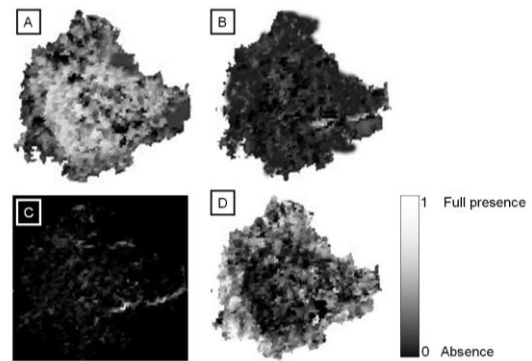
Figure 3: LC abundance maps (of 2006) for builtup, vegetation, water bodies and others. (Self Compiled)

classified (real proportion) and MODIS based abundance map (predicted proportions), and Wilcoxon signed rank test. The bivariate plot (figure 4) was helpful in visualising the accuracy of prediction by mixture models. While most of the points fall between the two 20 % difference lines, some points are outside the lines indicating that there could be higher or lower estimation than the actual values. The Pearson's product-moment correlation was 0.84 (p-value < $2.2e^{-16}$). 10 % of the difference pixels between the LISS-III proportion and the MODIS abundance were randomly selected at the same spatial locations in the two images by random number generation. These difference data values failed when subjected to normality test (table 3).

Figure 4: BDF of LISS-III classified and MODIS based abundance map. (Self Compiled)

Table 3: Normality tests for the difference in LISS-III and MODIS proportions (Self Compiled)

Normality test	p-value
Shapiro-Wilk	$2.2e^{-16}$
Anderson-Darling	$2.2e^{-16}$
Kolmogorov-Smirnov	$2.2e^{-16}$
Cramer-von Mises	Infinity
Lilliefors	$2.2e^{-16}$

The data points corresponding to builtup proportion in a MODIS pixel and corresponding LISS-III pixels were then subject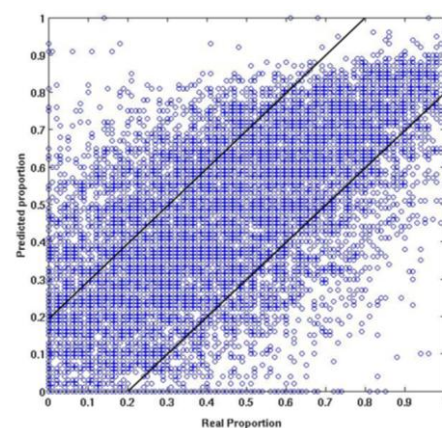ed to box-plot and histogram analysis. The distribution was symmetrical, hence Wilcoxon signed rank test with continuity correction was performed (r = 0.66, p-value < $2.2e^{-16}$), which showed less evidence against null hypothesis – "*true location of median of the difference between two data sets is equal to 0*".

The abundance image was further analysed with a minimum detectable threshold of 10 % and in increments of 10 % (i.e., 20 to 30 %, 30-40 %, …., 90 to 100 %) as shown in figure 5. Objects representing different brightness classes of impervious surface are typically selected to be mapped based on the tonal variations in the builtup landscape, which constitute spectral classes. The results hold great promise for improved accessibility and accuracy of this important urban indictor at the local and city level. Table 4 depicts the percentage impervious surface from abundance map.
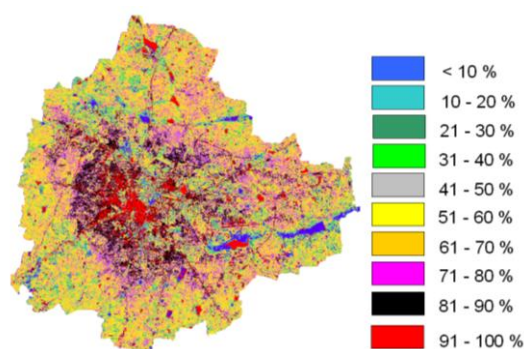

Figure 5: Percent impervious surface layer for the Bangalore city. (Self Compiled)

4.3 Forest fragmentation indices: Supervised classification was performed on temporal datasets for Bangalore city with the Bayesian classifier using the open source programs (i.gensig, i.class and i.maxlik) of Geographic Resources Analysis Support System (http://wgbis.ces.iisc.ernet.in/grass). Accuracy assessment was done using field knowledge, and visual interpretation which showed an overall accuracy of 72 %, 75 %, 71 %, 77 % 85 % and 55 % for the year 1973, 1992, 1999, 2000, 2006 and 2007. The class statistics is given in table 5. From the classified raster data, urban class was extracted and converted to vector representation for computation of precise area in hectares indicating 466 % increase in built up area from 1973 to 2007 as evident from temporal analysis

Table 4: Percent Impervious surface from abundance map (Self Compiled)

Percent Impervious surface	Area	
	Ha	%
0 – 10 %	7019.57	9.97
11 – 20 %	5853.89	8.31
21 – 30 %	7410.17	10.52
31 – 40 %	10126.27	14.38
41 – 50 %	10199.57	14.48
51 – 60 %	9149.63	12.99
61 – 70 %	9863.94	14.01
71 – 80 %	7050.32	10.01
81 – 90 %	3485.47	4.95
91 – 100 %	274.69	0.39

leading to a sharp decline of 61% area in water bodies mostly attributing to intense urbanisation process. Rapid urbanisation and sprawl has many detrimental effects including the loss of valuable agricultural and eco-sensitive (e.g. wetlands, forests) lands, enhanced energy consumption and greenhouse gas emissions from increasing private vehicle use and also from modern glazed architectures. Vegetation has decreased by 63 % from 1973 to 2007. Using the results from classification, forest fragmentation indices were computed as shown in figure 6 and the statistics are presented in table 6.

Table 5: Greater Bangalore land cover statistics (Self Compiled)

Class → Year ↓		Built up	Vegetation	Water Bodies	Others
1973	Ha	5448	46639	2324	13903
	%	**7.97**	**68.27**	**3.40**	**20.35**
1992	Ha	18650	31579	1790	16303
	%	**27.30**	**46.22**	**2.60**	**23.86**
1999	Ha	23532	31421	1574	11794
	%	**34.44**	**45.99**	**2.30**	**17.26**
2000	Ha	24163	31272	1542	11346
	%	**35.37**	**45.77**	**2.26**	**16.61**
2006	Ha	29535	19696	1073	18017
	%	**43.23**	**28.83**	**1.57**	**26.37**
2007	Ha	30876	17298	1005	19143
	%	**45.19**	**25.32**	**1.47**	**28.01**

Applying forest fragmentation indices to a time series LC data provided a quantitative assessment of the pattern of forest fragmentation at each date and a means for tracking trends in forest fragmentation. Patch forest which was only 2.45 % in 1973 has increased up to 9.6 % in 2006 and interior forest

Table 6: Composition of forest fragmentation (Self Compiled)

| Fragmentation Categories	1973		1992		1999		2000		2006	
	Ha	%	Ha	%	Ha	%	Ha	%	Ha	%
Patch	1120	2.45	1950	6.34	1788.6	5.91	1944	6.47	1810	9.57
Transitional	3789	8.28	4259	13.84	3816	12.62	3999	13.31	3956	20.92
Edge	14717	32.16	10709	34.81	9516	31.46	10593	35.25	6050	31.99
Perforated	1453	3.18	1447	4.70	1410	4.66	1219	4.06	1859	9.83
Interior	24675	53.93	12401	40.31	13715	45.35	12291	40.91	5236	27.69
Total	45756	100	30766	100	30244	100	30047	100	18909	100
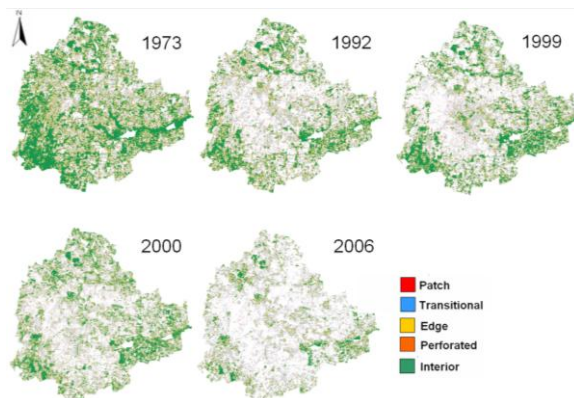
Figure 6: Forest fragmentation map (1972, 1992, 1999, 2000 and 2006). (Self Compiled)

has decreased from 54 % in 1972 to 27.7 % in 2006.

Using forest fragmentation indices, the state of the fragmentation for the city was developed. While the forest fragmentation map produced valuable information, it was difficult to visualise the state of forest fragmentation for tracking the trends and to identify the areas where forest restoration might prove appropriate to reduce the impact of deforestation. The values of TFP and FC calculated (table 7) for the temporal data were plotted on a graph that specifies six conditions of forest fragmentation in figure 7. The TFP designations revealed that forest fragmentation become more severe as forest cover decreases from 100 percent cover towards 80 percent. Between 60 and 80 percent forest cover, the opportunity for re-introduction of forest to connect forest patches is greatest, and below 60 percent, forest patches become small and more fragmented. The FC regions were evenly split and designated high forest continuity (above 0.5) or low forest continuity (below 0.5). The amount of forest and continuity were high in 1973 and decreased substantially in 2006 (figure 6). Forest edges and perforations have less meaning where the amount of forest is low and percolation theory [14] identifies two critical values of Pf. In a completely forested landscape, for a completely random forest conversion on an infinite grid

Table 7: Total forest proportion and forest continuity (Self Compiled)

State of forest fragmentation index	19 73	19 92	19 99	20 00	20 06
TFP	0.7	0.	0.	0.4	0.2
FC	0.4	0.	0.	0.3	0.1
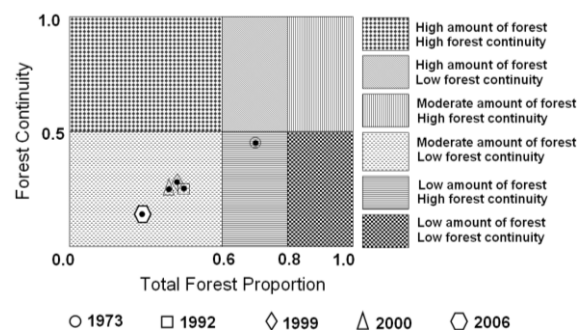
Figure 7: Six forest fragmentation conditions based on the values for Total Forest Proportion and Forest Continuity. (Self Compiled)

(and evaluating adjacency in cardinal directions), the residual forest is guaranteed to occur in identifiable patches when Pf falls below a critical value of about 0.4. Below that value, the nonforest pixels form a continuous path across the window. Conversely, as long as the residual forest is above a critical value of about 0.6, the forest pixels form such a path, and forest edges and perforations have more meaning. These values are used to define *patch* and *transitional* categories recognising that they are approximate because actual LC pattern is not random.

Forest fragmentation also depends on the scale of analysis (window size) and various consequences of increasing the window size are reported in [11]. The measurements are also sensitive to pixel size. Higher fragmentation occurs when finer grain maps are used over a fixed extent (window size). Finer grain maps identify more nonforest area where forest cover is dominant but not exclusive. The strict criterion for interior forest is more difficult

to satisfy over larger areas. Although knowledge of the feasible parameter space is not critical, there are geometric constraints. For example, it is not possible to obtain a low value of Pff when Pf is large. Percolation theory applies strictly to maps resulting from random processes; hence, the critical values of Pf (0.4 and 0.6) are only approximate and may vary with actual pattern. As a practical matter, when Pf > 0.6, nonforest types generally appeared as "islands" on a forest background, and when Pf < 0.4, forests appeared as "islands" on a nonforest background.

4.4 Urban Dynamics Characterisation:
Input data consisted of multi date images having three classes: urban, non-urban, and water bodies obtained from the supervised classification algorithm. Each single date fragmentation map consisted of three fragmentation classes – interior, perforated and patch. The final step in the urban growth model was to use two date fragmented image to create change map (1973 to 1992, 1992 to 1999, 1999 to 2000 and 2000 to 2006). The model produced urban growth maps, which consisted of developed land, non-developed land, water and the three types of growth (Infill growth, Expansion and Outlying growth) as shown in figure 8 and statistics are given in table 8.

Outlying growth have been further classified as – isolated, linear branching and clustered growth (figure 9). There were no perfect linear growth (linear branching surrounded by non-developed land). In all the cases, linear branching were surrounded by one of the other growth classes such as expansion growth, infill growth etc. Combining several temporal urban growth maps created an informative picture of the urban dynamics. Ward wise, impermeable areas were plotted against the urban population density to understand the increase in population density with the increase in the impermeable area. Increased paved surface and concentrated human activities has led to urban heat island effect, as there is increase in temperature between urban pixels compared to
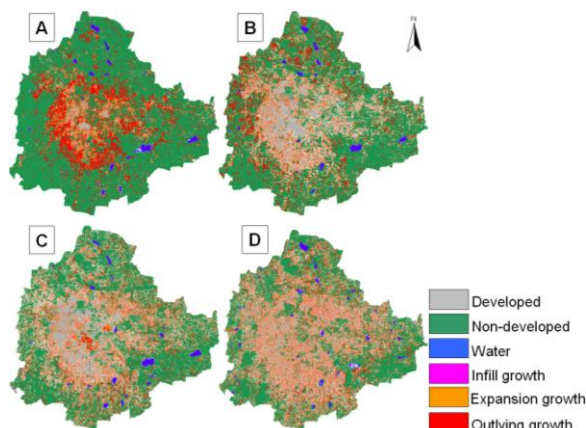

Figure 8: Urban growth map (A) 1973 to 1992, (B) 1992 to 1999, (C) 1999 to 2000, (D) 2000 to 2006.
(Self Compiled)
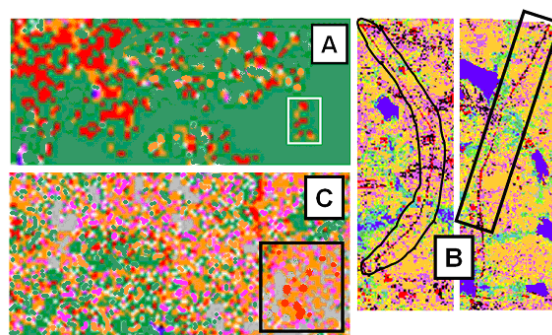
Figure 9: Types of urban outlying growth highlighted in boxes – (A) isolated growth, (B) linear branching (road/corridor), (C) clustered growth. (Self Compiled)

its surroundings. Visualisation helps the Local decision makers to see the implications of earlier decisions and policies and evolve appropriate LU policies for sustainable planning and management.

5. Conclusions

Urbanisation and urban sprawl seems inevitable in Indian cities as long as the growth is coupled with lack of holistic approaches in governance. Sections of the society will continue to cope up with skewed economic growth while attempting to protect natural resources.

Table 8: Changes in urban growth types from 1973 to 2006 (Self Compiled)

Urban Growth Type	1973 - 1992		1992 - 1999		1999 - 2000		2000 - 2006	
	Ha	%	Ha	%	Ha	%	Ha	%
Developed	6889	1.0	3818	5.6	2876	4.2	32380	4.74
Non-developed	48529	71	44034	64.6	42610	63	37922	55.54
Water	905	1.3	692	1.0	1434	2.1	952	1.39
Infill	720	1.1	2146	3.2	3088	4.5	4232	6.20
Expansion	5720	8.4	10078	14.8	13110	19	16412	24.04
Outlying	11520	17	7453	10.9	5054	7.4	5526	8.09
Total	68082	100	68220	100	68172	100	68282	100

Visualisation of urban dynamics based on data mining and modeling aid in capturing the information in an effective way. This would help in better planning for provision of basic amenities and also to adopt sustainable urban strategies. Orthogonal subspace projection mapped the impervious surface accurately evident from accuracy assessment. Forest fragmentation indices and the urban dynamics model show the change in type of land cover classes from vegetation to urban. Interior forest which was present in the city up to 54 % (in 1973) has come down to 28 % in 2006. Urban growth characterised by developed, infill, expansion and outlying types evidently illustrate the phenomenon of urbanising Greater Bangalore.

Acknowledgement

References:

[1] "*World Urbanization Prospects,*" Revision, Population Division, Department of Economic and Social Affaris, UN, 2005.

[2] T. V. Ramachandra, and U. Kumar, "*Geoinformatics for Urbanisation and Urban Sprawl pattern analysis. In: Geoinformatics for Natural Resource Management,*" (Eds. Joshi et al.). Nova Science Publishers, NY (In press), 2008.

[3] M. K. Arora, and S. Mathur, "*Multi-source classification using artificial neural network in rugged terrain,*" GeoCarto International, vol. 16, no. 3, pp. 37-44, 2001.

[4] R. O. Duda, P. E. Hart, and D. G. Stork, "*Pattern classification,*" A Wiley-Interscience Publication, Second Edition, ISBN 9814-12-602-0, 2000.

[5] Y. E. Shimabukuro, and A. J. Smith, "*The least-squares mixing models to generate fraction images derived from remote sensing multispectral data,*" IEEE Transactions on Geoscience and Remote Sensing, vol. 29, no. 1, pp. 16–20,1991.

[6] U. Kumar, N. Kerle, and T. V. Ramachandra, "*Contrained linear spectral unmixing technique for regional land cover mapping using MODIS data,*" In: Innovations and advanced techniques in systems, computing sciences and software engineering / ed by Elleithy, K., Berlin: Springer, 2008. ISBN: 978-1-4020-8734-9. paper 87. 9 p, 2008.

[7] A. A. Nielsen, "*Spectral mixture analysis: Linear and semi-parametric full and iterated partial unmixing in multi-and hyperspectral image data,*" International Journal of Computer Vision, vol. 42, no. 1, pp. 17-37, 2001.

[8] C-I Chang, "*Orthogonal Subspace Projection (OSP) Revisited: A Comprehensive Study and Analysis,*" IEEE Transactions on Geoscience and Remote Sensing, vol. 43, no. 3, pp. 502–518, 2005.

[9] J. D. Hurd, E. H. Wilson, S. G. Lammey, and D. L. Civco, "*Characterization of Forest Fragmentation and Urban Sprawl using time sequential Landsat Imagery,*" In ASPRS 2001 Annual Convention, St. Louis, MO, 2001.

[10] S. A. Levin, "*The problem of pattern and scale in ecology,*" Ecology, vol. 73, pp. 1943-1967, 1992.

[11] K., J. Riitters, R. O' Neill. Wickham, B. Jones, and E. Smith, "*Global-scale patterns of forest fragmentation,*" Conservation Ecology, vol. 4, no. 2-3, 2000. http://www.consecol.org/vol4/iss2/art3/

[12] J. D. Hurd, E. H. Wilson, and D. L. Civco, "*Development of a Forest Fragmentation Index to Quantify the rate of forest change,*" In ASPRS-ACSM Annual Conference and FIG XXII Congress, April 22-26, 2002.

[13] D. L. Civco, J. D. Hurd, E. H. Wilson, C. L. Arnold, and M. P. Prisioe, "*Quantifying and Describing Urbanizing landscape in the Northeast United States,*" Photogrammetry Engineering and Remote Sensing, vol. 68, no. 10, pp. 1083 - 1090, 2002.

[14] D. Stauffer, "*Introduction to percolation theory,*" Taylor and Francis, Philadelphia, Pennsylvania, USA, 1985.

Seismic Microzonation of Bangalore

T.G.Sitharam

sitharam@civil.iisc.ernet.in
Department of Civil Engineering, Indian Institute of Science, Bangalore - 560012.

Abstract

In the present study an attempt has been made to study the seismic hazard analysis considering the local site effects and to develop microzonation maps for Bangalore. Seismic hazard analysis and microzonation of Bangalore is addressed in this study in three parts: In the first part, estimation of seismic hazard using seismotectonic and geological information. All the earthquake sources and seismicity has been considered within a radius of 350 km from the Bangalore city for the study. Second part deals about site characterization using geotechnical and shallow geophysical techniques. An area of about 220 sq.km encompassing Bangalore Municipal Corporation has been chosen as the study area. There were over 150 lakes, though most of them are dried up due to erosion and encroachments leaving only 64 at present in BMP (Bangalore Mahanagara Palika) area. emphasizing the need to study site effects. In the last part, local site effects are assessed by carrying out one-dimensional (1-D) ground response analysis (using the program SHAKE 2000) using both borehole SPT data and shear wave velocity survey data within an area of BMP. Further, field experiments using microtremor studies have also been carried out (jointly with NGRI) for evaluation of predominant frequency of the soil columns. The same has been assessed using 1-D ground response analysis and compared with microtremor results. Further, Seed and Idriss's simplified approach has been adopted to evaluate the liquefaction susceptibility and liquefaction resistance assessment. Microzonation maps have been prepared for Bangalore city covering 220 sq. km area on a scale of 1:20000.

Key words: *Seismic hazard, Microzonation, site characterization, shear wave velocity, site response and liquefaction*

Introduction

Microzonation has generally been recognized as the most accepted tool in seismic hazard assessment and risk evaluation and it is defined as the zonation with respect to ground motion characteristics taking into account source and site conditions (ISSMGE/TC4, 1999). Making improvements on the conventional macrozonation maps and regional hazard maps, microzonation of a region generates detailed maps that predict the hazard at much larger scales. Damage patterns of many recent earthquakes around the world, including the 1999 Chamoli and 2001 Bhuj earthquakes in India, have demonstrated that the soil conditions at a site can have a major effect on the level of ground shaking. For example, in the Chamoli earthquake, epicenter located at more than 250 km away from Delhi caused moderate damage to some of the buildings built on filledup soil or on soft alluvium. The Bhuj earthquake caused severe damage not only in the epicentral region, but even in Ahmedabad, about 250 km away, which attributed to increased ground shaking of the soft alluvium. Mapping the seismic hazard at local scales to incorporate the effects of local ground conditions is the essence of microzonation.

Earthquake damage is commonly controlled by three interacting factors- source and path characteristics, local geological and geotechnical conditions and type of the structures. Obviously, all of this would require analysis and presentation of a large amount of geological, seismological and geotechnical data. History of earthquakes, faults/sources in the region, attenuation relationships, site characteristics and ground amplification, liquefaction susceptibility are few of the important inputs required. Effect of site amplification due to soil conditions and associated damage to built environment was amply demonstrated by many earthquakes during the last century. The wide spread

destruction caused by Guerrero earthquake (1985) in Mexico city, Spitak earthquake (1988) in Leninakan, Loma Prieta earthquake (1989) in San Francisco Bay area, Kobe earthquake (1995), Kocaeli earthquake (1999) in Adapazari are important examples of site specific amplification of ground motion even at location as far away as 100-300km from the epicenter (Ansal, 2004). These failures resulted from the effect of soil condition on the ground motion that translates to higher amplitude; it also modifies the spectral content and duration of ground motion. Site specific ground response analysis aims at determining this effect of local soil conditions on the amplification of seismic waves and hence estimating the ground response spectra for future design purposes. The response of a soil deposit is dependent upon the frequency of the base motion and the geometry and material properties of the soil layer above the bedrock. Seismic microzonation is the process of assessment of the source & path characteristics and local geological & geotechnical characteristics to provide a basis for estimating and mapping a potential damage to buildings, in other words it is the quantification of hazard. Presenting all of this information accordingly to develop hazard maps, for the use of planners, developers, insurance companies and common public is another important aspect of microzonation.

Scale and Methodology Adopted

Rapidly growing cities with increasing population are most vulnerable to natural hazards due to agglomeration of the population at one place. Preparation of the geotechnical microzonation maps provides an effective solution to overcome to some extent from seismic hazards. Seismic microzonation has been carried out to understand the effects of earthquake generated ground motions on soil or/and man-made structures. The main objective of a microzonation study is to use the obtained variation of the selected parameters for land use and city planning. Therefore it is very important that the selected microzonation parameters should be meaningful for city planners as well as for public officials. Ansal (2004) recommend that the national seismic zoning maps are mostly at small scale level (1:1,000,000 or less) and are mostly based on seismic source zones defined at similar scales. The seismic microzonation for a town requires 1:5,000 or even 1:1,000 scale studies and needs to be based on seismic hazard studies at similar scales. The general trend in conventional microzonation studies in India was to simplify the applied methodology by adopting the macrozonation seismic hazard maps as the primary source to estimate the earthquake hazard. In addition, due to the lack of sufficient geological and geotechnical data, a site simplification is used to define the site conditions with respect to local geological units.

Seismic Microzonation falls into the category of "applied research". That is why there is a need to upgrade and revise based on the latest information, Seismic microzonation was defined world wide based on region or country. However in Indian context, "Microzonation is a subdivision of a region into zones that have relatively similar exposure to various earthquake related effects. This exercise is similar to the macro level hazard evaluation but requires more rigorous input about the site specific geotechnical conditions, ground responses to earthquake motions and their effects on the safety of the constructions taking into consideration the design aspects of the buildings, ground conditions which would enhance the earthquake effects like the liquefaction of soil, the ground water conditions and the static and dynamic characteristics of foundations or of stability of slopes in the hilly terrain" –DST Expert Group on Microzonation of Delhi Chaired by Arya (1998) and the definition was endorsed by the DST subcommittee on Microzonation, Chaired by Narula (2001).

The microzonation level is graded based on the scale of the investigation and method of ground motion assessment. The technical committee on earthquake geotechnical engineering, TC4 of the International society of soil mechanics and foundation engineering (1993) states that the first grade (Level I) map can be prepared with scale of 1:1,000,000 – 1:50,000 and the ground motion was assessed based on the Historical earthquakes and existing information of geological and geomorphological maps. If the scale of the mapping is 1:100,000-1:10,000 and ground motion is assessed based on the microtremor and simplified geotechnical studies then it is called second grade (Level II) map. In the third grade (Level III) map ground motion has been assessed based on the complete geotechnical investigations and ground response analysis with a scale of 1:25,000-1:5,000. The steps in seismic microzonation has been subdivided into three major items:

1)   Evaluation of the expected input motion
2)   Local Site effects and ground Response analysis
3)   Preparation of microzonation maps.

Even though the seismic hazard analysis and microzonation has been grouped in to three major steps as above, there is a need to adopt step by step procedure to arrive at the final map for microzonation. Based on the grade and level of the microzonation map, a detailed methodology can be formulated with the above three basic steps. The steps followed for the seismic hazard assessment and microzonation of Bangalore in the present investigation is illustrated as a flow chart in Figure 1.

Seismic Study Area and Seismotectonic map

Seismotectonic map showing the geology, geomorphology, water features, faults, lineaments, shear zone and past earthquake events has been prepared for Bangalore which is as shown in Figure 2. A seismotectonic detail of the study area has been collected in a circular area having a radius of about 350 km around Bangalore. The sources identified from Seismotectonic Atlas (2000) and remote sensing studies are compiled and a map has been prepared using Adobe Illustrator version 9.0. The seismotectonic map contains 65 numbers of faults with length varying from 9.73 km to 323.5km, 34 lineaments and 14 shear zones. The map shows different rock groups with different colours. Faults, lineaments and shear zones are given different colours. Earthquake data collected from different agencies [United State Geological Survey (USGS), Indian Metrological Department (IMD), BARC Gauribidanur station Geological Survey of India (GSI) and Amateur Seismic Centre (ASC)] contain information about the earthquake size in different scales such as intensity, local magnitude, surface wave magnitude and body wave magnitudes. These magnitudes are converted to moment magnitudes (Mw) by using magnitude relations given by Heaton et al (1986).

The earthquake events collated and converted has been super imposed on the base map with available latitudes and longitudes. The earthquake events collated are about 1420 with minimum moment magnitude of 1.0 and a maximum of 6.2 and earthquake magnitudes are shown as circles with different diameters and colours. Sitharam and Anbazhagan (2007) have presented these aspects and new seismotectonic map has been developed and presented. The maximum occurred events near by the each source are assigned as the maximum source magnitude.

Geological formation of the study area is considered as one of the oldest land masses of the earth's crust. Most of the study area is classified as Gneissic complex/Gneissic granulite with major inoculation of greenstone and allied supracrustal belt. The geology deposits close to the eastern and western side of the study area is coastline having the alluvial fill in the pericratonic rift. The major tectonic constituents in the southern India include the massive Deccan Volcanic Province (DVP), the South Indian Granulite Terrain (SIGT), the Dharwar craton (DC), the Cuddapah basin (CB), the Godavari graben (GG) and the Mahanadi graben (MG), the Eastern and the Western ghats on the east and west coast of India, respectively. The Eastern Ghat region in general is a quiet zone, characterized by diffused low magnitude shallow focus earthquakes and an occasional earthquake of magnitude 5 to 6 (Mw).

The Indian shield region is marked by several rift zones and shear/thrust zones. Although this region is considered to be a stable continental region, this region has experienced many earthquakes of magnitude of 6.0 since the 18th Century and some of which were disastrous (Ramalingeswara Rao, 2000). Among them are the Mahabaleshwar (1764), Kutch (1819), Damooh hill (Near Jabalpur, 1846), Mount Abu (1848), Coimbatore (1900), Son-Valley (1927), Satpura (1938), Koyna, (1967), Latur (1993), and Jabalpur earthquake (1997). Nath (2006) highlighted that the most common cause for the Indian shield appears to be the compressive stress field in the Indian shield oriented NNE-SSW on an average as a consequence of the relentless India-Eurasia plate collision forces. Sridevi Jade (2004) highlighted that southern peninsular India moves as a rigid plate with about 20 mm/year velocity in the NNE direction (using Global positioning system measurement at Indian Institute of Science, Bangalore).
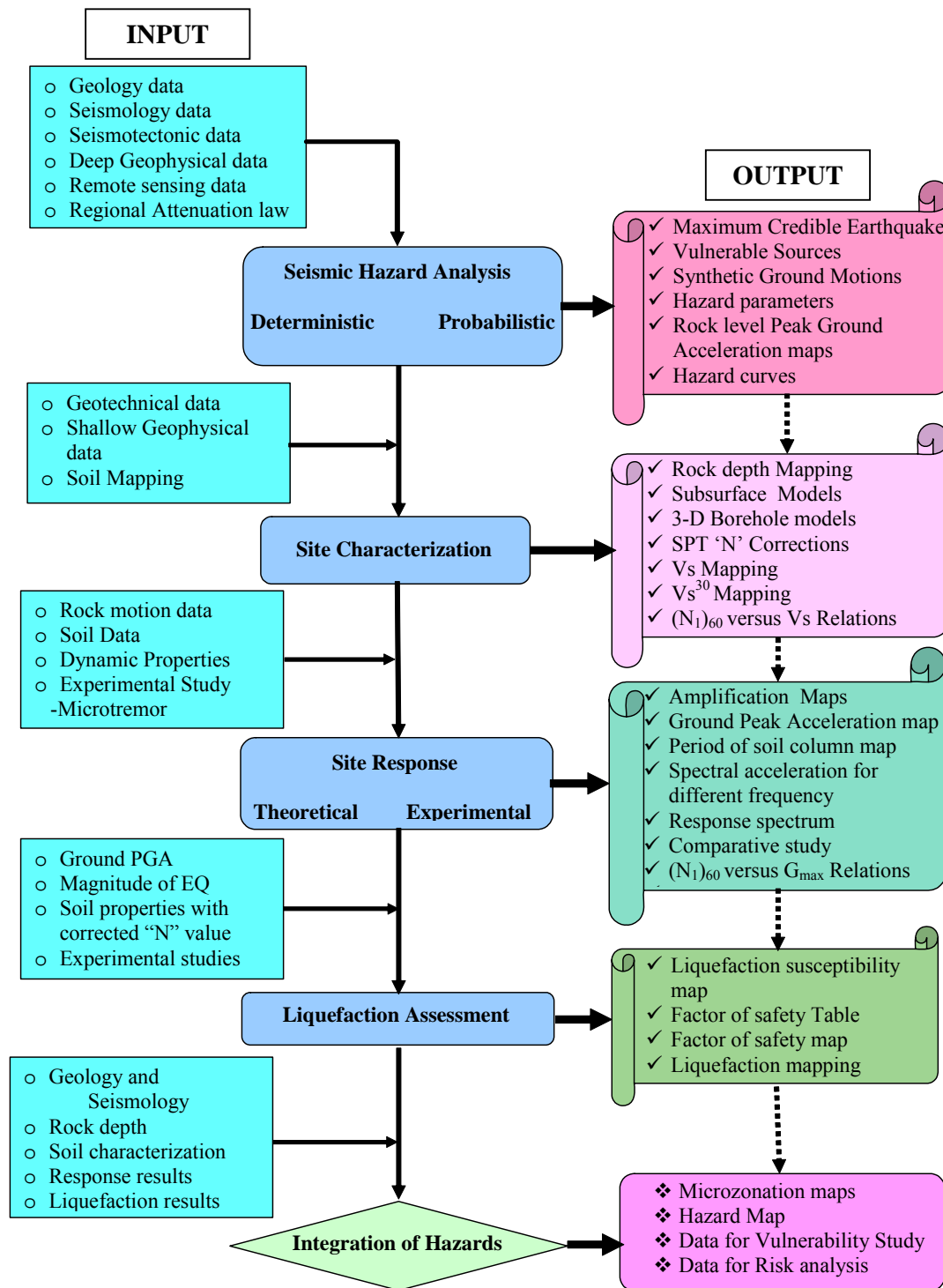
INPUT

- Geology data
- Seismology data
- Seismotectonic data
- Deep Geophysical data
- Remote sensing data
- Regional Attenuation law

OUTPUT

Seismic Hazard Analysis

Deterministic   Probabilistic

- ✓ Maximum Credible Earthquake
- ✓ Vulnerable Sources
- ✓ Synthetic Ground Motions
- ✓ Hazard parameters
- ✓ Rock level Peak Ground Acceleration maps
- ✓ Hazard curves

- Geotechnical data
- Shallow Geophysical data
- Soil Mapping

Site Characterization

- ✓ Rock depth Mapping
- ✓ Subsurface Models
- ✓ 3-D Borehole models
- ✓ SPT 'N' Corrections
- ✓ Vs Mapping
- ✓ Vs^{30} Mapping
- ✓ $(N_1)_{60}$ versus Vs Relations

- Rock motion data
- Soil Data
- Dynamic Properties
- Experimental Study -Microtremor

Site Response

Theoretical   Experimental

- ✓ Amplification Maps
- ✓ Ground Peak Acceleration map
- ✓ Period of soil column map
- ✓ Spectral acceleration for different frequency
- ✓ Response spectrum
- ✓ Comparative study
- ✓ $(N_1)_{60}$ versus G_{max} Relations

- Ground PGA
- Magnitude of EQ
- Soil properties with corrected "N" value
- Experimental studies

Liquefaction Assessment

- ✓ Liquefaction susceptibility map
- ✓ Factor of safety Table
- ✓ Factor of safety map
- ✓ Liquefaction mapping

- Geology and Seismology
- Rock depth
- Soil characterization
- Response results
- Liquefaction results

Integration of Hazards

- ❖ Microzonation maps
- ❖ Hazard Map
- ❖ Data for Vulnerability Study
- ❖ Data for Risk analysis

Figure 1: Flow Chart for Seismic Hazard and Microzonation
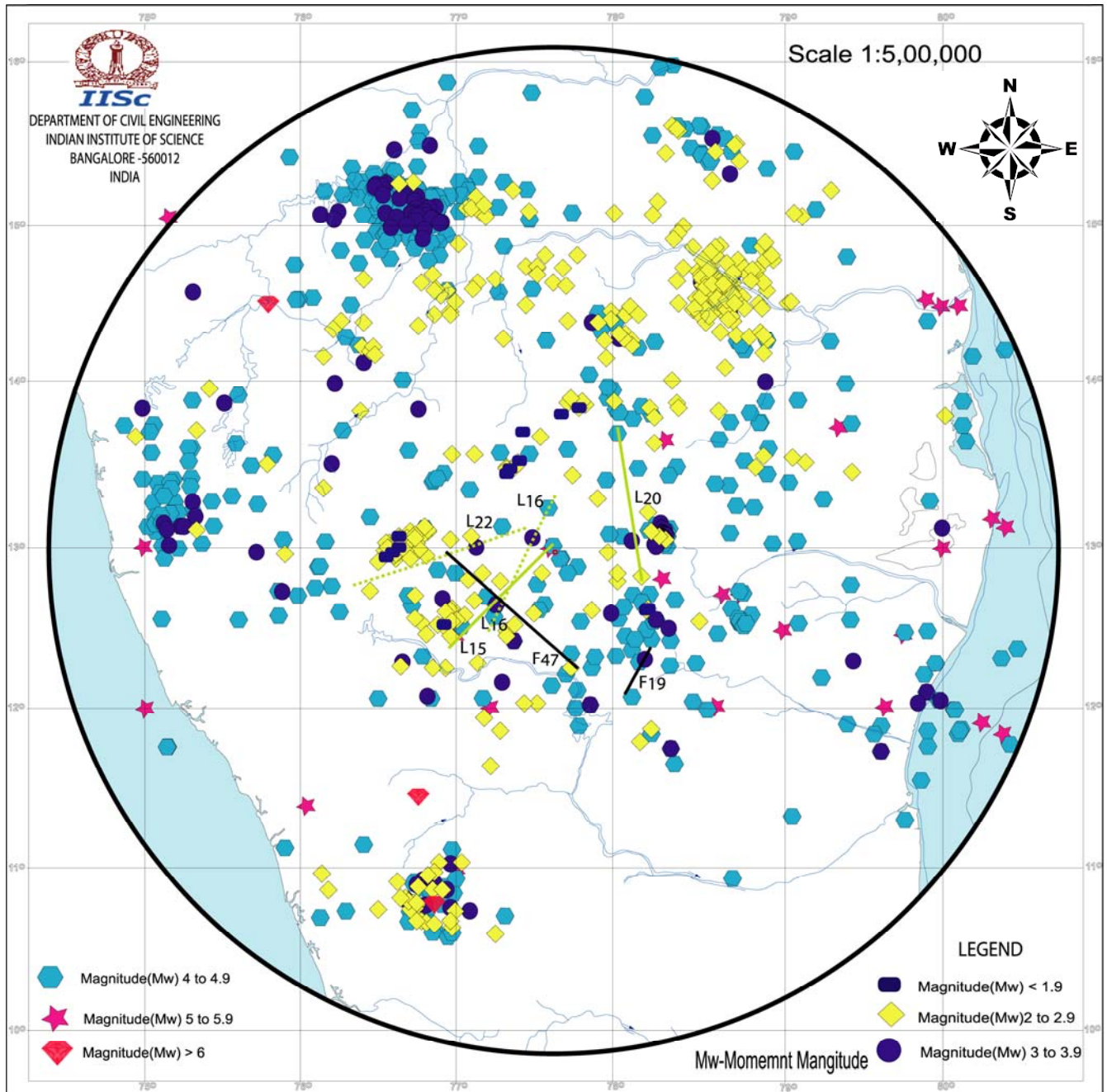
Figure 2: Seismotectonic map of Map of Bangalore region six seismogenic sources

In general, for the evaluation of seismic hazards for a particular site or region, all possible sources of seismic activity must be identified and their potential for generating future strong ground motion should be evaluated. The seismic sources are broadly classified as point source, line source and area sources. The seismic sources for this study were identified as line sources and mapped using geological, deep geophysical and remote sensing studies. The well defined and documented seismic sources are published in the Seismotectonic Atlas-2000 published by Geological Survey of India (SEISAT, 2000). Geological survey of India has compiled all the available geological, geophysical and seismological data for the entire India and has published a seismotectonic map in the year 2000.

Seismotectonic atlas contains 43 maps in 42 sheets of 3º x 4º sizes with scale of 1:1 million, which also describes the tectonic frame work and seismicity. This has been prepared with the intention that it can be used for the seismic hazard analysis of Indian cities. Ganesha Raj and Nijagunappa (2004) have also mapped major lineaments for Karnataka state with lengths more than 100 km using satellite remote sensing data and correlated with the earthquake occurrences. They have highlighted that there are 43 major lineaments and 33 earthquake occurrences with magnitude above 3 (since 1828) in the study area. About 23 of these earthquakes were associated with 8 major lineaments, which they have named as active lineaments. Both the above data have been used for the generated newly seismotectonic map of the study area (Sitharam et al, 2006 and Sitharam and Anbazhagan, 2007).

These sources matches well with major seismic sources considered by Bhatia et al (1997) for Global Seismic Hazard Assessment Program (GSHAP). The preferred fault plane solutions for the region generally indicate north-east south-west orientation with left-lateral strike slip motion. Alternate set of solution indicated in region is the thrust faulting along north-west orientation. GSHAP has delineated sources 70, 71 and 74 based on localized concentration of seismicity, along the Eastern Ghat region. The seismic source 72 is delineated to account some recent concentrated seismic activity in down south, near Trivandrum (Kerala state) along the western margin. It appears that this region has also been active in the historical times. In addition, the region around Latur is numbered as a seismic source zone 76. The source 69 covers the Godavari Graben region which had experienced a moderate sized earthquake of Magnitude 5.3 (known as Bhadrachalam earthquake), in the year 1969. The region around Bellary and Coimbatore have been demarcated as source zones 75 and 73 respectively on account of having experienced moderate sized earthquakes in the past (Bhatia et al, 1997).

Study Area for Microzonation

Bangalore city covers an area of over 220 square kilometers and it is at an average altitude of around 910 m above mean sea level (MSL). It is the principal administrative, industrial, commercial, educational and cultural capital of Karnataka state, in the South India (Figure 3). It experiences temperate and salubrious climate and an annual rainfall of around 940 mm. There were over 150 lakes, though most of them are dried up due to erosion and encroachments leaving only 64 at present in an area of 220 sq km. These tanks were once distributed throughout the city for better water supply facilities and are presently in a dried up condition, the residual silt and silty sand forming thick deposits over which buildings/structures have been erected. These soil conditions may be susceptible for site amplification during excitation of seismic waves. The population of Bangalore region is over 6 million. It is situated on a latitude of 12º 58' North and longitude of 77º 37' East. Bangalore city is the fastest growing city and fifth biggest city in India. Bangalore possesses many national laboratories, defence establishments, small and large-scale industries and Information Technology Companies. These establishments have made Bangalore a very important and strategic city. Because of density of population, mushrooming of buildings of all kinds from mud buildings to RCC framed structures and steel construction and, improper and low quality construction practice, Bangalore is vulnerable even against average earthquakes (Sitharam et al, 2006). The recent studies by Ganesha Raj and Nijagunappa (2004), Sitharam et al. (2006) and Sitharam and Anbazhagan (2007) have suggested that Bangalore need to be upgraded from the present seismic zone II (BIS, 2002) to zone III based on the regional seismotectonic details and hazard analysis. Hence sub soil classification for the Bangalore region is important to evaluate seismic local site effects for an earthquake.
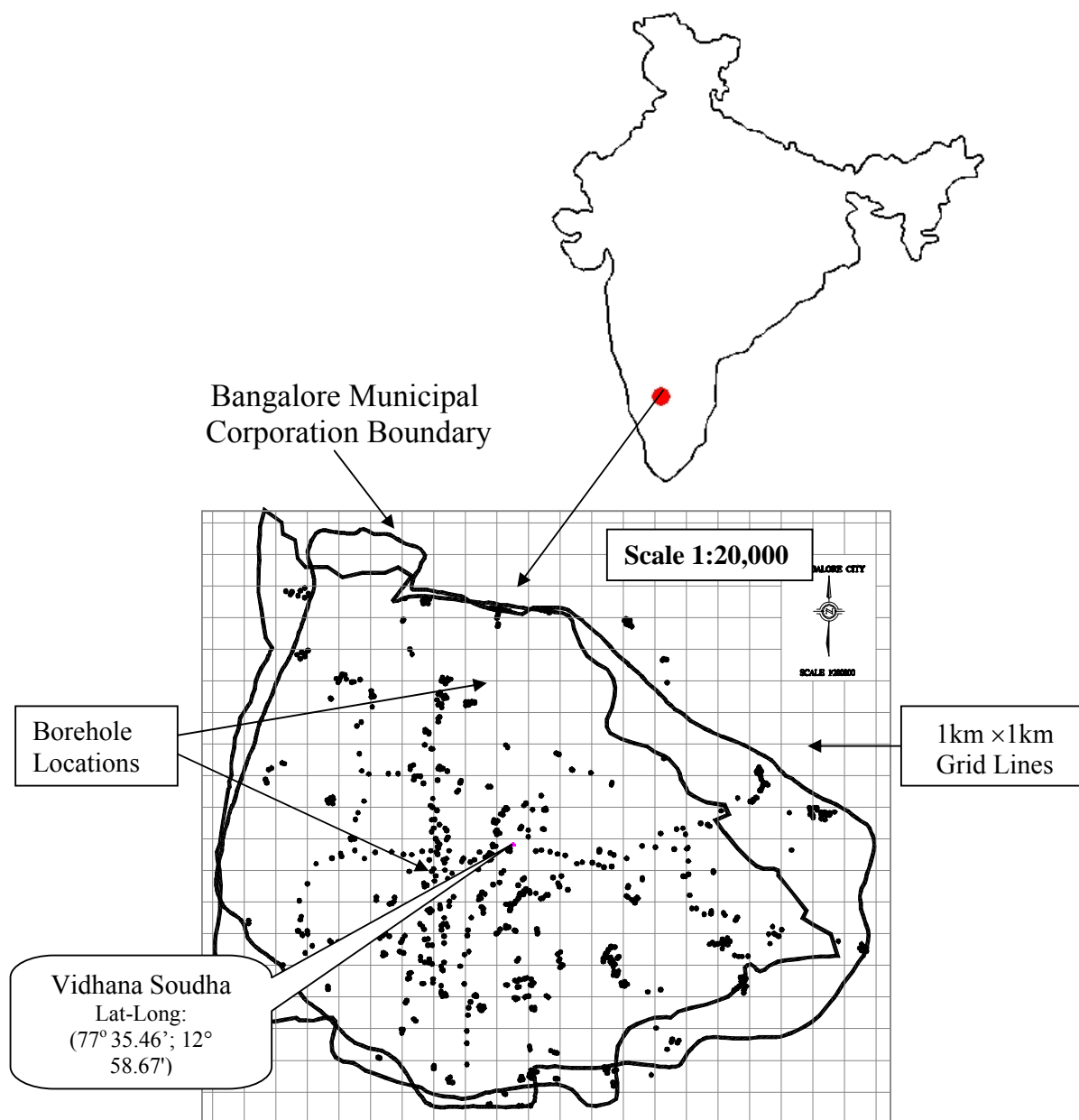
Figure 3: Study area with SPT borehole locations

Deterministic Seismic Hazard Analysis

Deterministic Seismic Hazard Analysis (DSHA) for Bangalore has been carried out by considering the past earthquakes, assumed subsurface fault rupture lengths and point source synthetic ground motion model. The seismic sources for region have been collected by considering seismotectonic atlas map of India and lineaments identified from satellite remote sensing images. Analysis of lineaments and faults help in understanding the regional seismotectonic activity of the area. Maximum Credible Earthquake (MCE) has been determined by considering the regional seismotectonic activity in about 350 km radius around Bangalore. Earthquake data are collected from IMD, USGS, NGRI, CESS, BARC, ASC and other public domain sites. Source magnitude for each source is chosen from the

maximum reported past earthquake close to that source and shortest distance from each source to Bangalore is arrived from the newly prepared seismotectonic map of the area. Using these details, and, attenuation relation developed for southern India by Iyengar and Raghukanth (2004), the peak ground acceleration (PGA) has been estimated. A parametric study has been carried out to find the fault subsurface rupture length using past earthquake data and Wells and Coppersmith (1994) relation between the subsurface lengths versus earthquake magnitudes. About more than 60% of earthquake magnitude matches for the subsurface length corresponding to 3.8% of the total length of fault. Assuming 3.8 % of the total length of fault as the subsurface rupture length, the expected maximum magnitude for each source has been evaluated and PGA is estimated for these magnitudes. Further seismological model developed by Boore (1983, 2003) SMSIM program has been used to generate synthetic ground motions from seismogenic sources identified in the above two methods. Typical ground motion and spectral acceleration at rock level is shown in Figures 4 and 5. From the above three approaches maximum PGA of 0.15g was estimated for Bangalore. This value was obtained for a maximum credible earthquake (MCE) having a moment magnitude of 5.1 from a source of Mandya-Channapatna-Bangalore lineament. Considering this lineament and MCE, a synthetic ground motion has been generated for 850 borehole locations (Figure 3) and they are used to prepare PGA map at rock level (Figure 6).
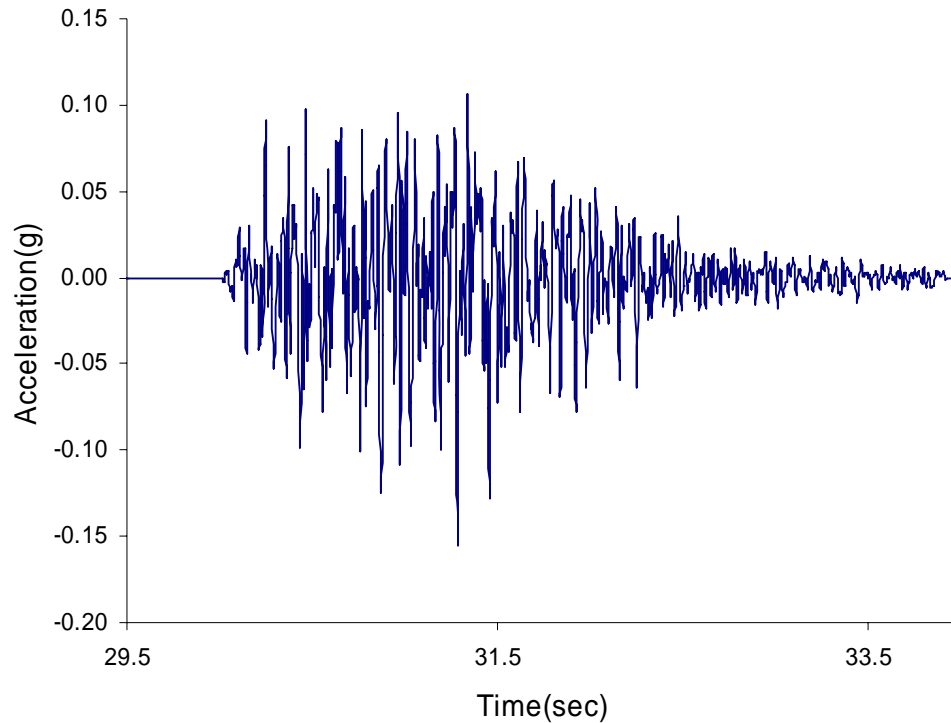

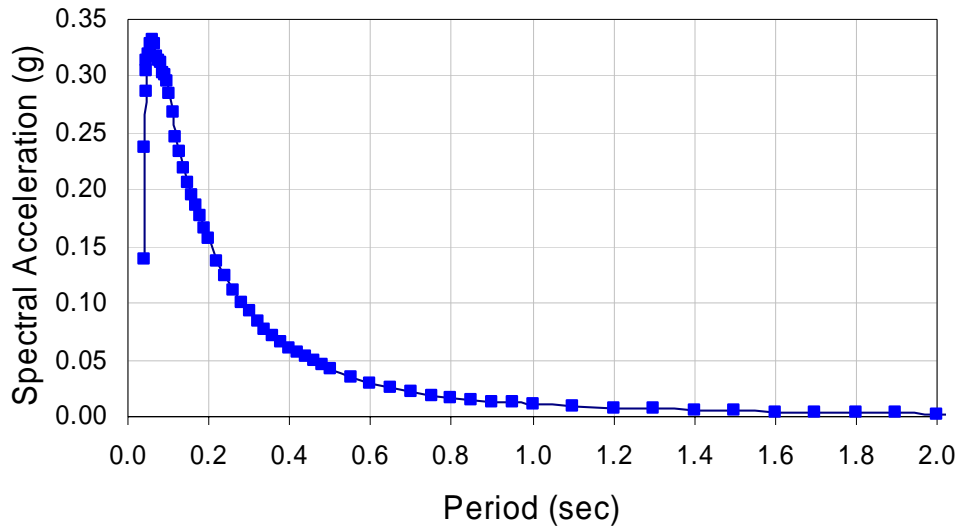**Figure 4: Typical synthetic ground motion for rock site**

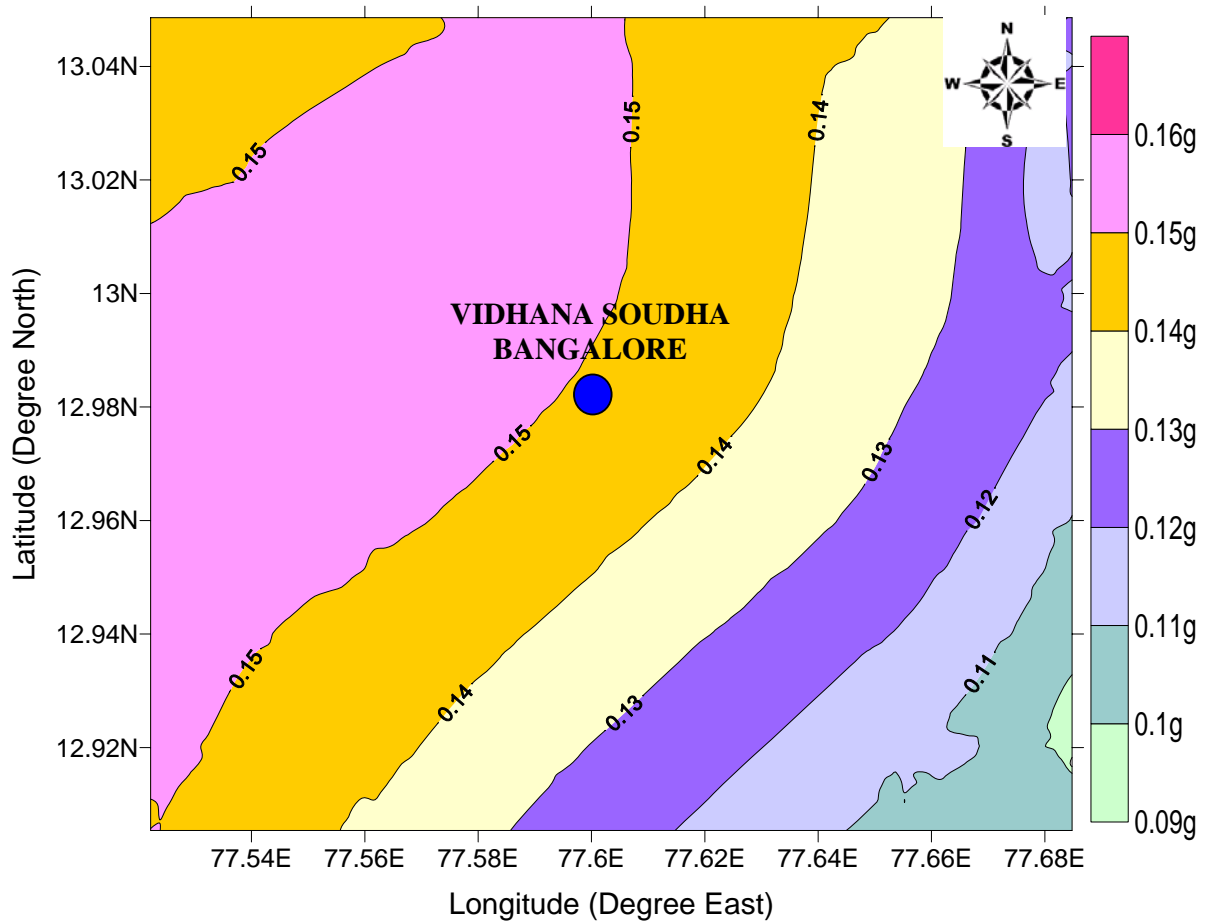**Figure 5: Typical Response spectra at Rock level**

Figure 6: Rock Level PGA Map for Bangalore

Probabilistic Seismic Hazard Analysis

Analyses have been carried out considering the seismotectonic region covering a circular area with a radius of 350km keeping Bangalore as the center. Seismic hazard parameter 'b' has been evaluated considering the available earthquake data using (1) Gutenberg–Richter (G-R) relationship and (2) Kijko and Sellevoll (1989, 1992) method utilizing extreme and complete catalogs. The 'b' parameter was estimated to be 0.87 from G - R relation and 0.87± 0.03 from Kijko and Sellevoll method. The obtained results are comparable with the 'b' values published earlier for southern India. Further, probabilistic seismic hazard analysis for Bangalore region has been carried out considering six seismogenic sources. From the analysis, mean annual rate of exceedance and cumulative probability hazard curve for Peak Ground Acceleration (PGA) and Spectral Acceleration (SA) have been generated. The mean annual rate of exceedance versus peak ground acceleration for all the sources at rock level is shown in Figure 7. Cumulative mean annual rate of exceedance versus spectral acceleration for period of 1 second and 5% damping (represented as hazard curve) is shown in Figure 8. In addition, Uniform Hazard Response Spectrum (UHRS) at rock level is also developed for the 5 % damping corresponding to 10 % probability of exceedance in 50 years. The peak ground acceleration (PGA) value of 0.121g obtained from the present investigation and it is comparable to PGA values obtained from deterministic seismic hazard analysis (DSHA) for the same area by Sitharam et al (2006) and Sitharam and Anbazhagan (2007). However, the PGA value obtained from the current investigation is higher than the Global Seismic Hazard Assessment Program (GSHAP) maps of Bhatia et al (1997) for the shield area. The study brings that the probabilistic and deterministic approaches will lead to similar answers complementing each other and provides additional insights to the seismic hazard assessment.
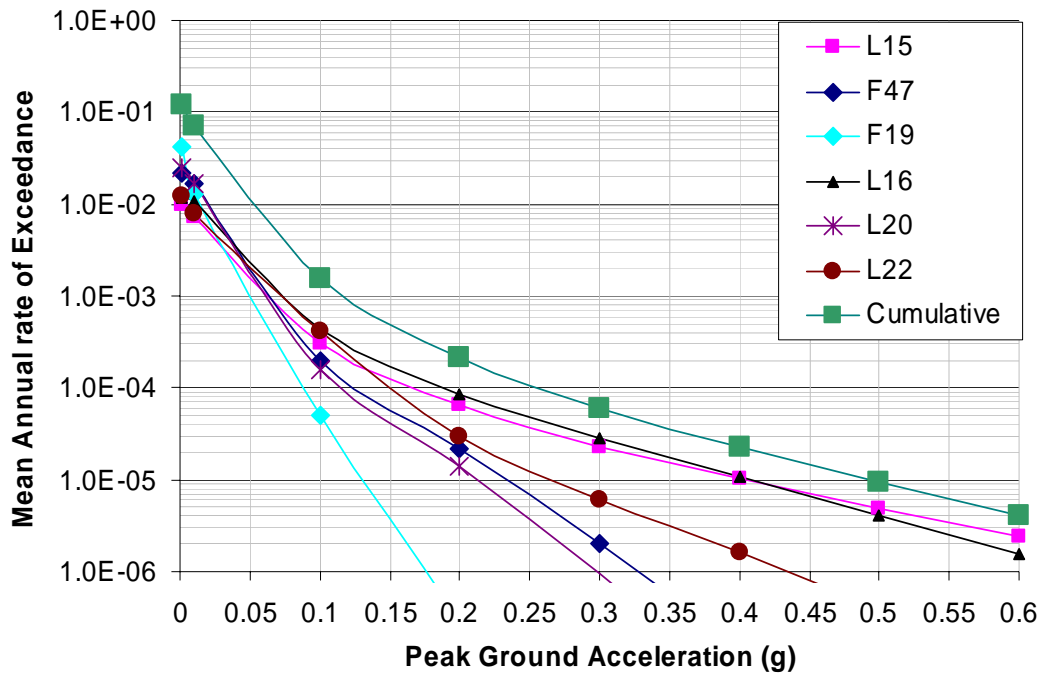

Figure 7: Hazard curves for different sources at the rock level for Bangalore

Site Characterization using geotechnical data (SPT)

The 3-D subsurface model with geotechnical data has been generated with development of base map of Bangalore city (220sq.km) with several layers of information (such as Outer and Administrative boundaries, Contours, Highways, Major roads, Minor roads, Streets, Rail roads, Water bodies, Drains, Landmarks and Borehole locations). GIS database for collating and synthesizing geotechnical data available with different sources and 3-dimensional view of soil stratum presenting various geotechnical parameters with depth in appropriate format has been developed. Figure 9 shows the GIS

model of borehole locations with respect to water features. Figure 10 shows the isometric view of some boreholes by overlapping of layers to get a 3-D projection. In the context of prediction of reduced level of rock (called as "engineering rock depth" corresponding to about Vs > 700 m/sec) in the subsurface of Bangalore and their spatial variability evaluated using geostatistical models such as ordinary kriging technique, Artificial Neural Network (ANN) and Support Vector Machine (SVM). Observed SPT 'N' values are corrected by applying necessary corrections, which can be used for engineering studies such as site response and liquefaction analysis.
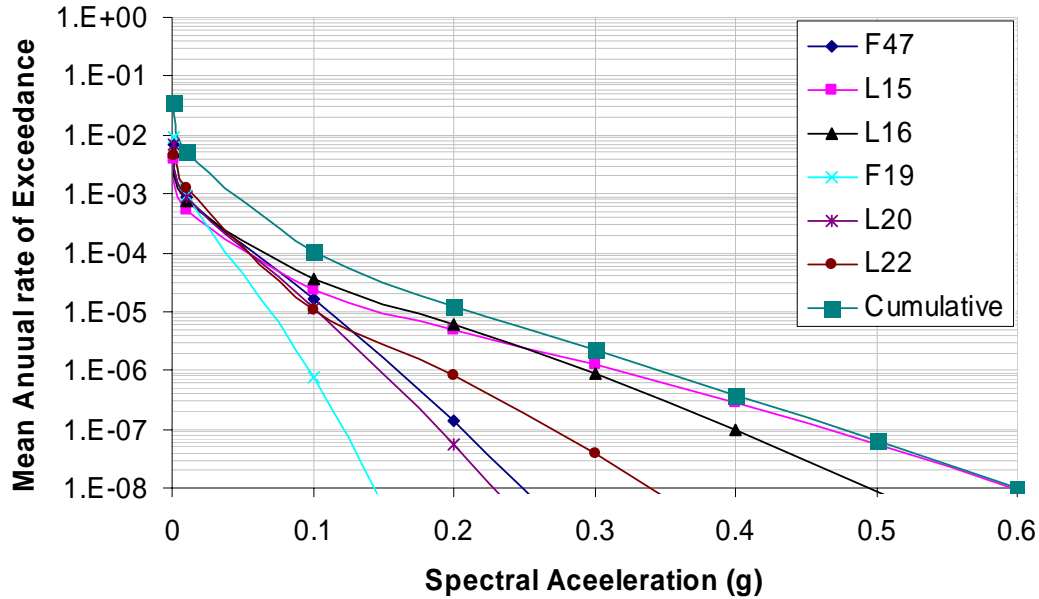
Figure 8: Spectral acceleration at the rock level corresponding to a period of 1s and 5% damping for Bangalore

From the 3-D subsurface model of geotechnical bore log data developed by Sitharam et. al, (2007), authors have identified that the overburden thickness of study area varies from 1m to about 40m. Subsurface profile information like unit weight, ground water level, SPT 'N' values are obtained from borehole data collected and compiled in the study area for the development of geotechnical subsurface model. With their wide distribution of data in the study area, these bore holes are considered to represent the typical features of soil profiles. Based on the nature of soils, classification of soils has been done for general identification of soil layers. Layer thickness and type of material are summarized in Table1. The 'N' values measured in the field using Standard penetration test procedure have been corrected for various corrections, such as:(a) Overburden Pressure (C_N), (b) Hammer energy (C_E), (c) Bore hole diameter (C_B), (d) presence or absence of liner (C_S), (e) Rod length (C_R) and (f) fines content (C_{fines}) (Seed et al., 1983; Skempton, 1986; Youd et al., 2001 and Cetin et al., 2004). First, corrected 'N' value i.e., $(N_1)_{60}$ are obtained using the following equation:

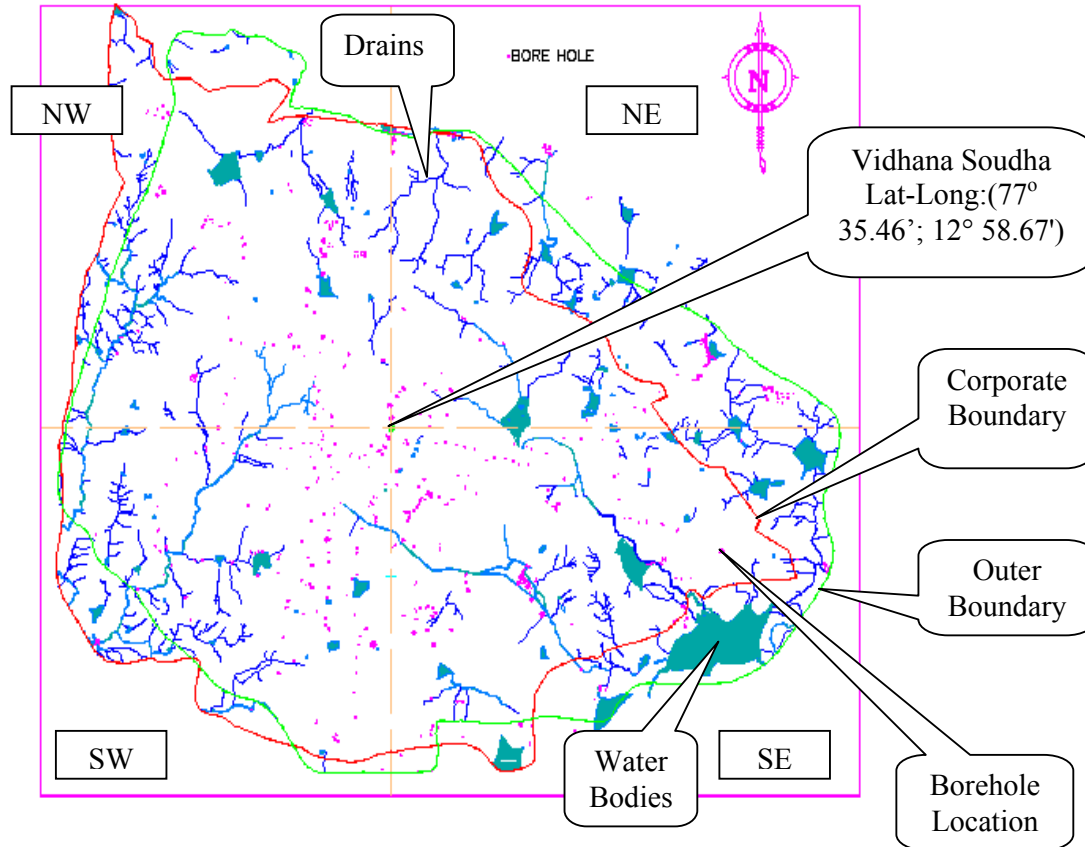$$(N_1)_{60} = N \times (C_N \times C_E \times C_B \times C_S \times C_R) \tag{1}$$

Figure 9: GIS model of borehole locations with respect to water features
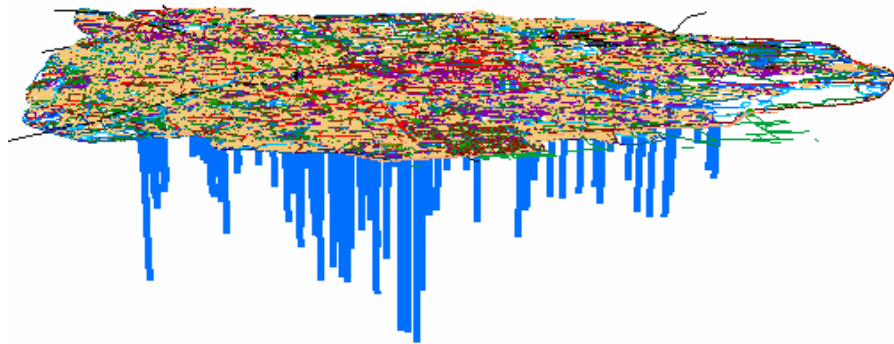

Figure 10: GIS model of borehole locations in 3-D view

Then this corrected 'N' values $(N_1)_{60}$ is further corrected for fines content based on the revised boundary curves derived by Idriss and Boulanger (2004) for cohesionless soils as described below:

$$(N_1)_{60cs} = (N_1)_{60} + \Delta(N_1)_{60} \tag{2}$$

$$\Delta(N_1)_{60} = \exp\left[1.63 + \frac{9.7}{FC + 0.001} - \left(\frac{15.7}{FC + 0.001}\right)^2\right] \tag{3}$$

FC = percent fines content (percent dry weight finer than 0.074mm).
A typical "N" correction calculation table for a borehole data is shown in Table 2.

Table 1: Soil Distribution in Bangalore

Layer	Soil Description with depth and Direction			
	Northwest	Southwest	Northeast	Southeast
First Layer	Silty sand with clay 0-3m	Silty sand with gravel 0-1.7m	Clayey sand 0-1.5m	Filled up soil 0-1.5m
Second layer	Medium to dense silty sand 3m-6m	Clayey sand 1.7m-3.5m	Clayey sand with gravel 1.5m-10m	Silt sandy with clay 1.5m-9m
Third Layer	Weathered Rock 6m-17m	Weathered Rock 3.5m-8.5m	Silty sand with Gravel 10m-15.5m	Sandy clay 9m-17.5m
Fourth layer	Hard Rock Below the 17m	Hard Rock Below 8.5m	Weathered rock 15.5m-27.5m	Weathered Rock 17.5m-38.5m
Fifth Layer	Hard Rock	Hard Rock	Hard Rock Below 27.5m	Hard Rock Below 38.5m

Site characterization using Shear Wave Velocity profiles by MASW

Site characterization has also been carried out using measured shear wave velocity with the help of shear wave velocity survey using MASW. MASW (Multichannel Analysis of Surface Wave) is a geophysical method, which generates a shear-wave velocity (*Vs*) profile (i.e., *Vs* versus depth) by analyzing Raleigh-type surface waves on a multichannel record. MASW system consisting of 24 channels Geode seismograph with 24 geophones of 4.5 Hz capacity were used in this investigation. The shear wave velocity of Bangalore subsurface soil has been measured and correlation has been developed for shear wave velocity (Vs) with the standard penetration tests (SPT) corrected 'N' values. About 58 one-dimensional (1-D) MASW surveys and 20 two-dimensional (2-D) MASW surveys has been carried out with in 220 sq.km Bangalore urban area. The test locations are selected such a way that these represent the entire city subsurface information (Figure 11). Most of the survey locations are selected in flat ground and also in important places like parks, hospitals, schools and temple yards etc. The optimum field parameters such as source to first and last receiver, receiver spacing and spread length of survey lines are selected in such a way that required depth of information can be obtained. All tests has been carried out with geophone interval of 1m, source has been kept on both side of the spread and source to the first and last receiver were also varied from 5m, 10m and 15m to avoid the effects of near-field and far-field. These source distances will help to record good signals in very soft, soft and hard soils. The exploration services section at the Kansas Geological Survey (KGS) has suggested offset distance for very soft, soft and hard soil as 1m to 5m, 5m to 10m and 10m to 15m respectively (Xu et al., 2006).

Dispersion curves and shear velocity 1-D and 2-D have been evaluated using SurfSeis software. The average shear wave velocity for the depth "d" of soil is referred as V_H. The average shear wave velocity up to a depth of H (V_H) is computed as follows:

$$V_H = \sum d_i / \sum (d_i / v_i) \tag{4}$$

Where $\sum d_i$ = cumulative depth in m.
For 30m average depth, shear wave velocity is written as:

$$Vs^{30} = \frac{30}{\sum_{i=1}^{N} \left(\frac{d_i}{v_i} \right)} \tag{5}$$

13

Table 2. Typical "N" correction Table for borelog

Borehole 4														Water Table = 1.4 m/19-11-2005
Depth	Field	Density	T.S	E.S	C_N	Correction Factors For				$(N_1)_{60}$	F.C	$\Delta(N_1)_{60}$	Corrected N value
m	N Value	kN/m³	kN/m²	kN/m²		Hammer Effect	Bore hole Dia	Rod Length	Sample Method		%		$(N_1)_{60cs}$
1.50	19	20.00	30.00	30.00	1.47	0.7	1.05	0.75	1	15.36	48	5.613	21
3.50	28	20.00	70.00	50.38	1.29	0.7	1.05	0.8	1	21.26	43	5.597	27
4.50	26	20.00	90.00	60.57	1.22	0.7	1.05	0.85	1	19.79	60	5.602	25
6.00	41	20.00	120.00	75.86	1.12	0.7	1.05	0.85	1	28.77	48	5.613	34
7.50	55	20.00	150.00	91.14	1.04	0.7	1.05	0.95	1	40.02	37	5.541	46
9.00	100	20.00	180.00	106.43	0.97	0.7	1.05	0.95	1	67.84	28	5.270	73
10.50	100	20.00	210.00	121.71	0.91	0.7	1.05	1	1	66.90	28	5.270	72
12.50	100	20.00	250.00	142.09	0.84	0.7	1.05	1	1	61.70	28	5.270	67

T.S - Total Stress

E.S - Effective Stress

C_N – Correction for overburden correction

$(N_1)_{60}$ – Corrected 'N' Value before correction for fines content

F.C – Fines content

$\Delta(N_1)_{60}$ – Correction for Fines content
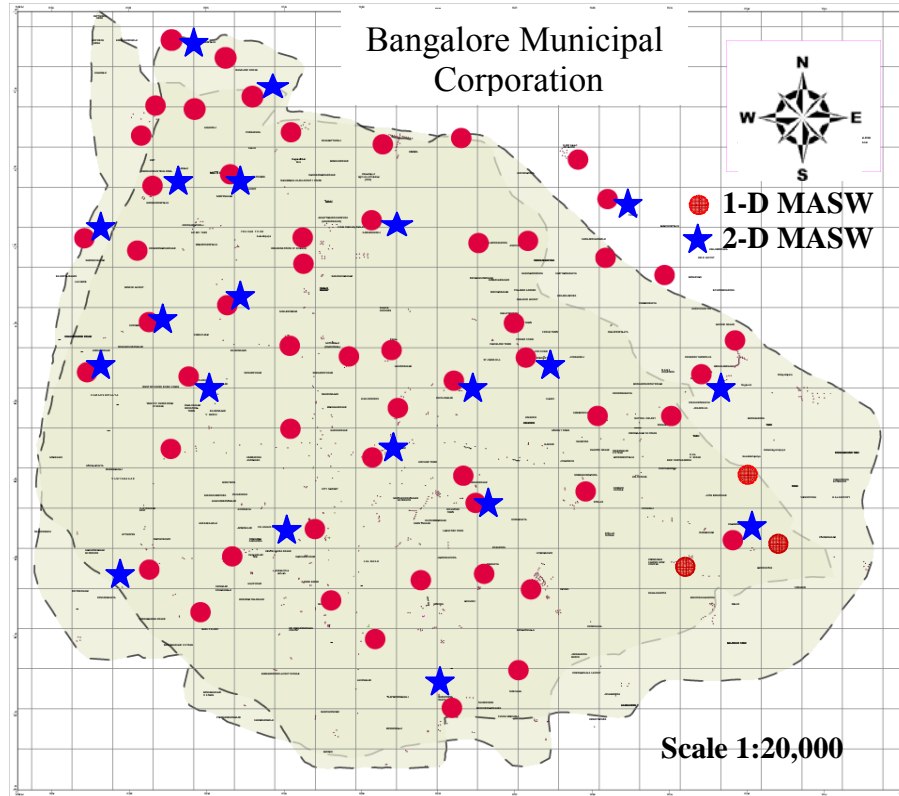
$(N_1)_{60cs}$ – Corrected 'N' Value

Figure 11: Study area with Marked MASW Testing Locations

where d_i and v_i denote the thickness (in meters) and shear-wave velocity in m/s (at a shear strain level of 10^{-5} or less) of the ith formation or layer respectively, in a total of N layers, existing in the top 30 m. Vs^{30} is accepted for site classification as per NEHRP (National Earthquake Hazard Research Programme) classification and also UBC classification (Uniform Building Code in 1997) [Dobry et al. 2000; Kanli et. al, 2006]. In order to figure out the average shear wave velocity distribution in Bangalore, the average velocity has been calculated using the equation (4) for each location. A simple spread sheet has been generated to carry out the calculation, as shown in Table 3. The Vs average has been calculated for every 5m depth interval up to a depth of 30m and also average Vs for the soil overburden has been calculated. Usually, for amplification and site response study the 30m average Vs is considered. However, if the rock is found within a depth of about 30m, near surface shear wave velocity of soil has to be considered. Otherwise, Vs^{30} obtained will be higher due to the velocity of the rock mass. In Bangalore the soil overburden thickness varies from 1m to about 40m. Hence, for overburden soil average Vs has also been calculated based on the soil thickness corresponding to the location, which is also shown in column 4 of Table 3. Using 1-dimensional shear wave velocity, the average shear wave velocity of Bangalore soil has been evaluated for depths of 5m, 10m, 15m, 20m, 25m and 30m (Vs^{30}) depths. Figure 12 shows the map of average shear wave velocity for a depth of 30m. The calculated average shear wave velocities are grouped according to the NEHRP site classes (Table 4) and map has been generated. The sub soil classification has been carried out for local site effect evaluation based on average shear wave velocity of 30m depth (Vs^{30}) of sites using NEHRP and UBC classification. Bangalore falls into "site class D" type of soil. Mapping clearly indicates that the depth of soil obtained from MASW is closely matching with the soil layers in the bore logs.

Table 3: Typical average shear wave velocity calculation

Depth (m)	Vs (m/s)	Soil thickness [d_i] (m)	Average Vs Soil-7.2m	Average Vs-5m	Average Vs-10m	Average Vs-15m	Average Vs-20m	Average Vs-25m	Average Vs-30m
-1.22	316	-1.2	259	265	286	310	338	362	306
-2.74	250	-1.5							
-4.64	255	-1.9							
-7.02	241	-2.4							
-10.00	388	-3.0							
-13.71	355	-3.7							
-18.36	435	-4.6							
-24.17	527	-5.8							
-31.43	424	-7.3							
-39.29	687	-7.9							

Table 4: Site Classes for average shear wave velocity

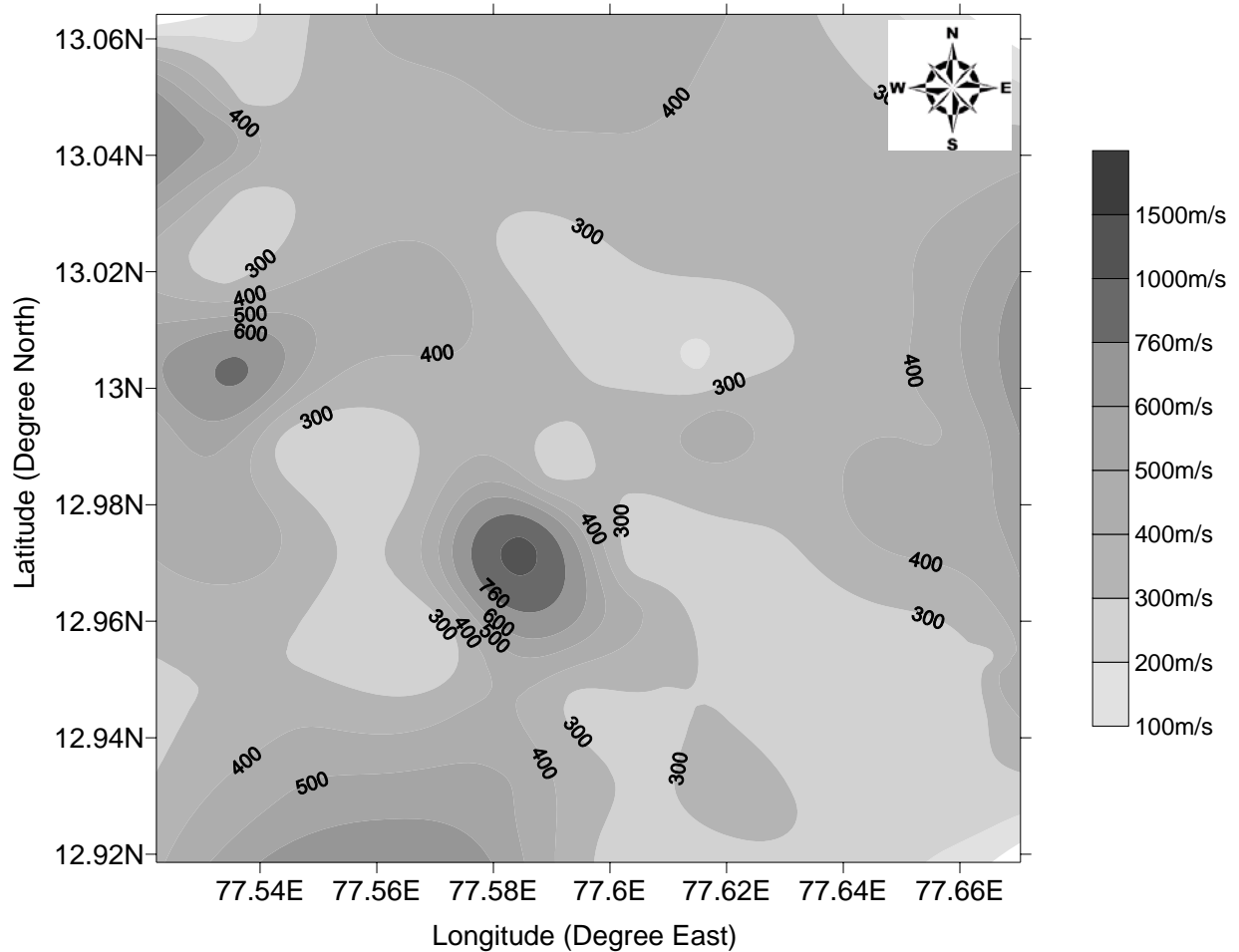| Site Class	Range of average shear wave velocity (m/s)
A	$1500 < Vs^{30}$
B	$760 < Vs^{30} \leq 1500$
C	$360 < Vs^{30} \leq 760$
D	$180 < Vs^{30} \leq 360$
E	$Vs^{30} < 180$

Figure 12: Average shear wave velocity for 30m Depth

Mapping of Subsurface Layers

2-D MASW test has been carried out at 20 locations with minimum length of 12m. Inbuilt kriging operation has been used to make interpolation of each mid point velocity and generate the 2-D *Vs* profile for a mid point of first spread line to mid point of last spread line. Typical 2-D velocity profile is shown in Figure 13. From Figure 13, it is clear that shallow depth shear wave velocities are with in the range of 360m/s. When depth increases, the shear wave velocities also increase. General observation from the 2-D Vs profiles, material layers of velocity 300m/s and above is dipping, falling and tilting, which may be due to the undulation and variation in original ground elevation. Also there is no considerable ground layering anomaly present in the subsurface and few locations where filled up soil is found (earlier tank beds which are encroached for habitation).
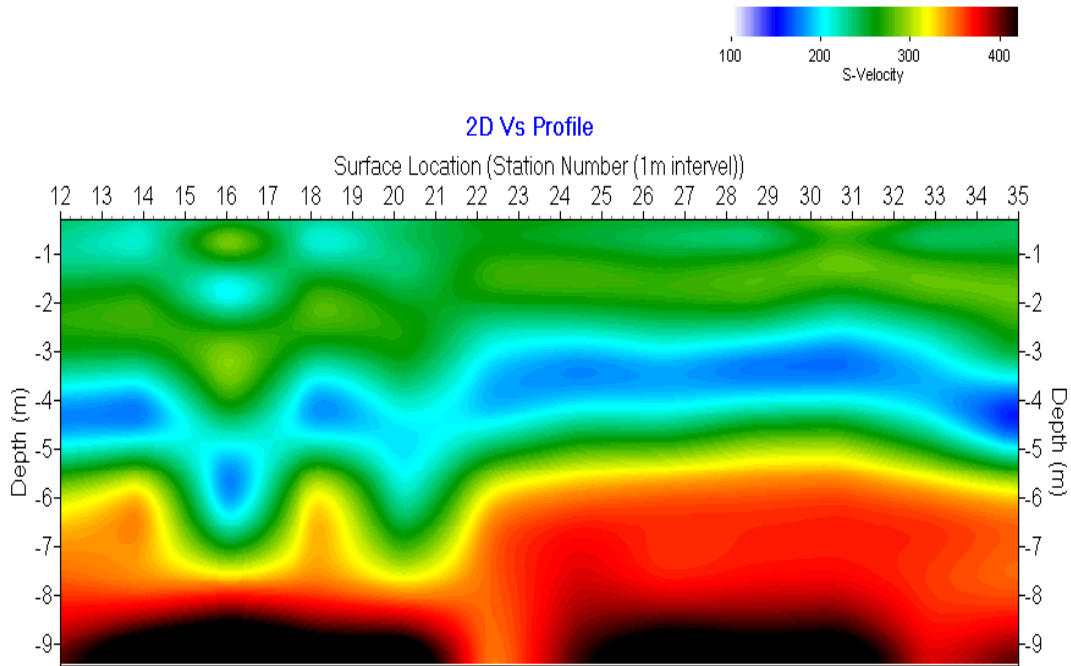
17

Figure 13: 2-D spatial variation of shear wave velocity

Correlation between $(N_1)_{60cs}$ AND V_S

The measured shear wave velocity at 38 locations were close to SPT boreholes, which are used to generate the correlation between the shear wave velocity and corrected 'N' values using a power fit. Prediction of ground shaking response at soil sites requires knowledge of shear modulus of the soil, which is directly expressed in terms of shear wave velocity. It is preferable to measure Vs directly by using field tests. However, presently it is not feasible to make Vs measurements at all the locations. Hence to make use of abundant available penetration measurements to obtain Vs values, correlation between Vs and penetration resistance are being done. Velocity calculated using 1-D MASW which represents Vs at mid point of each survey line, has been used for this purpose. About 162 data pairs of Vs and SPT corrected below count have been used for the regression analysis. The Vs values are selected from the 1-D MASW results corresponding to SPT "N" value at different depths. The regression equation developed between Vs and $(N_1)_{60cs}$ is given in equation 6 (with regression coefficient of 0.84):

$$Vs = 78[(N_1)_{60cs}]^{0.40} \tag{6}$$

Where, Vs is the shear wave velocity in m/s and $(N_1)_{60cs}$ is the corrected SPT 'N' value.

Japan Road Association (JRA, 1980) equations (equation 7 -for clayey soil and equation 8- for sandy soil), relating Vs and N_{60} are given below:

$$Vs = 100(N_{60})^{1/3} \quad \text{(JRA, 1980)- For clayey soil} \tag{7}$$

$$Vs = 80(N_{60})^{1/3} \quad \text{(JRA, 1980)} \quad \text{- For Sandy soil} \tag{8}$$

The coefficients are close to the value for the sandy soil. From the comparison between JRA equations with newly developed equation (6), it is clear that the fitted equation lies between the JRA equations for sandy and clay equations for wide range of "$(N_1)_{60cs}$" values, because the soil overburden in Bangalore has sand and silt with some percentage of clay content. Also, developed relationship between shear wave velocity and corrected 'N' values corresponds well with the published relationships of Japan Road Association.

Local site effects and Site Response

Bangalore city, a fast growing urban center, with low to moderate earthquake history and highly altered soil structure (due to large reclamation of land) is been the focus of this work. There were over 150 lakes, though most of them are dried up due to erosion and encroachments leaving only 64 at present in an area of 220 sq km. In the present study, an attempt has been made to assess the site response using geotechnical, geophysical data and field studies. The subsurface profiles of the study area within 220sq.km area was represented by 160 geotechnical bore logs (Figure 14) and 58 shear wave velocity profiles obtained by MASW survey. The data from these geotechnical and geophysical technique have been used to study the site response. These soil properties and synthetic ground motions for each borehole locations are further used to study the local site effects by conducting one-dimensional ground response analysis using the program SHAKE2000. The non-linearity of the shear modulus and damping is accounted for by the use of equivalent linear soil properties using an iterative procedure to obtain values for modulus and damping compatible with the effective strains in each layer as discussed above. The degradation curves for sand and rock used for the present work are those proposed by Seed and Idriss (1970) and Schnabel (1973) respectively. The response and amplification spectrum have been evaluated for each layer of borehole location. The map shows the peak acceleration at ground surface, amplification factor, period of the soil column, peak spectral acceleration, frequency corresponding to the peck spectral acceleration and the response spectrum at the ground surface of frequency of 1.5Hz, 3Hz, 5Hz, 8Hz and 10Hz for a 5% damping ratio. The microzonation maps prepared indicates a medium variation in amplification potential. There is a need for quantifying the number of times the PHA value at bedrock is amplified by the time it reaches the ground surface as stated in the previous section. The term "Amplification Factor" is hence used here to refer to the ratio of the peak horizontal acceleration at the ground surface to the peak horizontal acceleration at the bedrock. This factor is evaluated for all the boreholes using the PHA at bedrock obtained from the synthetic acceleration time history for each borehole and the peak ground surface acceleration obtained as a result of ground response analysis using SHAKE 2000. With the amplification factors varying from 1 to 4.7 and period of soil column from 0.08 to 4.5 seconds, the region is moderately amplifying. The amplification factor map for Bangalore City is shown in Figure 15. The spectral acceleration (SA) values for all the locations at 1.5 Hz, 3 Hz, 5Hz, 8 Hz and 10 Hz are computed and SA corresponding to a frequency of 8Hz is shown in Figure 16. A peculiar feature of the study region is that it has reclaimed land from silted lakes/tanks leading to significant variations in ground response.
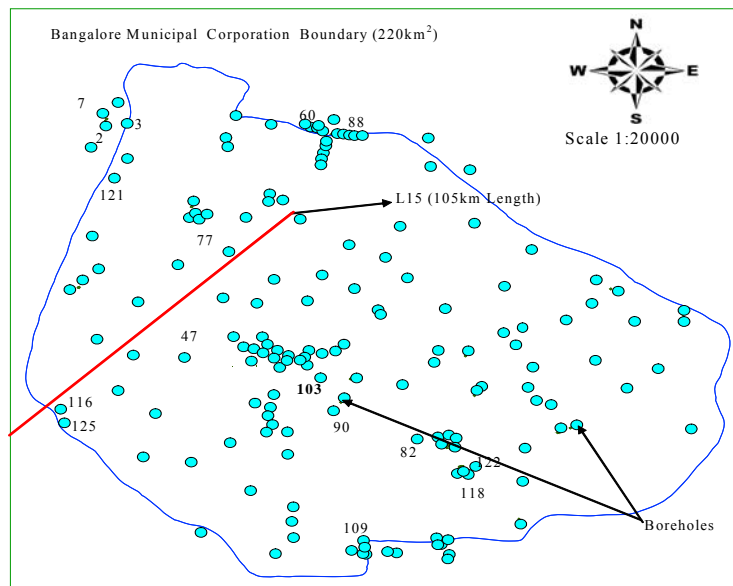

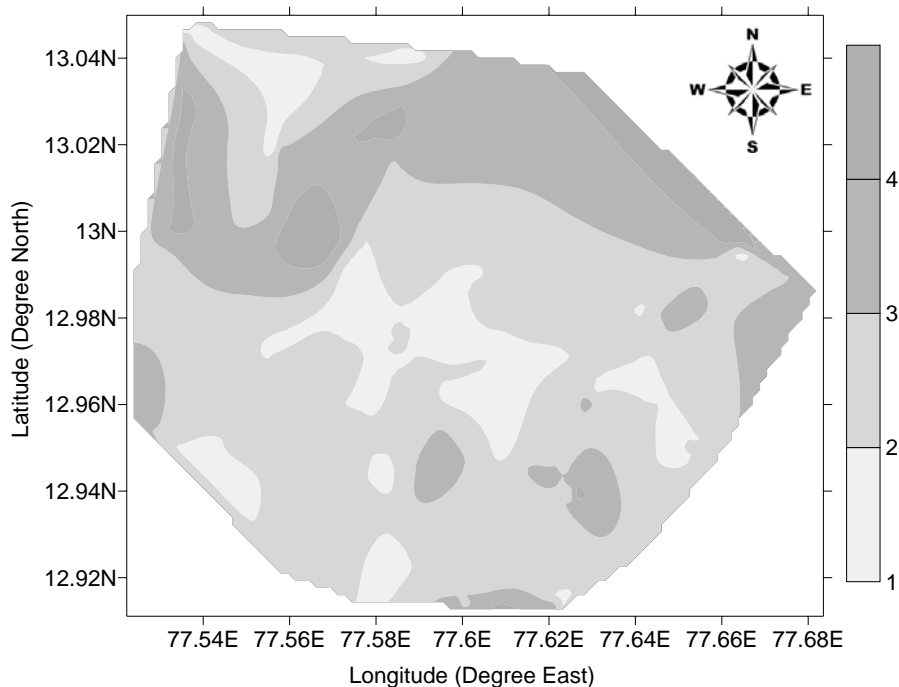**Figure 14: Location of the selected boreholes for site response study in Bangalore City**

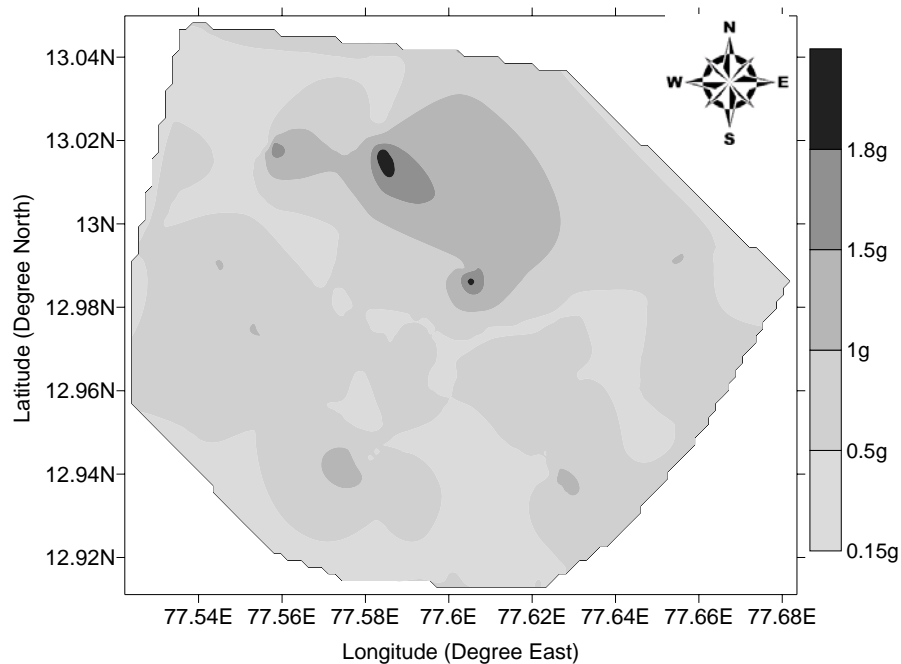**Figure 15: Amplification Factor map for Bangalore City**

Figure 16: Spectral Acceleration Map of Bangalore City at 8 Hz Frequency

Site Response study using shear wave velocity

Growth of geophysical methods particularly SASW (spectral analysis of surface wave) and MASW are being increasingly used for the site response study and microzonation of cities world wide. Shear wave velocities (Vs) measured using geophysical method are widely used to get better results of site response studies than SPT data.   Because, wave propagation theory shows that ground motion amplitude depends on the density and shear wave velocity of subsurface material (Bullen, 1965; Aki and Richards, 1980). Usually density has relatively little variation with depth but shear wave velocity

is the logical choice for representing site conditions. The response spectrum for 5% damping at the ground surface obtained for 160 borehole locations and 58 MASW survey locations clearly indicate that the range of spectral acceleration (SA) at different frequencies varied from 0.01 to 2.17g. Response parameter obtained using MASW data is comparable with the results of SPT. However results from MASW is lower than the results from SPT. Peak spectral acceleration values at lower period using MASW data is lower than SPT data, but the higher period values matches well for both the data. The shape of the amplification spectrum obtained using both data matches well, however values of amplification ratio from MASW data is lower than the SPT data, typical one is shown in Figure 18.
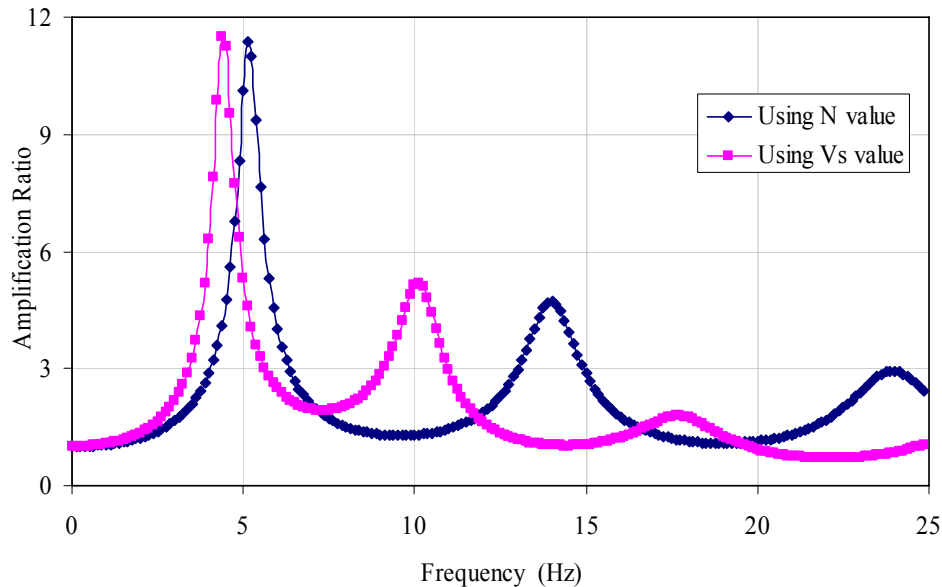
Figure 18: Typical Amplification Ratio Using Both Data

Predominant Frequency of Soil using site Response study

A single parameter widely used to categorize the soil for a ground motion is the predominant frequency, which is mainly, depends on the soil column height and its properties. The predominant frequency is defined as frequency of vibration corresponding to the maximum value of Fourier amplitude. In this study predominant frequency of soil column is obtained from Fourier spectrum estimated using SHAKE2000. Predominant frequencies of each borelog are estimated using both SPT data and MASW data. Results shows that predominant frequencies are similar from both analysis and varies from 3Hz to 12Hz using SPT data and 3.5Hz to 12Hz using MASW data. To find the variation of predominant frequencies from both method, the site response study (SHAKE2000 analyses) 33 points by SPT and MASW methods are considered. Predominant frequencies corresponding to these locations are presented in Figure 19. Figure 19 shows that predominant frequencies obtained from both data are comparable; values above the symbol are obtained using SPT data and below the symbol are obtained using MASW data. Table 5 shows that most of the study area has higher predominant frequency (3 Hz to 12.5 Hz) from both methods.
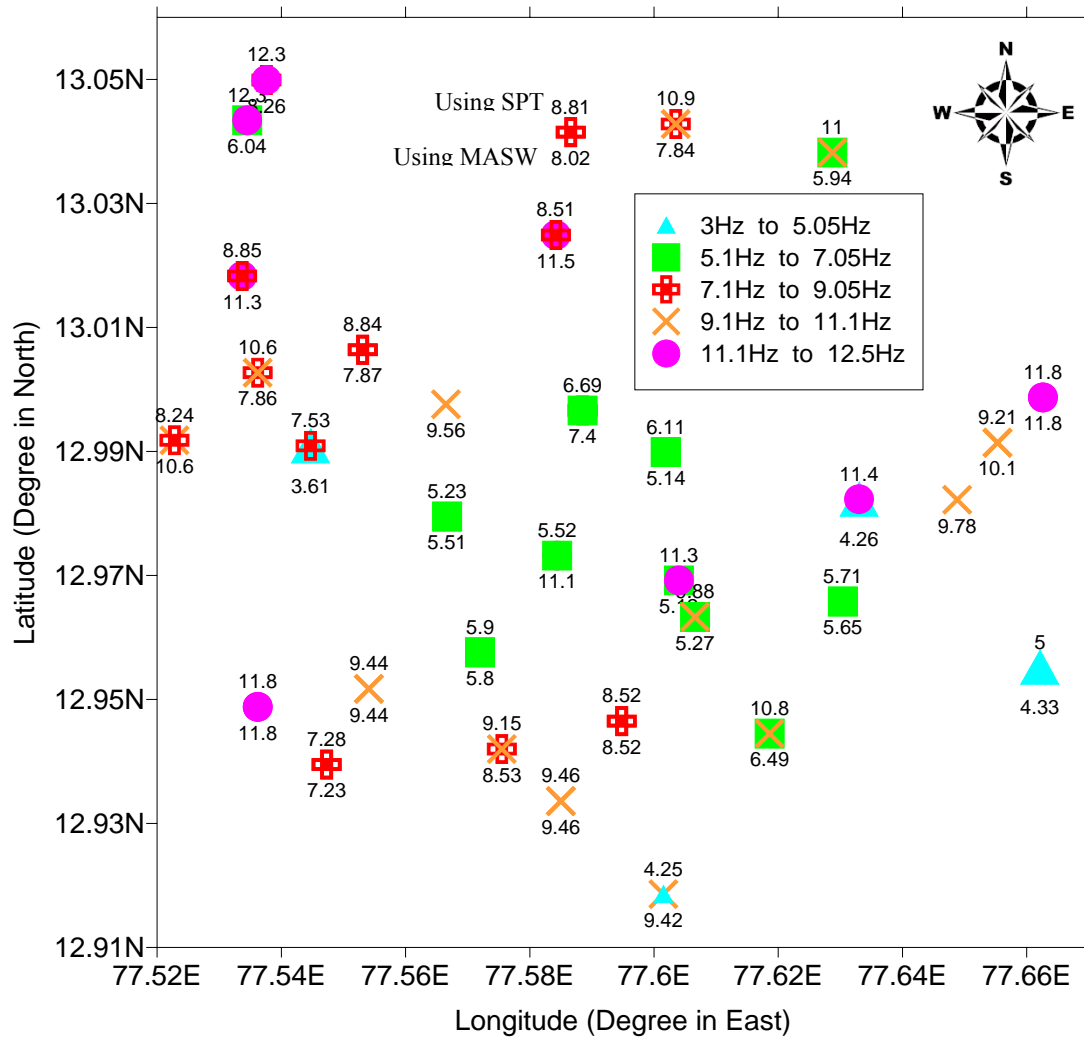
Figure 19: Predominant Frequencies using SPT and MASW Data

Table 5: Predominant frequency Ranges

Predominant Frequency Range (Hz)	Symbols	Numbers of sites	
		Using SPT	Using MASW
3.0 to 5.0	▲	3	3
5.1 to 7.0	■	6	9
7.1 to 9.0	✚	8	9
9.0 to 11.0	✕	9	7
11.1 to 12.5	●	8	5

Correlation between (N₁)₆₀cs and Gmax

Ground response study using SPT data and MASW data for same locations clearly shows that results obtained from SPT data are higher than MASW data result. Even though input motion, densities, thickness of layer and analysis procedures are same for both results, variation in the output may be due to another important input of dynamic soil properties. In SHAKE2000 dynamic soil properties such as shear modulus are evaluated based on the inbuilt equation (equation 13 in SHAKE2000) developed by Imai and Tonouchi (1982) which is given below:

$$G_{max}(kips/ft^2) = 325[(N_1)_{60cs}]^{0.68}$$ (Imai and Tonouchi, 1982)   (9)

The shear wave velocity is back calculated from the well known equation of $G = \rho Vs^2$. In response study using MASW data, shear modulus (G$_{max}$) is calculated by accounting the both density as well as in-situ shear wave velocities, which is given below:

(10)

Where

ρ density $G_{max} = \rho Vs^2$ om the undisturbed sample in SPT boreholes
Vs shear wave velocity measured using the MASW testing.

Dynamic properties obtained from SPT test correspond to high strain values when compared to MASW test which gives properties at low shear strains. Also the factor affecting G$_{max}$ depends on soil parameters, but in SHAKE2000, G$_{max}$ is calculated based on the inbuilt equation developed for some region. From this study it is felt that Shake programme can be effectively used by using G$_{max}$ equation for the region or the in-situ shear wave velocity for shake analysis. Studies show that the site response obtained from SHAKE2000 using MASW data is reasonably good when compared to using SPT data. The SPT data can be effectively used for site response analysis, if regional G$_{max}$ equation is developed. To fulfill this requirement an attempt has been made to correlate the measured G$_{max}$ (calculated from measured shear wave velocity and densities of each layer) of each borehole to corrected SPT-N values. About 38 locations MASW data were very close to the SPT bore hole. From 38 locations about 195 data pairs of *Vs* and SPT corrected blow count have been used for the regression analysis. The regression equation developed between *Vs* and *(N₁)₆₀cs* is given in equation 11:

$$G_{max} = 13.86[(N_1)_{60cs}]^{0.68}$$ (11)

Where, G$_{max}$ –Low strain maximum shear modulus in MN/m²,
        (N₁)₆₀cs – Corrected SPT "N" Value.

Power regression fitting gives the highest R squared value of 0.87. The comparison between Imai and Tonouchi (1982) equations (equation 9) with newly developed equation (11) are given in Figure 20. Fitted equation (11) matches up to a corrected SPT-N [(N₁)₆₀cs] value of 30 with Imai and Tonouchi (1982) equation. Beyond the "(N₁)₆₀cs" values of 30 fitted equation G$_{max}$ is lower than the Imai and Tonouchi (1982) equation.

Site response Using Micro Tremor (Jointly with NGRI)

The site response studies also carried out experimentally based on recording the ambient noise for a selected period of duration. The noise was recorded at 54 different locations in 220sq.km area of Bangalore city using L4-3D short period sensors (CMG3T) equipped with digital data acquisition system. In this study, Nakamura method was adopted by NGRI for obtaining the transfer function at various sites in Bangalore. The general layout of the Horizontal to Vertical Spectral Ratio technique (HVAR) is shown in Figure 21. The surface sources for the ambient noise generate Rayleigh waves which affect the vertical and horizontal motion equally in the surface layer. The spectral ratio of the horizontal component to the vertical component of the time series provides the transfer function at a given site. The dominant peak is well correlated with the fundamental resonant frequency. The predominant frequencies obtained from experimental result range between 1.2 Hz -11 Hz, which matches well with the 1-dimensional ground response analysis presented earlier.
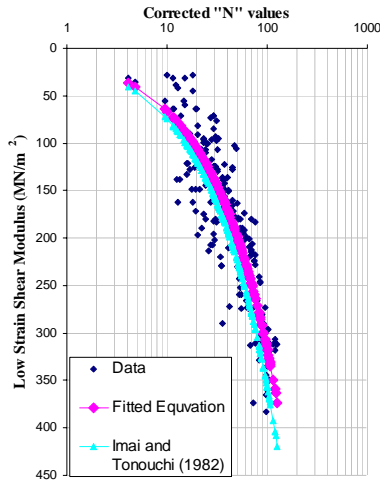
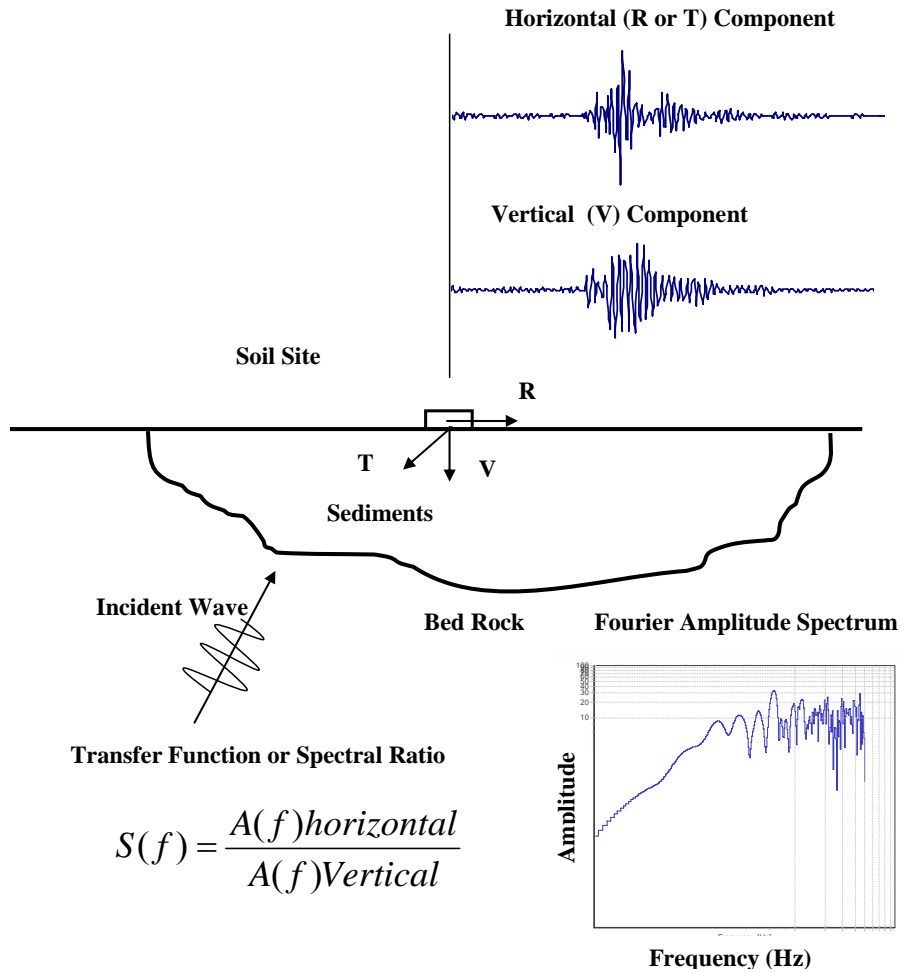**Figure 20: Comparison of shear modulus equations**

$$S(f) = \frac{A(f)horizontal}{A(f)Vertical}$$

Figure 21: Horizontal to Vertical Spectral Ratio Technique –Layout

Comparison of Predominant Frequency

Even though the Microtremor and MASW was carried out separately, about 43 points are comparatively closer to each other. These points are further used to compare the predominant frequency of Bangalore soil. Site response studies using SPT and MASW data shows that the predominate frequency of Bangalore soil varies from 3Hz to 12Hz. But a microtremor studies shows that the predominant frequency of Bangalore soil varies from 1.5Hz to 12Hz. The predominant frequency estimated from Microtremor and site response using MASW is shown in Figure 22. From Figure 22 the values above the symbol obtained using MASW site response study and values below the symbols are obtained using microtremor. Figure 8.33 also clearly shows that in most of the locations predominant frequency from both the method matches well. Most of the study area has predominant frequency of 3 Hz to 12 Hz from site response using SHAKE and microtremor studies, which is shown in Table 4.

Predominant Frequency Range (Hz)	Symbols	Numbers	
		Using MASW	Using Microtremor
3.0 to 5.0		7	16
5.1 to 7.0	▲	15	10
7.1 to 9.0	■	11	5
9.0 to 11.0	✚	6	2
11.1 to 12.5	✕	4	3
1.5 to 2.9	●	-	7

Table 4: Predominant Frequency using site response study and Microtremor

25

Liquefaction Hazard Assessment

To study the liquefaction hazard in Bangalore, the liquefaction hazard assessment has been carried out using standard penetration test (SPT) data and soil properties. Factor of Safety against liquefaction of soil layer has been evaluated based on the simplified procedure of Seed and Idriss (1971) and subsequent revisions of Seed et al (1983), Youd et al (2001) and Cetin et al (2004). Cyclic Stress Ratio (CSR) resulting from earthquake loading is calculated by considering moment magnitude of 5.1 and amplified peak ground acceleration. Cyclic Resistant Ratio (CRR) is arrived using the corrected SPT 'N' values and soil properties. In the cyclic stress approach, the generation of pore pressure related to the cyclic shear stresses and earthquake loading represented same. The earthquake loading can be evaluated using Seed and Idriss (1971) simplified approach as given below:

$$\text{Cyclic stress ratio (CSR)} = 0.65 \left(\frac{a_{max}}{g} \right) \left(\frac{\sigma_{vo}}{\sigma_{vo}'} \right) r_d \tag{12}$$

In this equation $0.65 \dfrac{a_{max}}{g}$ represents 65 % of the peak cyclic shear stress, a_{max} is peak ground surface acceleration, g is the acceleration of gravity, σ_{vo} and σ_{vo}' are total and effective vertical stresses and r_d = stress reduction coefficient. For the calculation of stress reduction coefficient many correlations are available which are discussed in detail in the NCEER workshop report (NCEER, 1997; Youd et al 2001). NCEER, (1997) and Youd et al (2001) recommends that for routine practice and non-critical projects, the equations given by Liao and Whitman (1986) may be used to estimate average values of r_d and is given below:

$$r_d = 1.0 - 0.00765_z \quad \text{for z} \le 9.15 \text{ m} \tag{13}$$
$$r_d = 1.174 - 0.0267z \quad \text{for } 9.15 \text{ m} < z \le 23 \text{ m} \tag{14}$$

Cyclic resistance ratio (CRR) is arrived based on corrected 'N' value from a plot of CRR versus corrected 'N' value from a large amount of laboratory and field data. Liquefaction resistance of soil depends on how close the initial state of the soil is to the state corresponding to the "failure". The liquefaction resistance can be calculated based on the laboratories tests and in-situ tests. Cyclic resistance ratio (CRR) is arrived based on corrected "N" value as per Seed et al. (1985), Youd et al., (2001); Cetin et al., (2004). Seed et al. (1985) presents a plot of CRR versus corrected "N" value from a large amount of laboratory and field data. The corrected "N" values are used to calculate the CRR for the magnitude of 7.5 earthquake using equation proposed by Idriss and Boulanger (2005) which as given below:

$$CRR = \exp\left\{ \frac{(N_1)_{60cs}}{14.1} + \left(\frac{(N_1)_{60cs}}{126} \right)^2 - \left(\frac{(N_1)_{60cs}}{23.6} \right)^3 + \left(\frac{(N_1)_{60cs}}{25.4} \right)^4 - 2.8 \right\} \tag{15}$$

However this estimation is proposed for an earthquake magnitude of 7.5. For the present study, for the earthquake moment magnitude of 5.1 has to be considered, so the necessary Magnitude Scaling Factor (MSF) has been evaluated. The magnitude-scaling factor used in the present study for the magnitude less than 7.5 is given below (Seed and Idriss, 1982):

$$MSF = \left[\frac{10^{2.24}}{M_W^{2.56}} \right] \tag{16}$$
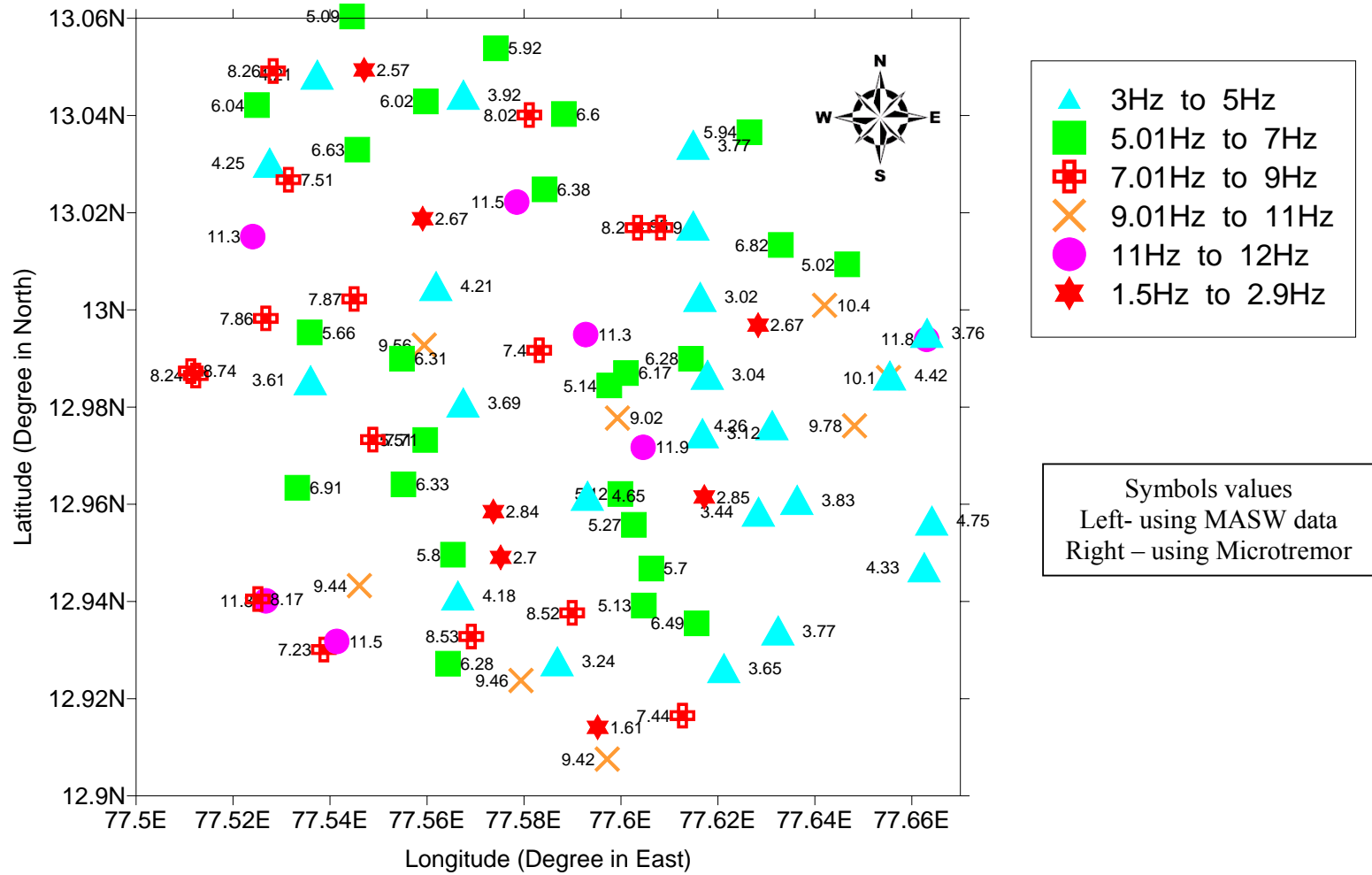
Figure 21: predominant frequency from Microtremor and Site Response using Shear wave Velocity

Factor of safety against liquefaction: The cyclic stress ratio caused by the earthquake is greater than the cyclic resistance ratio of in situ soil then liquefaction could occur. The factor of safety against liquefaction is defined as follows:

$$FS = \left(\frac{CRR_{7.5}}{CSR}\right)MSF \qquad (17)$$

Factor of safety against liquefaction is calculated using stress ratios and accounting necessary magnitude scaling factor for maximum credible earthquake. A simple spread sheet was developed to carryout the calculation for each bore log. The factor of safety against liquefaction is grouped together for the purpose of classification of Bangalore (220 sq. km) area for a liquefaction hazard. Using 2-D base map of Bangalore city, the liquefaction hazard map was prepared using AutoCAD and Arc GIS packages. The results are grouped as four groups for mapping and presented in the form of 2-dimensional maps. Figure 22 shows the map of factor of safety against liquefaction (FS) for Bangalore city to the local magnitude of 5.1. About 90% of the area in Bangalore have heigher factor of safety and are non-liquefiable. This study shows that Bangalore is safe against liquefaction except at few locations where the overburden is sandy silt with presence of shallow water table.

Cyclic triaxial experiments on undisturbed soil samples

Undisturbed samples were collected from few locations in (south west region) Bangalore city to verify the liquefaction potential of the soil. This is done by conducting cyclic triaxial test in the laboratory on the undisturbed soil samples collected from Boreholes locations of 482, 810 and 91. The test has been carried out as per ASTM: D 3999 (1991) in strain controlled mode. Cyclic triaxial tests are carried out with double amplitude axial strains of 0.5%, 1% and 2% with a frequency of 1Hz. A typical cyclic triaxial test results are presented in Figures 23 and 24. Figure 23 shows the variation of deviatoric stress versus strain plot for more than 120 cycles of loading (axial strain = 0.25%; applied confining pressure 100 KPa, for the undisturbed sample corresponding to depth 3m below GL, in-situ density of the soil sample 2.0 gm/cc with in-situ moisture content 15%, at 3.0m depth). Figure 24 shows the pore pressure ratio versus number of cycles. From these plots it is clear that even after 120 cycles, the average pore pressure ratio is about 0.94 and deviatoric stress versus strain plots has not become flat, indicating no liquefaction. The resistance to liquefaction is very high. The calculated factor of safety against liquefaction results, for this borehole is also very high indicating no liquefaction. These results match well with the lab test results (Sitharam et al 2007).
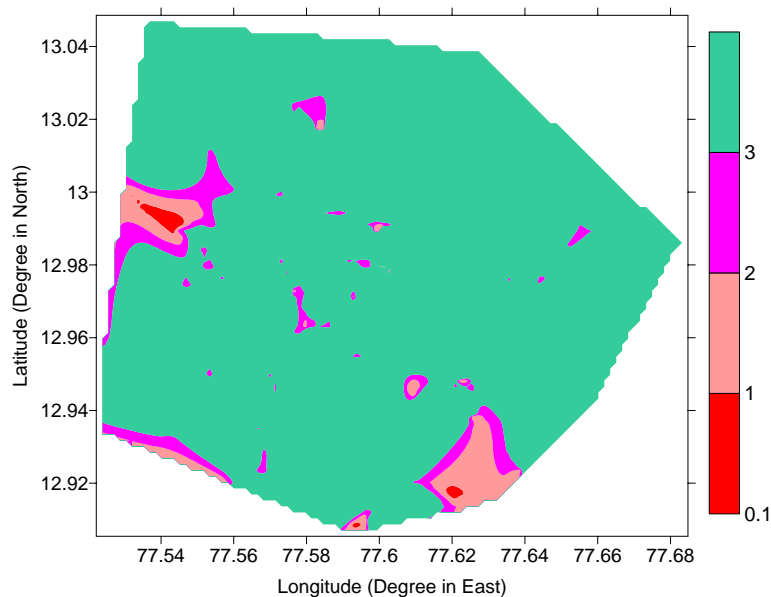

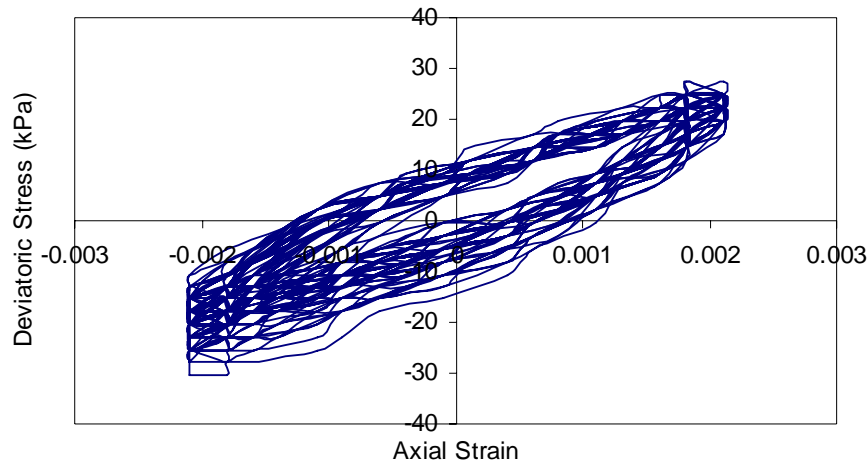**Figure 22: Distribution Factor of safety against Liquefaction**

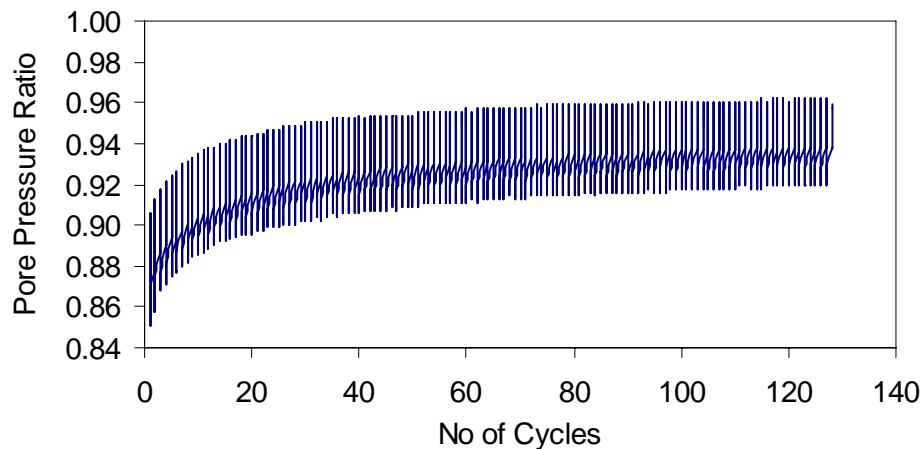**Figure 23: Typical hysteresis loops from a Cyclic Triaxial test**

Figure 24: Typical Pore Pressure Ratio Plot with number of cycles

Summary

This study shows that, expected peak ground acceleration (PGA) at rock level for Bangalore is about 0.15g using DSHA. Seismic parameter 'b' value is estimated as 0.87, which is slightly higher than the published values which may be due to increase in seismotectonic activity of the region. PSHA used to quantify the uncertainty involved in the hazard analysis, which also gives similar peak ground acceleration of 0.136g. Generally PSHA estimates a lower PGA values compared to that of PGA values obtained from DSHA. Mean annual rate of exceedance for particular acceleration is obtained for both PGA and spectral accelerations. Uniform hazard spectra at rock level and return period have been evaluated. Site characterization using SPT data has been carried out and 3-D subsurface model has been generated using GIS. Field SPT 'N' values are corrected by applying necessary corrections for further use in engineering applications. Site characterization also carried out using measured shear wave velocity using MASW and average shear wave velocity at each 5m interval up to a depth of 30m was evaluated and presented. Based on soil average shear wave velocity

and 30m average shear wave velocity, as per NEHRP and IBC, Bangalore can be classified as "Site class D". Correlation between corrected SPT 'N' values and measured shear wave velocity has been developed. Theoretical 1-D site response study shows that the amplification factor is in the range of 1 to 4.7 and predominant frequency varies from 2 Hz to 12Hz. The results of site response studies using SPT data and MASW data are comparable. Ground response parameters evaluated using MASW data are slightly lower values when compared to the parameters obtained using SPT data. Correlation between corrected SPT 'N' values and low strain shear wave modulus has been developed. Field study of microtremor also shows similar values of predominant frequencies for these sites. Predominant frequency obtained from these three methods matches very well. Liquefaction hazard map has been generated using factor of safety against Liquefaction. Which is evaluated based on SPT borehole information. At few locations undisturbed soil samples were collected and liquefaction testing has been carried out using laboratory cyclic triaxial testing. Liquefaction study shows that Bangalore is safe against liquefaction except at few locations where the overburden is sandy silt with presence of shallow water table.

Acknowledgements

References

Aki, K. and Richards, P.G. (1980), "Quantitative seismology", *W.H. Freeman, San,* Vol. 1

Ansal, A., Laue, J., Buchheister, J., Erdik, M., Springman, S.M., Studer, J. and Koksal, D. (2004), "Site Characterization and Site Amplification for a Seismic Microzonation Study in Turkey", *Proceedings 11th International Conference on Soil Dynamics and Earthquake Engineering, 3rd International Conf. On Earthquake Geotechnical Engineering, April 2004; Berkeley, California, USA,* pp 1-8.

Bhatia, S. C., Ravi Kumar, M., and Gupta, H.K. (1997)," A Probabilistic Seismic Hazard Map of India and Adjoining Regions", *http://www.seismo.ethz.ch/gshap/ict/india.html*, pp 1-12.

Boore, D. M. (1983), "Stochastic simulation of high-frequency ground motions based on seismological models of the radiated spectra", *Bull. Seism. Soc. Am.,* Vol. 73, 1865-1894.

Boore, D. M. (2003), "Simulation of ground motion using the stochastic method", *Pure and Applied Geophysics,* Vol. 160, pp 635-675.

Bullen, K.E. (1965), "An introduction to the theory of seismology", *Cambridge Univ. Press, Cambridge, U.K.*

Cetin, K.O, Seed, R.B., Kiureghian, A.D., Tokimatsu, K., Harder, L.F. Jr., Kayen, R.E., and Moss, R.E.S. (2004), "Standard penetration test-based probabilistic and deterministic assessment of seismic soil liquefaction potential", *Journal of Geotechnical and Geoenvironmental Engineering,* Vol. 12, pp 1314-1340.

Dobry, R., R. D., Borcherdt, C. B., Crouse, I. M., Idriss, W. B., Joyner, G. R. Martin, M. S., Power, E. E., Rinne and R. B. Seed, (2000), "New site coefficients and site classification system used in recent building seismic code provisions", *Earthquake Spectra,* Vol. 16, pp 41–67.

Ganesha Raj. K., and Nijagunappa, R. (2004)," Major Lineaments of Karnataka State and their Relation to Seismicity" *Remote Sensing Based Analysis, Jr.Geol.Soc.India,* Vol.63, pp.430-439.

Idriss, I. M. and Boulanger, R. W. (2005), "Evaluation of Liquefaction Potential, Consequences and Mitigation" *Invited Expert Lectures, Proc. Indian Geotechnical Conference-2005, 17-19 December 2005, Ahmedabad, INDIA,* pp 3-25.

Idriss, I. M., and Boulanger, R. W. (2004), "Semi-empirical procedures for evaluating liquefaction potential during earthquakes." *Proc., 11th International Conference on Soil Dynamics and Earthquake Engineering, and 3rd International Conference on Earthquake Geotechnical Engineering, D. Doolin et al., eds., Stallion Press,* Vol. 1, pp 32-56.

Imai. T and Tonouchi. K, (1982), "Correlation of N-value with S-wave velocity and shear modulus", Proceedings, 2nd European Symposium on Penetration Testing, Amsterdam, pp 57-72.

Kanli, A.I., Tildy, P., Pronay, Z., Pinar, A. and Hemann, L. (2006), "Vs^{30} mapping and soil classification for seismic site effect evaluation in Dinar region , SW Turkey", *Geophysics J. Int,* Vol. 165, pp 223-235.

Kijko, A. and Sellevoll, M. A. (1989), "Estimation of earthquake hazard parameters from incomplete data files. Part I Utilization of extreme and complete catalogs with different threshold magnitudes" *Bull. Seismol. Soc. Am.,* Vol. 79, pp 645–654.

Kijko, A. and Sellevoll, M. A. (1992), "Estimation of earthquake hazard parameters from incomplete data files. Part II. Incorporation of magnitude heterogeneity," *Bulletin of the Seismological Society of America, Feb 1992,* Vol.82, pp 120 - 134.

Liao, S. S. C., and Whitman, R. V. (1986), ''Catalogue of liquefaction and non-liquefaction occurrences during earthquakes.'' *Res. Rep., Dept. of Civ. Engrg., Massachusetts Institute of Technology, Cambridge, Mass.*

Nath,S.K. (2006), "Seismic Hazard and Microzonation Atlas of the Sikkim Himalaya", *published by Department of Science and Technology, Government of India, India.*

Ramalingeswara Rao, B. (2000), "Historical Seismicity and deformation rates in the Indian Peninsular Shield", *Journal of Seismology,* Vol. 4, pp 247-258.

Schnabel, P. B., (1973), "Effects of Local Geology and Distance from Source on Earthquake Ground Motion," *Ph.D. Thesis, University of California, Berkeley, California.*

Seed, H. B., and I. M. Idriss, (1971), "Simplified procedure for evaluating soil liquefaction potential," *Journal of the Soil Mechanics and Foundation Division, ASCE,* Vol.97, No.9, pp 1249-1274.

Seed, H. B., and Idriss, I. M., (1970), "Soil Moduli and Damping Factors for Dynamic Response Analyses," Rep. No. EERC-70/10, *Earthquake Engineering Research Center, University of California, Berkeley, California*

Seed, H. B., Idriss, I. M., and Arango, I. (1983), "Evaluation of Liquefaction potential Using Field Performance Data," *Journal of Geotechnical Engineering,* Vol. 109, No. 3, March, pp 458-482.

Seed, H.B., and I.M., Idriss, (1982), "Ground Motions and Soil Liquefaction during Earthquakes, Monogr.5", *Earthquake Engineering Research Institute, University of California, Berkeley.*

Seismotectonic Atlas of India-(2000), *published by Geological Survey of India.*

Sitharam, T. G. and Anbazhagan, P. (2007), "Seismic Hazard Analysis for the Bangalore Region", Natural Hazards, Vol. 40, pp 261–278.

Sitharam, T. G., Anbazhagan, P. and Ganesha Raj, K. (2006), "Use of remote sensing and seismotectonic parameters for seismic hazard analysis of Bangalore", *Natural Hazards Earth System Sci.,* Vol. 6, pp 927–939.

Skempton, A. W. (1986), "Standard Penetration Test Procedures." *Geotechnique,* Vol.36, No.3, pp.425-447.

Sridevi Jade, (2004), "Estimation of plate velocity and crustal deformation in the Indian sub-continent using GPS geodesy", *Current Science,* Vol.86, pp 1443-1448.

Wells, D.L., Coppersmith, K.J. (1994), "New empirical relationships among magnitude, rupture length, rupture width, rupture area, and surface displacement", *Bull. Seismol. Soc. Am. 4 (84), 975– 1002.*

Xu, Y., Xia, J., and Miller, R.D., (2006), "Quantitative estimation of minimum offset for multichannel surface-wave survey with actively exciting source", *Journal of Applied Geophysics,* vol 59, No. 2, pp117-125.

Youd, T.L., Idriss, I.M., Andrus, R.D., Arango, I., Castro, G., Christian, J.T., Dobry, R., Liam Finn, W.D., Harder Jr., L.H., Hynes, M.E., Ishihara, K., Koester, J.P., Liao, S.S.C, Marcuson, W.F., Marting, G.R., Mitchell, J.K., Moriwaki, Y., Power, M.S., Robertson, P.K., Seed, R.B, And Stokoe, K.H. (2001), "Liquefaction Resistance of Soils: Summary from the 1996 NCEER and 1998. NCEER/NSF Workshops on Evaluation of Liquefaction Resistance of Soils", *Journal of Geotechnical and Geoenvironmental Engineering,* pp 817 – 833.

OSGeo-India

About OSGeo

The Open Source Geospatial Foundation, abbreviated as"OSGeo" ,is an independent ,non profit organization established to support growing requirements of the open source geospatial community. The foundation will serve as an organizing body, a public technology commons, a development community manager, and event sponsor.

About India chapter

Geospatial tools, have gained tremendous support and popularity in India for the past decade or so. Many proprietary software systems with their applications have capurtred the requirements of users in Academia, Industry, Governemnt, local bodies of governance and a host of stakeholders involved in Infrastructure development in the country. The geospatial industry has grown substantially and is poised to grow further. Nevertheless, the benefits of a such growth are polarised towards a small segment of the society, primarily due to high costs of proprietary software in procuring, maintenance and outreach. So far such systems were seen as something to be used for high level planning and complex scientific operations by large corporates and Govt research agencies or departments only. The benefits that could potentiall accrue due to use of open source geo spatial systems are enormous given that India is one of the leading worldwide provider of IT services.

With recent developments in the areas of right-to-information and National Map Policy (http://dst.gov.in/whats_new/press_releases05/cabinet-approves.htm), there is a widespread and increased awareness towards use of geospatial tools. A large portion of geodata will now be freely available. Most goverement departments are now trying to find easier ways to manage, update and publish information for the public. There are also large number of NGOs and citizen organisations, working in areas such as ubran poverty, town planning, solid waste management,rural development, education,environmental issues and many more.

However, growth of GIS is hindered by highly priced proprietory softwares and unavailability of public geodata. Many of such licenced softwares remain unutilized in various government offices because they require either extensive training or easy availability on multiple locations. All this can be changed by the use of Free/Opensource software tools. There is hardly any proprietory GIS software that can show text in Unicode standard in maps . This is significant since all governmet data and most educational institutions work in local language media . FOSS4G has already shown this solution. Thus, Free/Opensource Geospatial softwares can be used for developing systems where more and more community participation and involvement is sought.

The OSGeo India Chapter is formed to fulfill the mission and objectives described in this document. OSGeo India Chapter will follow the Local Chapter Guidelines stipulated by OSGeo and cooperate closely with OSGeo Board in promoting the use and development of OSGeo projects in India. The OSGeo India Chapter will strive to serve anyone interested in Open Source Geospatial Solutions and related issues, and to cover all the activities associated with the application, development and promotion of Open Source Geospatial solutions in India.

Mission

Promoting Free/Opensource Geospatial tools and publicly available Geodata

Advocacy of and promoting Localized GIS along with applications on webmapping

Act as a bridge between various groups like Developers, Application Users, NGOs, e-governance etc.

Mentor various FOSS GIS miniprojects by providing resources such as technical guidence, webspace etc.

Objectives

Follow up on indian language support in various free/opensource GIS tools like GRASS, MapServer etc.

Initiative for standardisation of publicly available geodata

Setting up WMS/WFS based geodata servers using publicly available geodata

Tolkit for localised GIS including with special focus on schools, governments, public causes such as child malnutririon, mass education.

Open source Geospatial tool list

Web Mapping

Map bender   http://www.osgeo.org/mapbender

Map Builder   http://www.osgeo.org/mapbuilder

Map Guide Open Source   http://www.osgeo.org/mapguide

MapServer   http://www.osgeo.org/mapserver

OpenLayers   http://openlayers.org/

Desktop Applications

GRASS   http://www.osgeo.org/grass

OSSIM   http://www.osgeo.org/ossim

Geospatial Libraries

GDAL/OGR   http://www.osgeo.org/gdal_ogr

GeoTools   http://www.osgeo.org/geotools

Metadata Catalog

GeoNetwork opensource   http://geonetwork-opensource.org/

OSGeo Foundation Mailing Lists

Announcements List - keep informed about updates in the Open Source Geospatial Foundation

Discussion List - **interact and get involved in the Open Source Geospatial Foundation.**

Discuss, comment, query and share your knowledge through mail_discuss@lists.osgeo.org

OSGeo-India

c/o International Institute of Information Technology
Gachibowli, Hyderabad 500032
Email: rajan@iiit.ac.in

GRASS http://wgbis.ces.iisc.ernet.in/grass	QGIS http://www.qgis.org/	**Open** **JUMP** http://openjump.org/
http://www.php.net/	http://www.tcl.tk/	http://qt.nokia.com/
http://www.apache.org/	http://mapserver.org/	http://jabref.sourceforge.net/
http://openmodeller.sourceforge.net/	**ILWIS** http://www.itc.nl/ilwis/	http://www.boutell.com/gd/
http://www.r-project.org/	http://www.gstat.org/	**I N K S C A P E** http://www.inkscape.org/
http://www.mysql.com/	http://www.postgresql.org/	http://postgis.refractions.net/
ATutor- Content Management System http://www.atutor.ca/	http://drupal.org/	http://www.joomla.org/

Welcome to Free & Open Source Software (FOSS) at CES, IISc, Bangalore, India

Home
GRASS Mirror site in India
GRDSS
Geovisualisation
What is FOSS ?
FAQs
Scripting Language
Open Web Server
Open Source Database
Open Content Management System

Home   E-mail
Geographic Resources Analysis Support System
    Geographic Resources Decision Support System

GEOVISUALISATION OF CHERUVANNUR VILLAGE PANCHAYAT, KOZHIKODE, KERALA, INDIA

Open Source GIS in India, Discussion Meeting, 16th November 2009, CiSTUP, IISc